

STUDIES IN PANEL FLUTTER AT HIGHER MACH NUMBERS

I. FLAT AND SLIGHTLY CURVED PANELS

AT MACH NUMBER 2.81

II. CYLINDRICAL SHELLS WITH BOUNDARY LAYER

Thesis by

William Judson Anderson

In Partial Fulfillment of the Requirements

For the Degree of

Doctor of Philosophy

California Institute of Technology

Pasadena, California

1963

ACKNOWLEDGMENT

The author would like to express his appreciation for the encouragement and guidance given by Dr. Y. C. Fung during the development of this thesis. Thanks are also due to Mr. Marvin Jessey for his many hours of work on the instrumentation and to Mrs. Martha Lamson for her help with numerical calculations.

A number of people cheerfully helped with the preparation of the thesis. The typing was done by Miss Helen Burrus and the figures were drawn by Mrs. Melenie Loosli. The equations were inked in by my wife Betty, who also helped with the rough typing.

During one year of research, the author was supported by a National Science Foundation Fellowship. The remaining three years of research, including all of the wind tunnel testing, were sponsored by the Air Force Office of Scientific Research. The author is grateful for the aid given by these two agencies.

I. FLAT AND SLIGHTLY CURVED PANELS

AT MACH NUMBER 2.81

ABSTRACT

Two series of panel flutter tests were carried out in the Jet Propulsion Laboratory's 12 inch supersonic wind tunnel. Flat and slightly curved panels were tested at Mach number 2.81.

The flat, rectangular panels were designed to study two-dimensional flutter. They were clamped at front and rear with free sides which extended into the boundary layer at the sides of the tunnel. These panels fluttered in a two-dimensional mode which occurred at a thickness ratio approximately 15 per cent different from the predictions of existing theory. One of the panels exhibited a three-dimensional "rocking" flutter which has not been observed or discussed before. A theory is developed for this type of flutter.

The slightly curved panels were shallow circular cylindrical shells with the generators perpendicular to the flow direction. These panels were all of aspect ratio one. It was found that the effect of curvature was destabilizing and that the effect of internal pressurization was stabilizing.

TABLE OF CONTENTS

PART I

Section	Page
Introduction	1
1. Flat Panels	2
1.1. Description of Model	3
1.2. Instrumentation	5
1.3. Test Procedure	6
1.4. Experimental Results	8
1.5. Theoretical Prediction of Three-Dimensional Flutter	11
1.6. Conclusions and Discussion of Flat Panel Results	21
2. Slightly Curved Panels	22
2.1. Description of Model	23
2.2. Instrumentation	25
2.3. Test Procedure	25
2.4. Experimental Results	26
2.5. Theoretical Effect of the Cavity	27
2.6. Conclusions for Curved Panels	33
References	35
Appendix	37
Tables	39

LIST OF FIGURES

Figure		Page
1	Two-Dimensional, Flat, Clamped Panel.	44
2	Flutter Boundaries for Two-Dimensional, Flat Panels.	44
3	Wind Tunnel Model for the Flat Panel Test.	45
4	Installation of Model in Wind Tunnel.	45
5	Flat Panel Assembly.	46
6	Flutter Amplitudes for 0.015" Flat Panels.	47
7	Thickness Ratio Required to Prevent Flutter.	48
8	Resonant Frequencies for a Flat Panel 0.0151" Thick.	49
9	Resonant Frequencies for a Flat Panel 0.0153" Thick.	50
10	Resonant Frequencies for a Flat Panel 0.0193" Thick.	51
11	Resonant Frequencies for a Flat Panel 0.0151" Thick.	52
12	Phase Lag for Two-Dimensional Flutter of Flat, Clamped Panels.	53
13	Static Pressure Differential Between Model Cavity and Free Stream.	54
14	Coordinate System for Three-Dimensional Flutter of a Simply-Supported Panel.	55
15	Method of Images.	55
16	Two-Term Fourier Series Representation of $g(z)$.	55
17	Three-Dimensional Flutter Solution.	56
18	Flutter Boundary for Three-Dimensional Case.	57
19	Wind Tunnel Model for Curved Panel Test.	58
20	Curved Panel Assembly, Inverted.	58
21	Bottom View of Model.	59

LIST OF FIGURES (contd.)

Figure		Page
22	View of Model Cavity.	59
23	Typical Theoretical Flutter Boundary for Curved Panels.	60
24	Flutter Amplitudes for Slightly Curved Panels.	61
25	Flutter Amplitudes for Slightly Curved Panels.	62
26	Experimental Flutter Boundaries for Slightly Curved Panels.	63
27	Effect of Static Pressure Differential on the Flutter of Slightly Curved Panels.	64
28	Phase Lag at Initiation of Flutter, Curved Panels.	65
29	Phase Lag for Curved Panel No. 1.	66
30	Phase Lag for Curved Panel No. 3.	67
31	Phase Lag for Curved Panel No. 4.	68
32	Curved Panel Over a Closed Cavity.	69
33	Curved Panel in Initial and Deflected Positions.	69
34	Cavity Effect on Natural Frequencies of Curved Panels.	70
35	Cavity Effect on Natural Frequencies of Curved Panels.	70

LIST OF SYMBOLS

A	Dynamic pressure parameter, $\frac{\rho_a U L^3}{D} = \frac{\tau_{pML}^3}{D}$
a	Speed of sound in the fluid
a _s	Speed of sound in the panel material
D	Bending rigidity, $\frac{Eh^3}{12(1 - \nu^2)}$
E	Modulus of elasticity of panel material
f	Frequency, cps
f _n (x)	See equation 1
g _a	Aerodynamic damping, $0.702 \sqrt{1 - \nu^2} (\rho/\rho_s)(a/a_s)(\frac{L}{h})^2$
g(z)	See equation 1
h	Panel thickness
I	Identity matrix
k	Reduced frequency, $\frac{\omega L}{U}$
L	Panel length; also T-V (in Lagrange's equations, only)
l ₁ , l ₂	Panel length and width, see figures 14 and 32.
M	Mach number
P	Flutter matrix
P _t	Total pressure of flow
p	Static pressure of flow
p̄(x, z, t)	Perturbation pressure
Q _m	Generalized forces
T	Temperature

$T(t)$	Kinetic energy
t	Time
U	Velocity in the fluid
$V(t)$	Potential energy
V_o	Volume of the cavity under the panel
w_3	Dynamic pressure parameter, $\frac{\tau_p M^2 l_1^3}{8\beta D}$
$w(x, z, t)$	Panel deflection, positive in positive y direction
x	Coordinate in streamwise direction
y	Coordinate normal to plane of plate
z	Coordinate in spanwise direction
β	$\sqrt{M^2 - 1}$
τ	Ratio of specific heats
ΔP	Static pressure differential across the panel, positive when the cavity is at a higher pressure than free stream
ΔV	Change in cavity volume caused by panel deflection
η_{mn}	See equation 4
λ	$\frac{\rho_s h \omega^2 l_1^4}{D}$
λ_1	$\frac{\rho_s h \omega^2 l_2^4}{D}$
μ_{mnp}	See equation 15
ν	Poisson's ratio
ρ	Fluid density
ρ_s	Panel density
$\psi(x)$	Phase lag
ω	Frequency, radians per second

INTRODUCTION

Panel flutter is the self-excited oscillation of a thin shell or a membrane which is exposed to a flow nearly parallel to its surface. It has become important in the past few years because missiles and spacecraft require very thin coverings. Flutter of the various geometrical shapes involved, under the various loading and thermal effects, becomes a complex problem.

A great deal of theoretical work has been done for panel flutter, but there has been relatively little experimental work. The flutter of buckled flat panels has been studied experimentally by Eisley (Ref. 1) and Sylvester (Ref. 2). Tests have been carried out on a variety of flat panels by Greenspon and Goldman (Ref. 3), Sylvester and Baker (Ref. 4), Lock and Fung (Ref. 5), and Tuovila and Presnell (Ref. 6). A comprehensive review of theoretical and experimental progress in the field of panel flutter is given by Fung in reference 7.

Two series of wind tunnel tests were carried out at the California Institute of Technology's Jet Propulsion Laboratory to study two specific types of panel flutter. The testing was done at a Mach number of 2.81 in the 12" supersonic wind tunnel. One series dealt with flat, rectangular panels which were mounted in such a way as to allow two-dimensional flutter, i. e. flutter with constant displacement across the span. A flexure arrangement was used to minimize mid-plane stress. The other series dealt with the flutter of slightly curved panels, as shown in figures 19 and 20. Note that the generators of the cylinder are perpendicular to the flow.

Of primary interest in the tests were the flutter boundaries, the flutter modes involved, and whether or not there was a form of frequency coalescence.

1. Flat Panels

The first series of tests was designed to study the two-dimensional flutter of flat panels with clamped edges and zero membrane stress (see figure 1). This is one of the simplest types of panel flutter, and provides a case where experiment can be compared with existing theory. The theoretical side is well understood for Mach numbers between 2 and 5 because linear piston theory can be applied.

The experimental panels were rectangular in shape and were clamped at the leading edge, free at the sides and attached to a flexure at the rear. The flexure was designed to allow neither deflection nor rotation of the trailing edge, but allowed it to translate so as to reduce the membrane stress. In essence, this flexure acted as a weak linear spring in resisting translation.

The theory for this case has been worked out in detail by Houbolt (Ref. 8) and Movchan (Ref. 9). Both used linear piston theory for the aerodynamic forces and were able to find exact solutions to the stability problem. Linear piston theory yields an aerodynamic pressure of the form

$$\bar{p}(x,t) = \frac{\rho U^2}{M} \frac{\partial w(x,t)}{\partial x} + \frac{\rho U}{M} \frac{\partial w(x,t)}{\partial t} ,$$

where $w(x,t)$ is the panel displacement.

Houbolt finds that, for zero membrane stress, flutter is controlled by two variables A and g_a . They are defined as

$$A = \frac{\rho_a U L^3}{D},$$

$$g_a = 0.702 \sqrt{1-v^2} \frac{\rho}{\rho_s} \frac{a}{a_s} \frac{L^2}{h^2},$$

where ρ_s is the panel density and a_s is the speed of sound in the panel material. The critical value of A at flutter is plotted in figure 2. Because g_a is generally very small at flutter, the value of $\frac{A}{\pi^4}$ is usually taken to be 6.52 for clamped panels and 3.52 for pinned panels. Houbolt points out that setting $g_a = 0$ is equivalent to neglecting the "aerodynamic damping" term $\frac{\rho U}{M} \frac{\partial w}{\partial t}(x, t)$ in the aerodynamic force.

In addition to the two-dimensional flutter discussed above, one of the panels exhibited a three-dimensional type of flutter. This flutter was characterized by a rocking motion with a nodal line down the center of the panel. Theory for this type of flutter is developed in section 1.5, using linear supersonic aerodynamic theory.

1.1. Description of Model

The panels were mounted in a wedge-shaped aerodynamic frame made of aluminum (figure 3). The model was positioned across the center of the test section (figure 4) and was isolated against vibration from the tunnel walls by "floating" it on rubber mounts. The model was designed so that no reflected shock waves hit it.

The experimental panel was mounted over a 1/2" deep cavity in the frame, thus exposing the panel to supersonic flow on one side and stagnant air on the other. The panel extended to within 1/2" of the wind tunnel walls, which was approximately the displacement boundary layer

thickness on the walls. It was hoped that this would give an approximation to two-dimensional flow over the panel. A $3/32$ " venting gap extended along each edge of the mounting panel, serving to equalize the static pressure between the cavity and the free stream.

Each of the panels was soldered into a three-piece assembly including a panel, a front mounting bar, and a flexure - all made of half-hard yellow brass (figure 5). The flexure was machined from a solid bar.

A surface plate was used to join the panel assembly and the aerodynamic frame. This was done by inverting the components, placing them on the plate and bolting the mounting bar and the flexure to the model.

Vibration tests were carried out to determine the lower natural frequencies of the panels. The results are given in Table I, along with theoretical values from Warburton (Ref. 14). Fair agreement was found between the experimental and theoretical values for the two-dimensional modes. The second frequency listed (the three-dimensional "rocking" mode) was higher experimentally than predicted by theory. This may have been due to an initial "droop" in the panels, which was a two-dimensional deflection with a value of about 0.015" at the center of the panels. A deflection of this type can stiffen the panel with respect to bending in the spanwise direction.

Some bench testing was also done to determine the effect of the presence of a finite cavity under the panel on the natural frequencies of the panel. Using a bench model (not the actual wind tunnel model) it was found that a $1/2$ " deep vented chamber on one side of a panel did have an effect on the order of one or two cycles per second.

It was necessary to add a mechanical stop in the model to limit the translation of the flexures to 0.004". This was done after several

runs in the tunnel had damaged a flexure due to the starting shock loads on the panel. The stop system consisted of two eccentric cams and an electric light system. The stops were rotated until contact was made with the flexures, closing an electrical circuit and lighting a bulb. Each cam was then backed off until 0.004" clearance was obtained. This stop system worked very well throughout the testing and prevented further damage to the flexures. The electric light system was connected during the running of the tests to insure that the stops were not hitting the flexures.

1.2. Instrumentation

Panel displacements were measured with three inductance pickups equally spaced along the centerline of the model. The pickups were manufactured by Electroproducts, Inc. of Chicago, and the carrier system was especially developed for panel flutter testing by the electronics laboratory at GALCIT*. A 100 kilocycle carrier was used. The pickups were mounted 0.13" from the bottom surface of the panels and the motion of the brass panels in the field generated by the pickup caused a change in signal. No mechanical contact with the panel was necessary.

The signals from the pickups in the model were recorded using an Ampex model FR-100A tape recorder. An FM system was used so that both static deflection (due to a possible pressure differential between cavity and free stream) and dynamic deflections could be recorded. Also, a Technical Products harmonic analyzer with plotter was used to prepare plots of the power spectral density of the panel's vibration.

*Graduate Aeronautical Laboratories, California Institute of Technology.

An Ad-Yu phase meter was used to determine the phase shift between the three pickup signals during flutter. This meter works on the zero-crossing principle.

Four electromagnets were mounted in the cavity of the frame. Using these magnets, it was possible to find the resonant frequencies of the panels during the preflutter analysis. In order to excite the brass panels this way, it was necessary to glue small strips of 0.012" soft iron on the underside of each panel.

Pressure taps were installed in the bottom of the cavity and on the forward upper surface of the aerodynamic frame. These taps allowed the monitoring of the static pressure differential between cavity and free stream. This pressure differential is designated by the symbol ΔP in the following discussions.

One thermocouple was mounted in the cavity bottom and another on the underside of one of the panels. It was found that the frame and the panel reached the same operating temperature, with the temperature on the frame lagging by about five minutes because of the larger mass involved.

1.3. Test Procedure.

The Jet Propulsion Laboratory's 12" supersonic wind tunnel was a continuous flow tunnel with variable geometry throat calibrated for discrete Mach numbers. The test section was 9" high and 12" wide. Total pressure and total temperature were the easily varied parameters. All testing was carried out at Mach number 2.81.

The tests were run by holding the temperature on the model constant and by raising the total pressure in increments. The following procedure was used:

1. A panel of desired thickness was chosen.
2. The panel assembly was bolted to the aerodynamic frame.
3. The temperature at mounting was noted.
4. The amount of droop at the center of the panel was measured. (This was a good measure of panel imperfection.)
5. The flexure stops were set to allow only 0.004" deflection.
6. The assembled model was put in the tunnel.
7. The natural frequencies of the panel were measured (no flow).
8. Flow was established and stabilized at the lowest P_t desired for the particular sequence of runs.
9. The stagnation temperature was adjusted so that the model temperature was within ± 1 degree F. of that at which the model was assembled.
10. The root-mean-square voltage of the signal from each pickup was measured.
11. The resonant frequencies were found using the magnets.
12. Five minutes of signals from the pickups were recorded.
13. The total pressure was raised to the next value and steps 9 through 12 repeated.

Eventually a P_t setting was found where the amplitude of vibration started to increase suddenly. Data points were then taken at closer increments in this region. The exact point of sharp rise in response was noted.

After the panel had started to flutter, Fastax moving pictures were taken. These pictures helped in the identification of the flutter mode.

1.4. Experimental Results

Two types of flutter were encountered during the tests. One was two-dimensional and the other was a three-dimensional type of flutter with a nodal line down the center of the panel. The latter type was not considered before, but it occurred at a lower value of the parameter A than the two-dimensional flutter.

Every panel which was tested exhibited flutter. Amplitudes of panel motion as functions of the total pressure of the wind tunnel are shown in figure 6 for both types of flutter and also for a case where three-dimensional flutter gradually faded into two-dimensional flutter.

The test results are shown in Table II. Each flutter point was obtained by increasing P_t in the manner outlined in the previous section. Each point represents the flutter of a particular panel as mounted on a particular day of running and is taken as the average of three or more sweeps through the flutter boundary. The spread of P_t at flutter for these sweeps was usually about 2 per cent. When total pressure was lowered in the tunnel, flutter subsided at the same point at which it had started.

The last case given, for the 0.0190" panel, is not to be trusted as highly as the other cases. A static pressure differential sufficient to bow the panel in about 0.060" existed at the high value of P_t needed to flutter this panel.

The two-dimensional flutter occurred at values of $\frac{A}{\pi^4}$ which were about 35 per cent lower than those predicted for clamped two-dimensional panels by Houbolt. Figure 7 shows the thickness ratio required to prevent flutter as a function of wind tunnel static pressure. It is seen that these flutter points lie between the theoretical curves for clamped and simply supported end conditions. The three-dimensional flutter occurred at values of $\frac{A}{\pi^4}$ in the neighborhood of 3.0.

Frequency surveys during the approach of flutter failed to turn up any frequency coalescence for either kind of flutter. It was possible to follow the resonant frequencies in the preflutter region by using the magnet excitation system or by a harmonic analysis of the panel's response (see figures 8 through 11). In some cases it was possible to follow these frequencies through the onset of flutter. In each case, it was easy to see that the flutter occurred at one of the resonant frequencies. The amplitude of the response at this frequency grew rapidly as flutter started, completely dwarfing the response at the other frequencies.

Some phase angle data were obtained, although not as much as desired (only one pickup carrier system was available for part of the test). The phase lag $\psi(x)$ will be defined by writing the displacement $w(x, t)$ in the following way:

$$\begin{aligned}
 w(x,t) &= \left\{ w_1(x) + i w_2(x) \right\} e^{i\omega t} \\
 &= \sqrt{w_1^2(x) + w_2^2(x)} e^{i[\omega t + \psi(x)]}
 \end{aligned}$$

Figure 12 shows the phase lag $\psi(x)$ for two-dimensional flutter. All points are for the 0.0151" and 0.0153" panels. The theoretical curve is taken from work by Houbolt (Ref. 2). Experimentally, the first pick-up (farthest upstream) is arbitrarily given a phase lag to fit the theoretical curve. The large change in phase lag occurs farther to the rear of the panel than expected, but the total phase lag agrees well.

A Fastax camera was used in several runs, and was actually the means by which the three-dimensional flutter was first identified.

The static pressure differential between the cavity and the free stream was measured for each run. There was nearly a linear relationship between this pressure differential and the total pressure at which the tunnel was run (see figure 13). The differential was quite small in the P_t range where flutter was initiated for the panels of 0.015" thickness. Other panel mountings produced somewhat different pressure relationships, but generally of the same type as shown in this figure.

All runs were made with close control on the model temperature in order to minimize mounting effects. An allowance of ± 1 degree F. was made. A check on the temperature effect proved that the flexure relieved thermal stress so effectively that a 15 degree change in temperature only changed the frequencies by 2 per cent. This survey was made with the tunnel running at slightly less than the flutter P_t . Hence, temperature effects were virtually eliminated.

The effect of the boundary layer on the panel has always been of some concern. In this testing, the transition from laminar to turbulent boundary layer occurred on the panel. In order to check this effect, identical runs were made with (a) no boundary layer trip, (b) with a trip of No. 220 grit, and (c) with a trip made of a single strand of 0.050" wire running across the nose of the model. It was found that although the No. 220 grit moved the transition point forward on the panel, three-dimensional flutter occurred at precisely the same P_t as with no trip. The 0.050" wire trip was then used to give a greater amount of disturbance and did cause a very thick turbulent boundary layer to be initiated immediately behind the wire. This did have an effect on the panel, delaying flutter until the two-dimensional type occurred at a higher P_t .

1.5. Theoretical Prediction of Three-Dimensional Flutter

Theoretical flutter boundaries for the three-dimensional case will be calculated using Lagrange's equations and linear supersonic aerodynamic theory. Ackeret quasi-static aerodynamic theory will also be used for comparison.

An attempt was made to solve the problem with clamped edge conditions but the aerodynamic forces became very involved algebraically. Hence it was decided to use simply-supported edge conditions, and to concentrate attention on the differences between two-dimensional and three-dimensional flutter for the simply-supported case as shown schematically in figure 14. The vertical displacement $w(x, z, t)$ is positive in the upward direction.

From Fastax pictures taken during the flutter tests, it was observed that there was a nodal line down the center of the panel at

$z = \frac{\ell_2}{2}$. For an approximate solution, the deflection will be taken as

$$w(x, z, t) = \sum_{n=1}^N a_n(t) f_n(x) g(z), \quad (1)$$

where

$$f_n(x) = \sin \frac{n\pi x}{\ell_1} \quad 0 \leq x \leq \ell_1$$

and

$$g(z) = \left[1 - \frac{2z}{\ell_2} \right] \quad 0 \leq z \leq \ell_2.$$

These functions do not satisfy the plate free-edge boundary conditions at $z = 0$ and $z = \ell_2$, but they do satisfy the simply-supported edge conditions at $x = 0$ and $x = \ell_1$.

The kinetic energy of the plate is

$$\begin{aligned} T(t) &= \frac{1}{2} \int_0^{\ell_2} \int_0^{\ell_1} \rho_s h \left[\frac{\partial w}{\partial t}(x, z, t) \right]^2 dx dz \\ &= \frac{1}{2} \rho_s h \frac{\ell_1 \ell_2}{6} \sum_{n=1}^N \dot{a}_n^2(t). \end{aligned}$$

From small deflection plate theory (Ref. 10), the potential energy is

$$\begin{aligned} V &= \frac{1}{2} D \int_0^{\ell_2} \int_0^{\ell_1} \left\{ \left(\frac{\partial^2 w}{\partial x^2} + \frac{\partial^2 w}{\partial z^2} \right)^2 - 2(1-\nu) \left[\frac{\partial^2 w}{\partial x^2} \frac{\partial^2 w}{\partial z^2} - \left(\frac{\partial^2 w}{\partial x \partial z} \right)^2 \right] \right\} dx dz \\ &= \frac{1}{2} D \sum_{n=1}^N \left[\frac{\ell_1 \ell_2}{6} \left(\frac{n\pi}{\ell_1} \right)^4 + 4(1-\nu) \left(\frac{\ell_1}{\ell_2} \right) \left(\frac{n\pi}{\ell_1} \right)^2 \right] a_n^2. \end{aligned}$$

The generalized forces are

$$\begin{aligned}
 Q_m &= - \int_0^{\ell_1} \int_0^{\ell_2} \bar{p}(x, z, t) \frac{\partial w(x, z, t)}{\partial a_m} dx dz \\
 &= - \int_0^{\ell_2} \int_0^{\ell_1} \bar{p}(x, z, t) \sin \frac{m\pi x}{\ell_1} g(z) dx dz \quad .
 \end{aligned} \tag{2}$$

Using Lagrange's equations

$$\frac{d}{dt} \frac{\partial L}{\partial \dot{a}_m} - \frac{\partial L}{\partial a_m} = Q_m \quad m = 1, 2, \dots, N$$

where

$$L = T - V,$$

we obtain

$$c_s h \frac{\ell_1 \ell_2}{6} \ddot{a}_m + D \left[\left(\frac{m\pi}{\ell_1} \right)^4 \frac{\ell_1 \ell_2}{6} + 4(1-\nu) \left(\frac{m\pi}{\ell_1} \right)^2 \left(\frac{\ell_1}{\ell_2} \right) \right] a_m = - \int_0^{\ell_2} \int_0^{\ell_1} \bar{p}(x, z, t) \sin \frac{m\pi x}{L} g(z) dx dz$$

$$(m = 1, 2, \dots, N) \quad .$$

Assuming that $a_m(t) \sim e^{i\omega t}$, where ω may be complex, we have

$$\left\{ D \left[\left(\frac{m\pi}{\ell_1} \right)^4 \frac{\ell_1 \ell_2}{6} + 4(1-\nu) \left(\frac{m\pi}{\ell_1} \right)^2 \left(\frac{\ell_1}{\ell_2} \right) \right] - c_s h \omega^2 \frac{\ell_1 \ell_2}{6} \right\} a_m = - \int_0^{\ell_2} \int_0^{\ell_1} \bar{p}(x, z, t) \sin \frac{m\pi x}{L} g(z) dx dz \tag{3}$$

$$(m = 1, 2, \dots, N) \quad .$$

We will first solve the set of equations 3 using Ackeret quasi-static theory for the aerodynamic pressure, just to get a feeling for the problem. The pressure is

$$\bar{p}(x, z, t) = \frac{\gamma_p M^2}{\beta} \frac{\partial w}{\partial x}(x, z, t) .$$

This will give no three-dimensional aerodynamic effects; however, as shown for two-dimensional flutter, Ackeret theory can give good results at the relatively low frequencies and high Mach numbers we are considering. The set of equations 3 become

$$\left[(m\pi)^4 + 24(1-\nu) \left(\frac{\ell_1}{\ell_2} \right)^2 (m\pi)^2 - \lambda \right] a_m + 32 w_3 \sum_{n=1}^N \eta_{mn} a_n = 0 \quad (m = 1, 2, \dots, N), \quad (4)$$

where

$$\lambda = \frac{e_s h \omega^2 \ell_1^4}{D}$$

$$w_3 = \frac{\gamma_p M^2 \ell_1^3}{8 \beta D}$$

$$\eta_{mn} = \begin{cases} 0 & \text{when } m+n = \text{even} \\ \frac{nm}{m^2 - n^2} & \text{when } m+n = \text{odd} \end{cases}$$

For the panels which were tested, $\left(\frac{\ell_1}{\ell_2} \right) = 0.8555$ and $\nu = 0.3$.

Equations 4 are a set of linear homogeneous algebraic equations. For a nontrivial solution for the a_n to exist, the determinant of the

coefficients of a_n must vanish. This leads to an eigenvalue problem of the form

$$\text{Det}(P - \lambda I) = 0$$

where P is a real matrix.

Experience with the case of two-dimensional flutter of flat panels has shown that a four-mode solution yields an eigenvalue only 1 per cent different from the exact value. Hence, a four-mode solution ($N = 4$) was carried out for this case. The Burroughs 220 digital computer was used.

It was found that for low values of the dynamic pressure parameter w_3 , the eigenvalues λ are real. As w_3 is raised, a critical value is obtained where a pair of conjugate complex eigenvalues appear, indicating flutter. Three-dimensional flutter occurs at

$$w_3 = 55.1$$

This compares with the two-dimensional flutter boundary (obtained using Ackeret theory) at $w_3 = 42.9$. The use of Ackeret theory hence provides no insight as to why the experimental three-dimensional flutter occurred at a lower value of w_3 than the two-dimensional flutter.

Let us now devote our attention to a solution of the flutter equations 4 using linearized supersonic aerodynamics. Any realistic study of this flutter should include a three-dimensional aerodynamic theory because the panel's aspect ratio is so small that most of the panel lies in the tip Mach cones. The basic ideas for potential supersonic flow over an oscillating thin wing were set down by Garrick and Rubinow (Ref. 11). Luke and St. John (Ref. 12) developed the forces on a panel

of finite span and infinite chord oscillating in a periodic spanwise displacement. We will use the work of Luke and St. John and hence incur all of the assumptions of linearized potential flow theory, i. e. that the fluid is inviscid and irrotational, and that disturbances at the panel are very small.

The upper and lower walls of the test section were sufficiently far from the model that no reflected waves hit it. However, the side walls do affect the panel. We will assume that they prevent cross flow at the edges of the panel. If, for the solution of the velocity potential, the panel is assumed to be extended outside the tunnel as shown in figure 15, the symmetry is such that this wall condition is satisfied (as in the method of images for subsonic flow). This leads naturally to the use of a superposition of solutions for sinusoidal $g(z)$ as developed by Luke and St. John.

Let us define one period of $g(z)$ as

$$g(z) = \begin{cases} 1 - \frac{2z}{l_2} & 0 \leq z \leq l_2 \\ 1 + \frac{2z}{l_2} & -l_2 \leq z < 0 \end{cases} \quad (5)$$

We then have the Fourier cosine series

$$g(z) = \frac{8}{\pi^2} \sum_{\bar{n}=1,3,5}^{\infty} \frac{1}{\bar{n}^2} \cos \frac{\bar{n}\pi z}{l_2} \quad .$$

Because of the complexity of the aerodynamic forces and because of the very rapid convergence of this series, only two terms are retained. The two term representation of $g(z)$ is shown in figure 16, and it appears satisfactory for our purposes. The set of equations 3 become

$$\left\{ D \left[\left(\frac{m\pi}{\ell_1} \right)^4 \frac{\ell_1 \ell_2}{6} + 4(1-\nu) \left(\frac{m\pi}{\ell_1} \right)^2 \left(\frac{\ell_1}{\ell_2} \right) \right] - \rho_s h \omega^2 \frac{\ell_1 \ell_2}{6} \right\} a_m = - \frac{8}{\pi^2} \int_0^{\ell_2} \int_0^{\ell_1} \bar{p}(x, z, t) \sin \frac{m\pi x}{L} \left[\cos \frac{\pi z}{\ell_2} + \frac{1}{9} \cos \frac{3\pi z}{\ell_2} \right] dx dz \quad (6)$$

$$(m = 1, 2, \dots, N) .$$

Luke and St. John's work shows that for $g(z) = \cos \frac{\bar{n}\pi z}{L}$ the pressure on the surface is of the form

$$\bar{p}(x, z, t) = \bar{p}_{\bar{n}}(x) \cos \frac{\bar{n}\pi z}{L} e^{i\omega t} .$$

Furthermore, because the problem is linear, for $g(z) =$

$$\frac{8}{\pi^2} \left[\cos \frac{\pi z}{\ell_2} + \frac{1}{9} \cos \frac{3\pi z}{\ell_2} \right], \text{ we have}$$

$$\bar{p}(x, z, t) = \frac{8}{\pi^2} \left[\bar{p}_1(x) \cos \frac{\pi z}{\ell_2} + \frac{1}{9} \bar{p}_3(x) \cos \frac{3\pi z}{\ell_2} \right] e^{i\omega t} .$$

The z dependence in the set of equations 6 can be integrated out to give

$$\left\{ D \left[\left(\frac{m\pi}{\ell_1} \right)^4 \frac{\ell_1 \ell_2}{6} + 4(1-\nu) \left(\frac{m\pi}{\ell_1} \right)^2 \left(\frac{\ell_1}{\ell_2} \right) \right] - \rho_s h \omega^2 \frac{\ell_1 \ell_2}{6} \right\} a_m = - \frac{32 \ell_2}{\pi^4} e^{i\omega t} \int_0^{\ell_1} \left[\bar{p}_1(x) + \frac{1}{81} \bar{p}_3(x) \right] \sin \frac{m\pi x}{L} dx \quad (7)$$

$$(m = 1, 2, \dots, N) .$$

The expression $\int_0^{\ell_1} \bar{p}_n(x, t) \sin \frac{m\pi x}{L} dx$ can be found in reference 9.

It is a little difficult to extract from this work, being involved in a Galerkin process and because of the use of non-dimensional coordinates.

However, one can arrive at the result that, for a displacement

$$w(x, z, t) = \sum_{n=1}^N a_n(t) \sin \frac{m\pi x}{\ell_1} \cos \frac{n\pi z}{\ell_2}.$$

$$\int_0^{\ell_1} \bar{p}_n(x) \sin \frac{m\pi x}{\ell_1} dx = \sum_{n=1}^N \frac{4D}{\ell_1^2} w_3 \left[\left(A_n + i \frac{k}{2} \frac{M^2 - 2}{\beta^2} \right) \bar{\delta}_{mn} + \left(\frac{n\pi}{2} - F_{n\bar{n}} \right) \bar{E}_{mn} - e^{-2J} (-i)^m (B_{mn\bar{n}} + C_{mn\bar{n}}) - D_{mn\bar{n}} \right] \frac{a_n}{(\ell_2/2)} \quad (8)$$

where

$$w_3 = \frac{\tau_p M^2 \ell_1^3}{8D\beta}$$

and

$$k = \frac{\omega L}{U}.$$

The remaining constants are defined in the Appendix.

The set of equations 7 become

$$\begin{aligned} \sum_{n=1}^N \left\{ \left[(n\pi)^4 + 24(1-\nu) \left(\frac{\ell_1}{\ell_2} \right)^2 (n\pi)^2 - \lambda + \frac{41}{81} i k \left(\frac{m^2 - 2}{\beta^2} \right) w_3 + \frac{1536}{\pi^4} w_3 \left(A_n + \frac{1}{81} A_{n3} \right) \right] \bar{\delta}_{mn} \right. \\ \left. + \frac{1536}{\pi^4} w_3 \left[\left(\frac{41}{81} n\pi - F_{n1} - \frac{1}{81} F_{n3} \right) \bar{E}_{mn} - (-i)^m e^{-2J} (B_{mn1} + \frac{1}{81} B_{mn3} + C_{mn1} + C_{mn3}) \right. \right. \\ \left. \left. - (D_{mn1} + \frac{1}{81} D_{mn3}) \right] \right\} a_n = 0 \end{aligned} \quad (9)$$

$$(m = 1, 2, \dots, N),$$

where

$$\lambda = e_s h \omega^2 \frac{\ell_1^4}{D} .$$

Again we have a system of homogeneous linear algebraic equations which can be cast into an eigenvalue problem with eigenvalue λ . The problem is of the form

$$\text{Det} (P - \lambda I) = 0 ,$$

where the complex matrix P is a function of M , k , w_3 , $\frac{\ell_1}{\ell_2}$, and ν .

A four-mode solution was carried out on the IBM 7090 digital computer for

$$\begin{aligned} M &= 2.81 \\ \frac{\ell_1}{\ell_2} &= 0.855 \\ \nu &= 0.3 \end{aligned}$$

In order to find neutrally stable solutions, i. e. where ω (and hence λ) is real, the following procedure is used. Values of k and w_3 are assumed and the eigenvalues λ are calculated. In general, the λ are complex, so w_3 is raised until a real λ is found. This yields a point on the flutter boundary which has values of k , w_3 , and λ associated with it. The results are shown in figure 17. It is interesting that for $k < 0.3$ there is little variation in λ and w_3 . Flutter occurs at $w_3 = 54.8 \pm 0.2$ over the range $0 < k < 0.3$.

For panels of the type used in the wind tunnel tests, we have

$$E = 15.0 \times 10^6 \text{ psi}$$

$$\rho_s = 0.0007971 \frac{\text{lb} \cdot \text{sec}^2}{\text{in}^4}$$

$$T = 210^\circ \text{ R}$$

$$\gamma = 1.4$$

The values of $\left(\frac{h}{\ell_1}\right)$ and p at flutter for this special case can be found by using the definitions of λ and w_3 . We have

$$\left(\frac{h}{\ell_1}\right) = \sqrt{\frac{\rho_s U^2}{E} \frac{1}{12(1-\nu^2)} \frac{k^2}{\lambda}}$$

$$p = \frac{8E\beta}{\gamma M^2} \left(\frac{h}{\ell_1}\right)^3 \frac{w_3}{12(1-\nu^2)}$$

Values of $\left(\frac{h}{\ell_1}\right)$ and p are calculated for each point on the flutter boundary with the results shown in figure 18. Even at sea level pressures, flutter occurs at $k < 0.32$.

The test panel which exhibited three-dimensional flutter in the wind tunnel had a value of $\left(\frac{h}{\ell_1}\right) = 0.00163$. A simply-supported panel of this thickness ratio would flutter at $k = 0.10$ and $w_3 = 54.65$.

We can now compare our results:

- | | | |
|----------------------|--------------------------|---------------|
| a) Two-dimensional | Ackeret theory | $w_3 = 42.9$ |
| b) Three-dimensional | Ackeret theory | $w_3 = 55.1$ |
| c) Three-dimensional | linear supersonic theory | $w_3 = 54.65$ |

These theoretical values are all for simply-supported ends. Flutter was found experimentally at $w \approx 39.0$.

When case a) is also worked out using Lagrange's equations (not included in this work), it is found that the basic difference between a) and b) is the twisting energy involved in the three-dimensional flutter. This is seen to raise the flutter boundary. The difference between b) and c) lies only in the aerodynamics. Linear supersonic theory lowers the three-dimensional flutter boundary only slightly compared with Ackeret theory.

We have not explained the occurrence of three-dimensional flutter at a lower dynamic pressure than two-dimensional flutter. This happened for only one of the three panels tested. It is possible that some imperfection in this panel assembly, coupled with unknown cavity and wall effects, made this panel more susceptible to rocking flutter.

1.6. Conclusions and Discussion of Results

The thickness ratio required to prevent two-dimensional flutter of flat, unstressed panels at Mach number 2.81 was found by experiment to be 15 per cent higher than the prediction of Houbolt's theory. The phase lag of the panels during two-dimensional flutter agreed fairly well with this theory. No coalescence of frequencies was observed, however.

A three-dimensional type of flutter occurred on one of the panels. The theory which was developed for this type of flutter indicates that it can appear only at dynamic pressures 28 per cent higher than that needed to precipitate two-dimensional flutter.

The differences between experiment and theory might have been due to a) imperfectly clamped end conditions b) the slight initial curvature in the panels c) the small static pressure differential between cavity and free stream, or d) the complicated flow conditions

at the edges of the panel. The clamping support at the ends was relatively rigid, however, as shown by the agreement between the two-dimensional natural frequencies and the theoretical results of Warburton (Ref. 14). The initial curvature might have had an effect similar to the initial curvature which is studied in section 2 and is shown to be destabilizing. The effect of a small static pressure differential was studied by Lock and Fung (Ref. 5) for the case of a two-dimensional panel with a different type of flexure than that used here. They found that small pressure differentials had little effect on the flutter boundaries. The flexure support relieved the membrane stress which would ordinarily have been induced by the loading. Because the pressure differential was small during the current tests, the effect was probably small, also. The flow conditions at the edge of the panel present an unknown factor in the experiments. The interaction between boundary layer, model cavity and moving panel edge is difficult to analyze. It is possible that these edge conditions were responsible for the appearance of the three-dimensional flutter at a low dynamic pressure.

2. Slightly Curved Panels

The second series of wind tunnel tests dealt with the flutter of initially curved panels. The panels were unstressed, very shallow, and of aspect ratio one.

The purpose of the tests was to find the effect of curvature on flutter boundaries, flutter modes and frequency coalescence. Data were also taken on the effect of pressurizing the cavity under the panel.

Some interesting theoretical results have been given for slightly curved panels by Yates and Zeijdel (Ref. 13). Using linear shallow shell theory and quasi-steady aerodynamics, they find that certain values of curvature are very destabilizing. A typical flutter boundary is shown in figure 23. It was not possible to obtain experimental data in the same form as presented in this figure, so comparison with this theory is difficult.

2.1. Description of Model

The model (figures 19, 21, and 22) was almost identical to the one used for flat panels. Again, the design was such that no reflected shock waves would hit the panel or model.

Four panel curvatures were tested. If we define w_0 as the deflection at the center of the panel and L as the length of the panel, the four curvatures were $\frac{w_0}{L} = 0$ (nominally flat), 0.007, 0.013, and 0.020. It was felt that $\frac{w_0}{L} = 0.007$ was the smallest nonzero curvature that could be manufactured with precision. Each of the panels had an unsupported length of 9", an unsupported width of 9" and a thickness of approximately 0.008".

Because the panels were to be firmly attached to a supporting frame, all materials had to be identical to prevent trouble with thermal expansion. It was decided to use spring cartridge brass for the panels; therefore half-hard cartridge brass was used for the rest of the model.

The square frames used to support the panels (figure 20) were built up from bar stock. They were machined into the proper radii of curvature by a contour milling process. In addition, solid blocks of aluminum were machined into female molds of the same radii as the frames. These blocks served as forms for shaping the flat sheet.

The panels were attached to the frames by an oven soldering process. They were pretinned around the edges by electroplating solder onto the surface. Then they were placed in the female molds and held to the curvature by a small quantity of steel shot. A coating of solder 0.005" thick was built up on the frames by heating them in an oven and flowing the solder onto the hot surface. After cooling, the frames were placed over the panels and the assembly was baked in an oven for several hours at 450° F. A good joint was obtained.

The cavity under the panel was made air tight for the tests merely by sealing around the edges of the panel with wind tunnel wax. The pressure differential ΔP was controlled during the tests with the use of a vacuum pump.

The natural frequencies of the four panels were studied on the bench. In order to check the effect of the model cavity, the panel assemblies were tested while installed in the model and also out in open air. The model cavity was not made air tight for this testing. It was found that the cavity had no significant effect on any of the natural frequencies except those of the simplest mode for each panel (the mode with nodal lines around the edges of the panel only). This frequency could not be found when the panel assembly was installed in the model. The results of the vibration tests are presented in Table III. The frequencies listed were taken with the panel assembly resting in the model cavity, except those given for the simplest mode of each panel. These were taken with the panel assembly out in open air.

Some simple calculations were done in order to clear up the effect of the cavity on the panel. This work is presented in section 2.5.

It is shown that cavity under the panel can greatly increase the simplest frequency. The higher modes are not affected as much.

It is desirable to have some theoretical frequencies to compare with the experimental values given in Table III. These can be calculated from the work in section 2.5. Table IV lists the frequencies for the curved panels under the assumption of freely-supported edges and no cavity effect. Because of the freely-supported edge conditions, these theoretical frequencies are all somewhat lower than the experimental values.

The vibration tests for the curved panels were done before the full significance of the cavity effect was known. The panels were disassembled before a full experimental study of the effect of a sealed cavity could be carried out.

2.2. Instrumentation

The instrumentation was identical to that used for the flat panel tests. Because the pickups were located slightly closer to each other than in the flat panel model, a slight "beat" due to interference was noticed in the pickup signal. This noise was only several millivolts rms and was eliminated by the use of small brass shields around the pickups (see figure 22).

2.3. Test Procedure

The test procedure was similar to that for flat panels; however, there were no stops to adjust or droop to measure in this case. The static pressure differential ΔP had to be monitored continuously. A tolerance of ± 0.001 psi was allowed for all ΔP settings.

2.4. Experimental Results

Each of the four panels fluttered. The flutter points are given in Table V. Curves of the panel response at the center pickup are given in figures 24 and 25. In general, the panels were almost motionless up to the flutter boundary, where large amplitude flutter occurred. This was not true for the one flat panel tested, however. The designation of a flutter boundary was somewhat arbitrary for this panel. It was decided to define flutter as motion for which the deflection at the center of the panel had an rms value equal to the thickness of the plate.

The flutter for these curved panels was much more violent than the flutter of the flat panels. Also, when panels 3 and 4 were internally pressurized to $\Delta P = 0.050$ psi, the static airloads became sufficiently high before flutter occurred to cause a static deflection. The front surface of the panel was pushed in and to the rear, while the back part of the panel was drawn outward toward the airstream.

As P_t was lowered, it was noticed that there was a tendency for the flutter to persist at slightly lower values of P_t than at which it had started. No data were taken on this phenomenon. All results given here were taken as P_t was being raised.

The flutter boundaries are shown in figures 26 and 27. The initial curvature is destabilizing. Even a slight amount of initial curvature has a significant effect. There appears to be little difference caused by the increase in curvature from $\frac{w^0}{L} = 0.013$ to $\frac{w^0}{L} = 0.020$. This is particularly evident in figure 27. The internal pressurization is stabilizing and appears to have a similar effect on each of the panels (i. e., the slopes of the curves in figure 27 are approximately the same).

Because of the large number of closely spaced frequencies, it was found almost impossible to follow the resonant frequencies of the curved panels. The magnetic excitation system did not work well and the harmonic analysis of turbulence response was difficult to interpret. These two methods complement each other and both are needed to gather any significant frequency data. None will be presented.

Phase angle data were obtained for panels 1, 3, and 4. Figure 28 shows the phase lag $\psi(x)$ for these panels just after the initiation of flutter. The panels with greater curvature have a greater amount of phase lag. Figures 29 through 31 give the remainder of the phase lag data which was taken at higher values of P_t than at the flutter boundary. Here it is seen that raising P_t (and hence raising the flutter frequency) lowers the amount of phase lag for panels 3 and 4. During the run of panel 2 ($\frac{w_o}{L} = 0.007$), one of the pickup lines was cut and all phase angle data were lost for that panel.

The use of spring brass for the panel material was fortunate. The panels were violently fluttered for hours without any noticeable damage.

2.5. Theoretical Effect of the Cavity

A simple calculation can be carried out to determine the effect of the closed cavity on the natural frequencies of the curved panels. Consider the case where the edges of the panel are "freely-supported". The cylindrical coordinate system is shown in figure 32. The angular variable is θ and the circular panel covers an arc of angle ϕ .

Because of the relatively low frequency of panel vibration and the small size of the cavity, it can be assumed that the air trapped in

the cavity is in equilibrium at all times. The cavity volume and pressure when the panel is undeflected will be called V_0 and p_0 , respectively. After the panel has deflected to a position $w(x, \theta, t)$, these quantities will be denoted by $V_0 + \Delta V$ and $p_0 + \bar{p}$ (see figure 33). Let us assume that the thermodynamic process which takes place in the air is adiabatic and reversible. The pressures for the undeflected and the deflected panel are then related by

$$p_0 V_0^\gamma = (p_0 + \bar{p})(V_0 + \Delta V)^\gamma \quad (10)$$

For infinitesimal vibrations,

$$\left| \frac{\Delta V}{V_0} \right| \ll 1.$$

The right hand side of equation 10 can be expanded to give

$$\bar{p} = - \frac{\gamma p_0 \Delta V}{V_0} + O \left(\left(\frac{\Delta V}{V_0} \right)^2 \right) \quad (11)$$

It can be shown that for $\left| \frac{w(x, \theta, t)}{R} \right| \ll 1$, the change in volume is given by

$$\Delta V = \int_0^L \int_0^\phi w(x, \theta, t) R \, d\theta \, dx.$$

Retaining only the linear term in equation 11, we have

$$\bar{p}(t) = - \frac{\tau p_0}{V_0} \int_0^L \int_0^\phi w(x, \theta, t) R \, d\theta \, dx . \quad (12)$$

The equation of motion which will be used for the shell is the modified Donnell equation, which is particularly useful for this type of loading. (See reference 15 for a discussion of this equation.) The deflection pattern of this shell segment corresponds to that of a cylinder with many circumferential waves. Therefore, the use of a Donnell type of equation is justified.

$$D \nabla^4 w + \frac{Eh}{R^2} \nabla^{-4} \frac{\partial^4 w}{\partial x^4} + \rho h \frac{\partial^2 w}{\partial t^2} - \bar{p}(t) = 0 . \quad (13)$$

The symbol ∇^{-4} is defined by $\nabla^{-4} \nabla^4 f(x, \theta, t) = f(x, \theta, t)$. The boundary conditions on $w(x, \theta, t)$ are

$$w(0, \theta, t) = w(l_2, \theta, t) = \frac{\partial^2 w}{\partial x^2}(0, \theta, t) = \frac{\partial^2 w}{\partial x^2}(l_2, \theta, t) = 0$$

$$w(x, 0, t) = w(x, \phi, t) = \frac{\partial^2 w}{\partial \theta^2}(x, 0, t) = \frac{\partial^2 w}{\partial \theta^2}(x, \phi, t) = 0 .$$

Consider a vibration mode of the form

$$w(x, \theta, t) = e^{i\omega t} \sin \frac{m\pi x}{l_2} \sin \frac{n\pi \theta}{\phi} .$$

This deflection satisfies the boundary conditions. If either m or n is even, the pressure $\bar{p}(t) = 0$ and there is no cavity effect. In this case, $w(x, \theta, t)$ satisfies equation 13 and is an eigenfunction of the problem. However, when m and n are both odd, there is a cavity effect.

If a general displacement of the form

$$w(x, \theta, t) = e^{i\omega t} \sin \frac{m\pi x}{l_2} \sum_{n=1}^N a_n \sin \frac{n\pi \theta}{\Phi} \quad (14)$$

is assumed, an approximate solution for the natural frequencies can be obtained by using Galerkin's method. The following set of equations results:

$$\sum_{n=1}^N a_n \left[\left[\left(\frac{n l_2}{R \Phi} \right)^2 + m^2 \right]^2 \pi^4 + 12(1-\nu^2) \left(\frac{l_2}{R} \right)^4 \left(\frac{R}{h} \right)^2 \frac{m^4}{\left[\left(\frac{n l_2}{R \Phi} \right)^2 + m^2 \right]^2} - \lambda_1 \right] \delta_{np} \quad (15)$$

$$+ \frac{768 \pi (1-\nu^2)}{\pi^4 m^2 n p} \left(\frac{p_0}{E} \right) \left(\frac{l_2}{h} \right)^3 \frac{l_2^2 R \Phi}{V_0} \mu_{mnp} \Bigg] = 0 \quad (p = 1, 2, \dots, N)$$

where

$$\lambda_1 = \frac{e_s h \omega^2 l_2^4}{D}$$

$$\mu_{mnp} = \begin{cases} 1 & \text{if } m, n, \text{ and } p \text{ are all even} \\ 0 & \text{if } m, n, \text{ or } p \text{ is odd} \end{cases}$$

For a shallow shell, we may assume that $R\phi = l_1$. Equation 15 then reduces to

$$\sum_{n=1}^N a_n \left[\left\{ \left[\left(\frac{n l_2}{l_1} \right)^2 + m^2 \right]^2 \pi^4 + 12(1-\nu^2) \left(\frac{l_2}{R} \right)^4 \left(\frac{R}{h} \right)^2 \frac{m^4}{\left[\left(\frac{n l_2}{l_1} \right)^2 + m^2 \right]^2} - \lambda_1 \right\} \delta_{np} \right. \\ \left. + \frac{768 \pi (1-\nu^2)}{\pi^4 m^2 n p} \frac{p_0}{E} \left(\frac{l_2}{h} \right)^3 \left(\frac{l_2^2 l_1}{V_0} \right) \mu_{mnp} \right] = 0 \quad (p = 1, 2, \dots, N) \quad (16)$$

The condition for existence of a nontrivial displacement is that the determinant of the coefficients must vanish.

A two-mode solution was carried out using the modes $m = 1$, $n = 1$, and $m = 1$, $n = 3$. The following average values, corresponding to the test panels, were used:

$$\frac{l_1}{l_2} = 1$$

$$V_0 = 48.6 \text{ in}^3$$

$$E = 15 \times 10^6 \text{ psi}$$

$$\nu = 0.3$$

$$\tau = 1.4$$

$$h = 0.008 \text{ inch}$$

The results are shown in figures 34 and 35. Curves are drawn for $p_0 = 1$ atmosphere (corresponding to the bench tests) and $p_0 = 1/20$

atmosphere. All of the wind tunnel tests were run at $p_0 < 1/20$ atmosphere. It is apparent that the closed cavity greatly increases the frequency of the simplest mode, especially for panels with small curvature. The effect on the mode for $m = 1, n = 3$ is much smaller.

The mode $m = 3, n = 1$ and higher modes could be investigated for cavity effect; however, it can be seen from the set of equations 15 that the cavity term becomes smaller compared to the bending and stretching terms for these modes.

It can be concluded that the simplest mode is greatly affected by the cavity, higher odd modes are affected only slightly and higher even modes are not affected at all. The important parameters for the cavity effect are the cavity static pressure and volume. The force which results from the presence of the cavity varies as $\frac{p_0}{V_0}$. If it is desired to reduce the cavity effect, then it is necessary to use a large volume under the test panel. The pressure p_0 usually must be adjusted to closely match the free stream static pressure of the wind tunnel (to avoid a large static pressure differential across the panel) and so it can not be reduced for the purpose of minimizing the cavity effect.

No flutter calculations were carried out using the simple cavity theory developed here. It might be expected, however, that the presence of the closed cavity would tend to stabilize a panel. This is because the pressure loading acts as a restoring spring force.

Tuovila and Presnell (Ref. 6) experimentally investigated the effect of changing the cavity size in a series of flat panel tests. They tested fiber-glass sandwich panels with foamed cores in the Mach

number range of 1.76 to 2.87. Three cavity depths were tried for a series of flat panels which were approximately 20" wide and 33" long. A 1/2" deep cavity was found to give a critical flutter dynamic pressure 40 per cent lower than that obtained with a 1 1/2" deep cavity. On the other hand, when the cavity depth was reduced to zero (with the panel touching the cavity bottom), no flutter was found.

The theory discussed above does not explain the decrease in critical dynamic pressure found by Tuovila and Presnell as their cavity depth decreased from 1 1/2" to 1/2". However, the assumption that the air in the cavity is in equilibrium is not valid if the chamber size is large enough for resonance phenomena to occur.

2.6. Conclusions for Curved Panels

The curved panels exhibited large amplitude flutter, the amplitude of which was of the order of the arch rise w_0/L . Several of the panels deflected visibly under the static airloads before flutter occurred. It was found that small amounts of initial curvature were destabilizing and that internal pressurization was stabilizing.

It was also found that the closed cavity under the panel can affect the natural frequencies of the panel, particularly that of the simplest mode. An expression was developed for the pressure in the cavity which can be easily included in flutter calculations. Enlarging the cavity size appears to be a way of reducing the effect of the cavity. The model used in the present tests was limited in size because of the possibility of blocking the flow in the wind tunnel. Because of the very low static pressure in the cavity during the tests, the three curved panels were probably not greatly affected; however, the flat panel with a closed cavity may have been stabilized somewhat.

The panels which were tested were very shallow, but it would be desirable to test even shallower panels. It will take extreme care to make shallower panels because of the close tolerances required.

REFERENCES

1. Easley, J. G.: The Flutter of a Two-Dimensional Buckled Plate with Clamped Edges in Supersonic Flow, Air Force Office of Scientific Research TN 56-296, California Institute of Technology, (July 1956).
2. Sylvester, M. A.: Experimental Studies of Buckled Rectangular Panels at Mach Numbers from 1.2 to 3.0 including Effects of Pressure Differential and of Panel Width-Length Ratio. NASA TN D-833 (May 1961).
3. Greenspan, J. E. and Goldman, R. L.: Flutter of Thin Panels at Subsonic and Supersonic Speeds. Air Force Office of Scientific Research TR 57-65, The Martin Company, Baltimore (1957).
4. Sylvester, M. A. and Baker, J. E.: Some Experimental Studies of Panel Flutter at Mach Number 1.3. NACA TN 3914 (February 1957).
5. Lock, M. H. and Fung, Y. C.: Comparative Experimental and Theoretical Studies of the Flutter of Flat Panels in a Low Supersonic Flow. Air Force Office of Scientific Research TN 670, California Institute of Technology (May 1961).
6. Tuovila, W. J. and Presnell, John C.: Supersonic Panel Flutter Test Results for Flat Fiber Glass Sandwich Panels with Foamed Cores. NASA TN D-827 (June 1961).
7. Fung, Y. C.: A Summary of the Theories and Experiments on Panel Flutter. Air Force Office of Scientific Research TN 60-224, California Institute of Technology (May 1960).
8. Houbolt, J. C.: A Study of Several Aerothermoelastic Problems of Aircraft Structures in High Speed Flight. Doctoral Thesis, E. T. H., Zurich (1958).
9. Movchan, A. A.: On Vibrations of a Plate Moving in a Gas. NASA Re-publication 11-22-58W (January 1959).
10. Timoshenko, S.: Theory of Plates and Shells. McGraw-Hill Book Co., Inc., New York, p. 50 (1940).
11. Garrick, I. E. and Rubinow, S. I.: Theoretical Study of Air Forces on an Oscillating or Steady Thin Wing in a Supersonic Main Stream. NACA Report 872 (1947).
12. Luke, Y. L. and St. John, A.: Supersonic Panel Flutter. WADC TR 57-252 (July 1957).

13. Yates, J. E. and Zeijdel, E. F.: Flutter of Curved Panels. Air Force Office of Scientific Research TR 59-163, Midwest Research Institute (September 1959).
14. Warburton, G. B.: The Vibration of Rectangular Plates. Proceedings of the Institution of Mechanical Engineers, Vol. 168, p. 371 (1954).
15. Batdorf, S. B.: A Simplified Method of Elastic-Stability Analysis for Thin Cylindrical Shells. NACA Report No. 874, (1947).

APPENDIX

The following definitions are necessary for the determination of the linear supersonic air forces in section 1.5. They are essentially those defined by Luke and St. John (Ref. 10). The subscripts \bar{n} have been added for clarity.

$$K = \frac{Mk}{2\beta^2}$$

$$\Gamma_{\bar{n}} = \sqrt{K^2 + \left(\frac{2\bar{n}\pi\ell_1}{\ell_2\beta}\right)^2}$$

$$\lambda_{r\bar{n}} = \Gamma_{\bar{n}} \cos \left(\frac{2r-1}{8}\pi\right)$$

$$a_{r\bar{n}} = -\frac{1}{2} \left\{ \left(KM - \frac{K}{2}\right)^2 + \Gamma_{\bar{n}}^2 \cos^2 \left(\frac{2r-1}{8}\pi\right) \right\}$$

$$b_{r\bar{n}} = \frac{i\Gamma_{\bar{n}}K}{\beta^2 2} \cos \left(\frac{2r-1}{8}\pi\right)$$

$$J = iKM$$

$$\epsilon_{rn\bar{n}} = \frac{1}{2} \left\{ \frac{(\lambda_{r\bar{n}} + n\pi/2)}{J^2 + (\lambda_{r\bar{n}} + n\pi/2)^2} - \frac{(\lambda_{r\bar{n}} - n\pi/2)}{J^2 + (\lambda_{r\bar{n}} - n\pi/2)^2} \right\}$$

$$\delta_{rn\bar{n}} = \frac{J}{2} \left\{ \frac{1}{J^2 + (\lambda_{r\bar{n}} + n\pi/2)^2} - \frac{1}{J^2 + (\lambda_{r\bar{n}} - n\pi/2)^2} \right\}$$

$$\eta_{rn\bar{n}} = \frac{J}{2} \left\{ \frac{1}{J^2 + (\lambda_{r\bar{n}} + n\pi/2)^2} + \frac{1}{J^2 + (\lambda_{r\bar{n}} - n\pi/2)^2} \right\}$$

$$\phi_{rn\bar{n}} = \frac{1}{2} \left\{ \frac{(\lambda_{r\bar{n}} + n\pi/2)}{J^2 + (\lambda_{r\bar{n}} + n\pi/2)^2} + \frac{(\lambda_{r\bar{n}} - n\pi/2)}{J^2 + (\lambda_{r\bar{n}} - n\pi/2)^2} \right\}$$

$$A_{n\bar{n}} = \sum_{r=1}^2 (a_{r\bar{n}} \eta_{rn\bar{n}} + b_{r\bar{n}} \phi_{rn\bar{n}})$$

$$F_{n\bar{n}} = \sum_{r=1}^2 (a_{r\bar{n}} \epsilon_{rn\bar{n}} - b_{r\bar{n}} \delta_{rn\bar{n}})$$

$$\bar{\delta}_{mn} = \begin{cases} 0 & m \neq n \\ 1 & m = n \end{cases}$$

$$\bar{\epsilon}_{mn} = \begin{cases} 0 & \text{if } (m+n) \text{ is even} \\ \frac{4m}{\pi(m^2-n^2)} & \text{if } (m+n) \text{ is odd} \end{cases}$$

$$B_{mn\bar{n}} = \sum_{r=1}^2 \left\{ b_{r\bar{n}} (\epsilon_{rm\bar{n}} \epsilon_{rn\bar{n}} - \delta_{rm\bar{n}} \delta_{rn\bar{n}}) + a_{r\bar{n}} (\epsilon_{rm\bar{n}} \delta_{rn\bar{n}} + \epsilon_{rn\bar{n}} \delta_{rm\bar{n}}) \right\} \sin 2\lambda_{r\bar{n}}$$

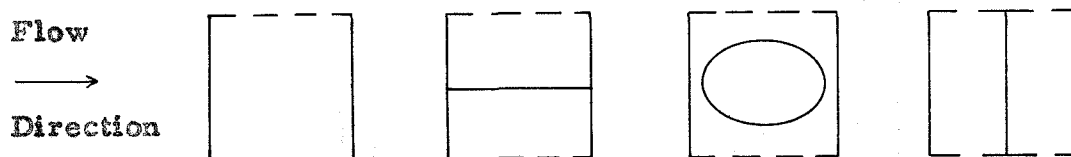
$$C_{mn\bar{n}} = \sum_{r=1}^2 \left\{ a_{r\bar{n}} (\epsilon_{rm\bar{n}} \epsilon_{rn\bar{n}} - \delta_{rm\bar{n}} \delta_{rn\bar{n}}) - b_{r\bar{n}} (\epsilon_{rm\bar{n}} \delta_{rn\bar{n}} + \epsilon_{rn\bar{n}} \delta_{rm\bar{n}}) \right\} \cos 2\lambda_{r\bar{n}}$$

$$D_{mn\bar{n}} = \sum_{r=1}^2 \left\{ -a_{r\bar{n}} (\epsilon_{rm\bar{n}} \epsilon_{rn\bar{n}} - \delta_{rm\bar{n}} \delta_{rn\bar{n}}) + b_{r\bar{n}} (\epsilon_{rm\bar{n}} \delta_{rn\bar{n}} + \epsilon_{rn\bar{n}} \delta_{rm\bar{n}}) \right\}$$

Two terms have been taken in the Bessel function expansion used by Luke and St. John (i. e. $q = 2$ in their notation). This is consistent with our use of $\bar{n} = 1, 3$ and does not introduce much error. Taking another term in the expansion (setting $q = 3$) would have increased the amount of work greatly.

TABLE I

NATURAL FREQUENCIES OF FLAT PANELS MOUNTED IN MODEL
(NO FLOW)



Panel No. 1, 0.0151"

Exper.	25.9 cps	40.6 cps	67.5 cps	69.0 cps
Theor.	26.2 cps	29.7 cps	---	71.9 cps

Panel No. 2, 0.0153"

Exper.	31.0 cps	44.2 cps	77.0 cps	72.4 cps
Theor.	26.5 cps	30.1 cps	---	72.7 cps

Panel No. 3, 0.0193"

Exper.	27.5 cps	39.0 cps	66.0 cps	87.0 cps
Theor.	32.9 cps	37.4 cps	---	90.0 cps

Flexure stiffnesses: No. 1 : 3,410 lb/in

No. 2 : 3,410 lb/in

No. 3 : 6,000 lb/in

The theoretical values are taken from Warburton (Ref. 14).

TABLE II

EXPERIMENTAL FLUTTER POINTS FOR FLAT PANELS

Panel Thickness in.	Type of Flutter	P_t cm Hg	p psi	T $^{\circ}R$	f cps	$\frac{A}{\pi}$	Comments
0.0151	3-D	60.0	0.421	204	30.5	2.84	
0.0151	3-D	64.0	0.449	211	41.6	3.04	
0.0151	3-D	71.0	0.498	210	44.0	3.37	
0.0151	3-D	59.0	0.414	210	39.0	2.80	
0.0151	3-D	60.0	0.421	210	42.0	2.84	Grit B. L. Trip
0.0151	2-D	100.0	0.702	210	89.0	4.74	Wire B. L. Trip
0.0153	2-D	86.2	0.605	211	64.5	3.93	
0.0153	2-D	95.0	0.667	211	63.5	4.33	
0.0190	2-D	252.0	1.769	226	117.0	6.00	$\Delta P = -0.07$ psi

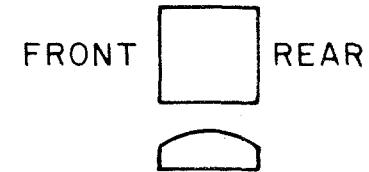
The values of p are calculated from P_t using isentropic flow relations.

TABLE III

NATURAL FREQUENCIES OF CURVED PANELS. BENCH TEST.

PANEL

ORIENTATION:



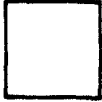
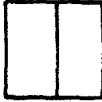
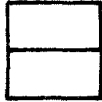
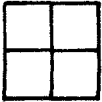
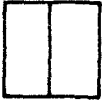
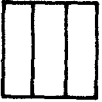
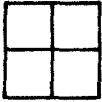
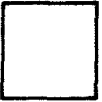
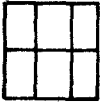
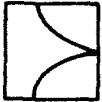

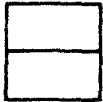
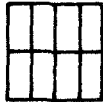



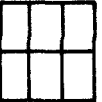
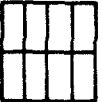
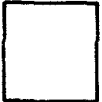
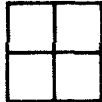
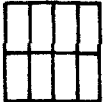
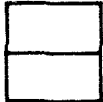

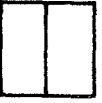
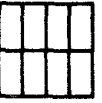
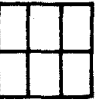



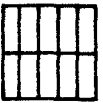
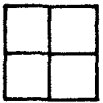
1									
	37.0	45.3	59.2	88.6					
2									
	49.2	76.8	86.2	88.4	116	121	127	130	155
3									
	85	96	136	148	152	157	196	202	210
4									
	113	115	172	182	208	209	232	240	257

TABLE IV

THEORETICAL NATURAL FREQUENCIES OF CURVED PANELS

(Freely-supported boundary conditions. No cavity effect. Calculated from equation 16.)

PANEL	ORIENTATION:		FRONT		REAR	
1		13		33		33
				33		53
2		41		63		84
				84		69
				90		-
				104		112
				125		125
3		60		71		113
				116		136
				141		127
				188		207
4		73		83		107
				144		194
				146		208
				187		237

TABLE V
EXPERIMENTAL FLUTTER POINTS FOR CURVED PANELS

Panel	h in	$\frac{w_0}{L}$	R in	V_0 in^3	ΔP psi	P_t cm Hg	P psi	T $^{\circ}\text{R}$	$\frac{A}{\pi}$	f cps
1	0.0082	0	∞	40.5	0	60.5	0.425	207	16.50	84
					0.0250	84.0	0.589	209	22.91	116
					0.0500	110.5	0.775	210	30.14	144
2	0.0076	0.007	160.75	45.6	0	19.5	0.137	205	6.81	109
					0.0290	48.3	0.339	207	16.55	125
					0.0500	60.9	0.427	206	20.87	137
3	0.0082	0.013	86.60	49.5	0	21.0	0.147	208	5.73	82
					0.0290	44.0	0.309	204	12.00	137
					0.0500	60.5	0.425	206	16.50	
4	0.0077	0.020	56.34	55.0	0	17.5	0.123	210	5.76	105
					0.0683	61.5	0.432	209	20.26	178

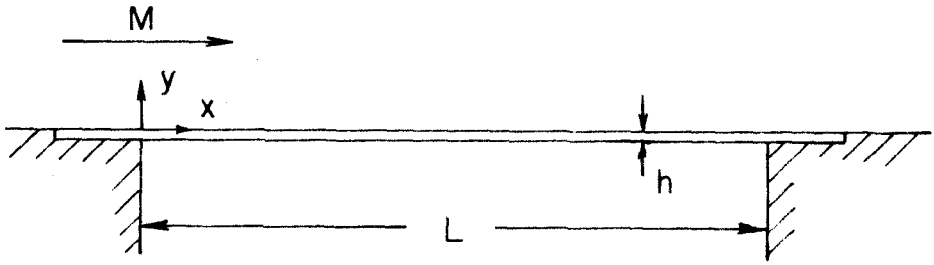


Fig. 1. Two-Dimensional, Flat, Clamped Panel.

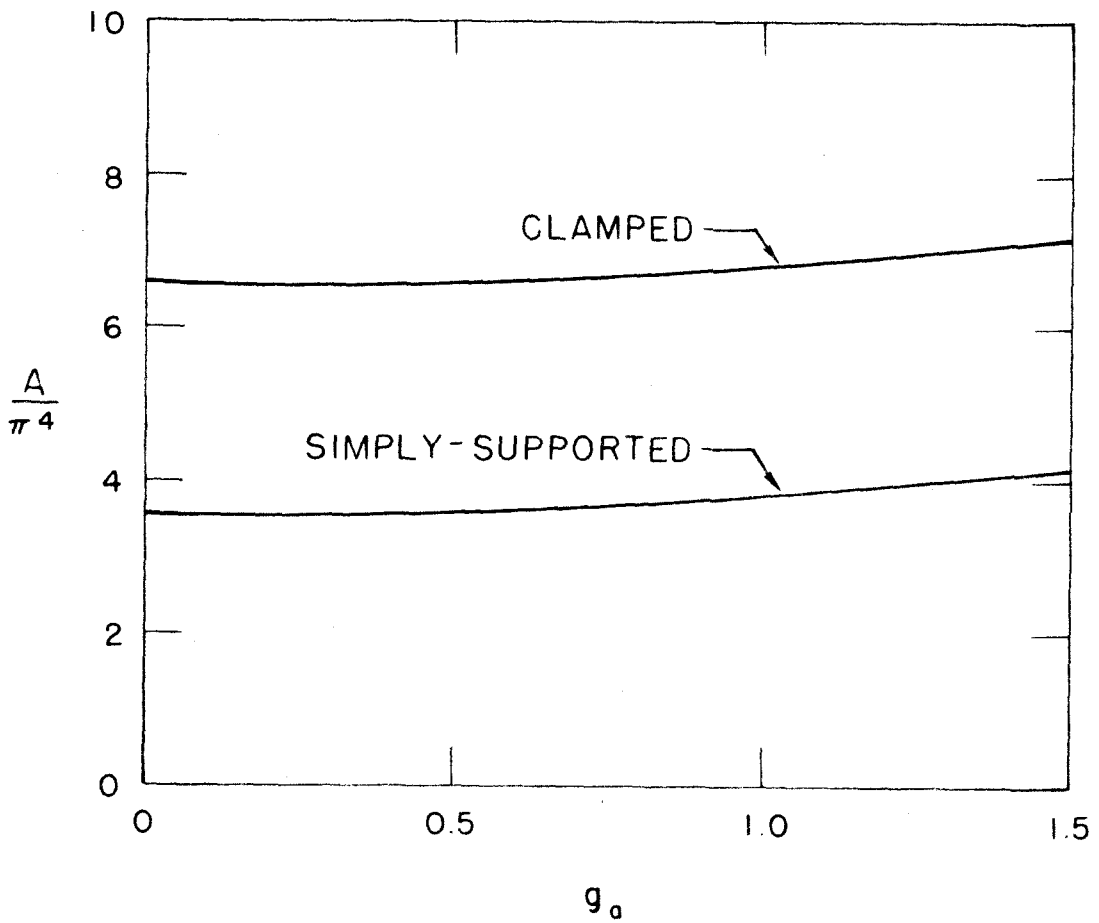


Fig. 2. Flutter Boundaries for Two-Dimensional, Flat Panels with Zero Membrane Stress. (Houbolt, Ref. 8).

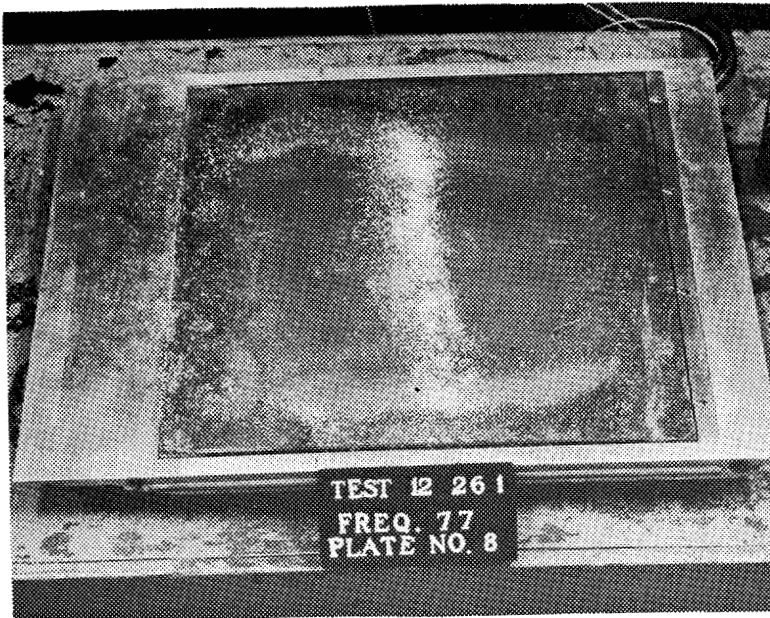


Fig. 3. Wind Tunnel Model for the Flat Panel Test.
(Shown During Vibration Tests on the Bench.)

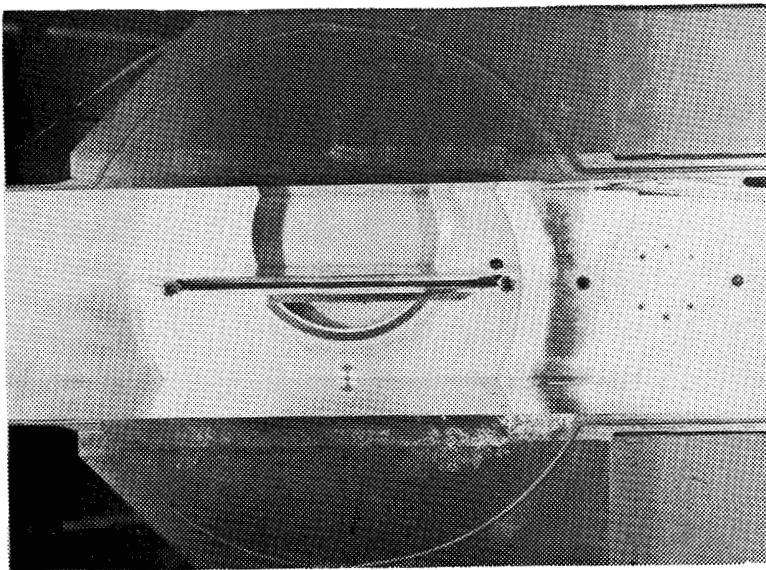


Fig. 4. Installation of Model in Wind Tunnel.
(Flow from Left to Right.)

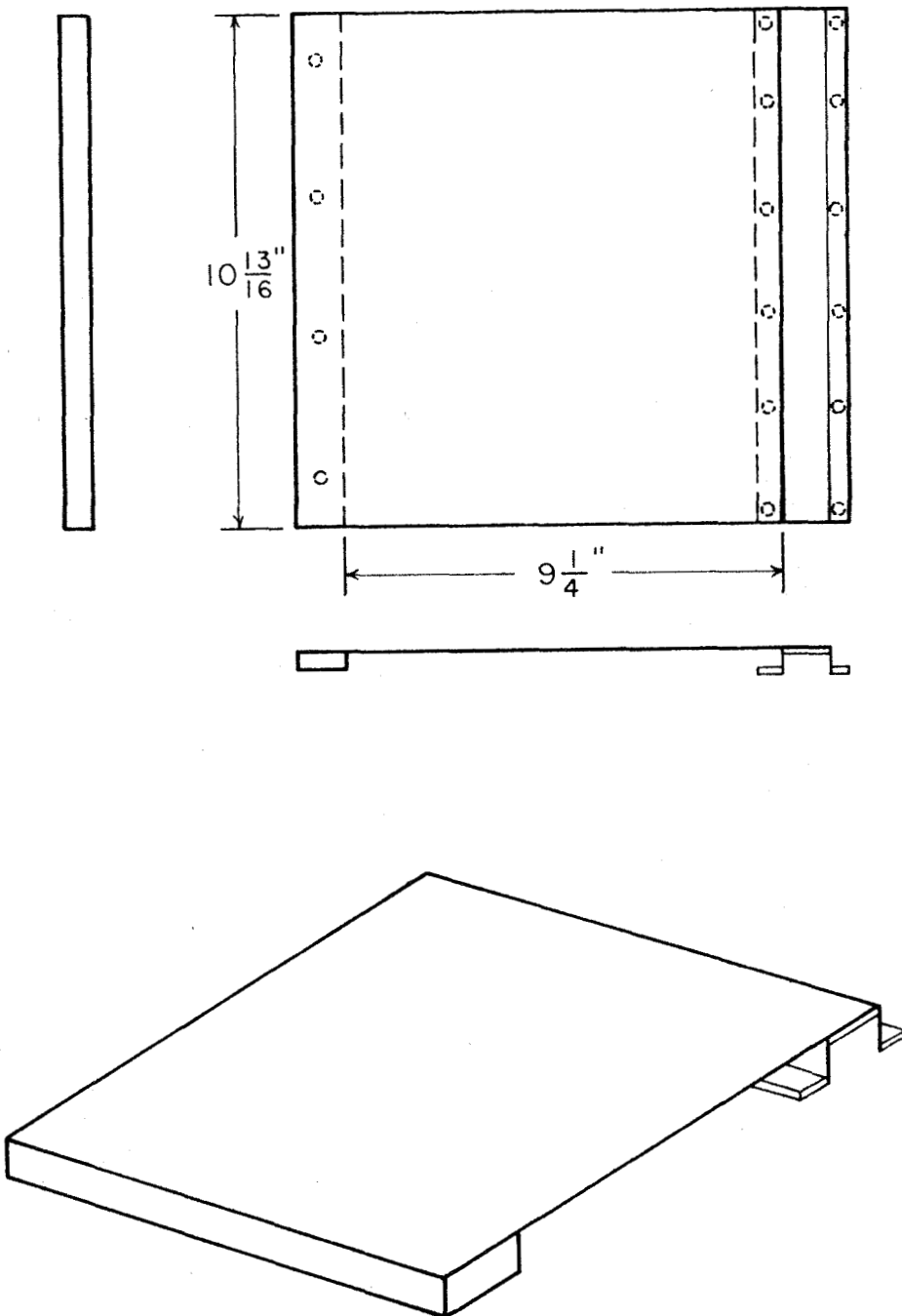


Fig. 5. Flat Panel Assembly.

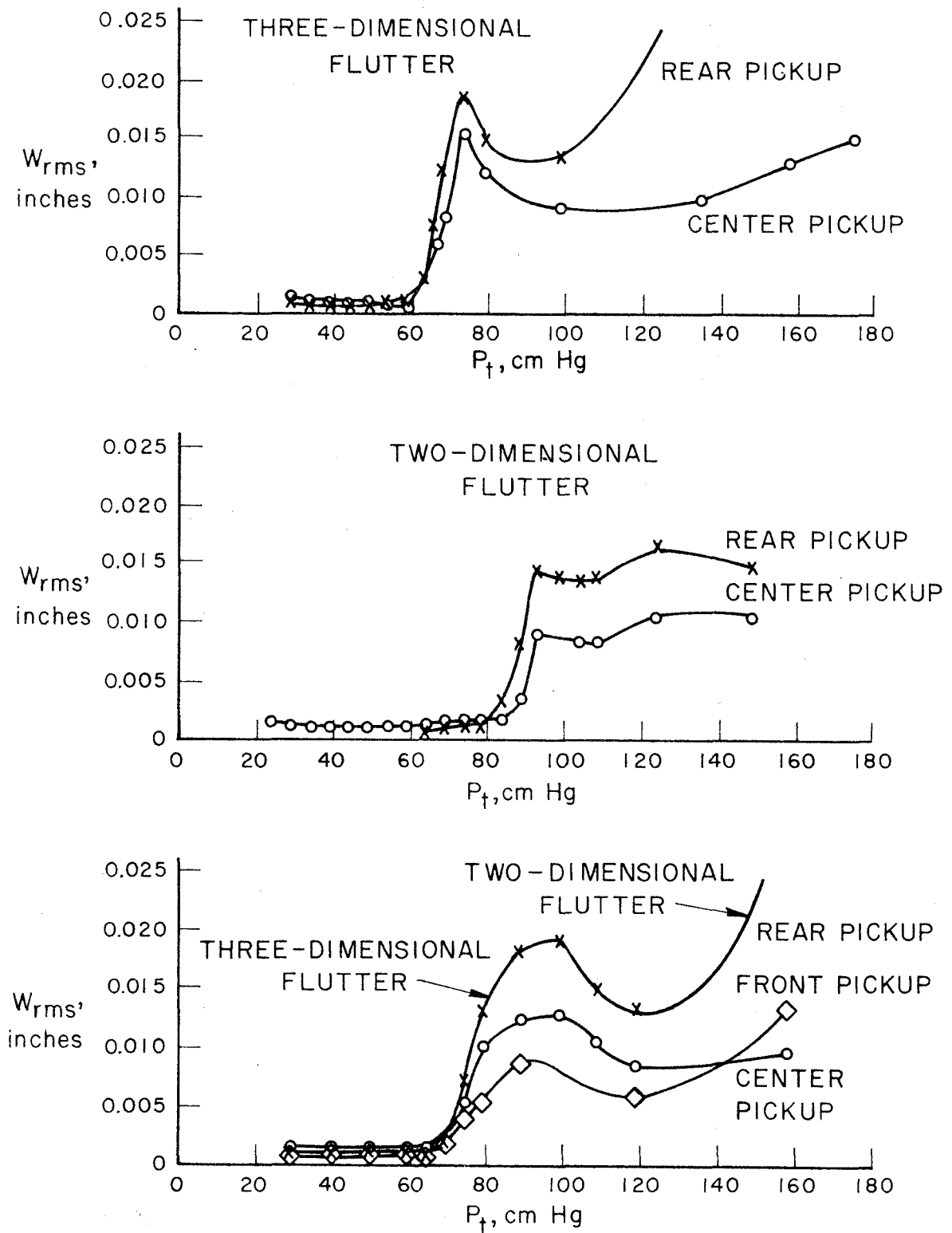


Fig. 6. Flutter Amplitudes for 0.015" Flat Panels.

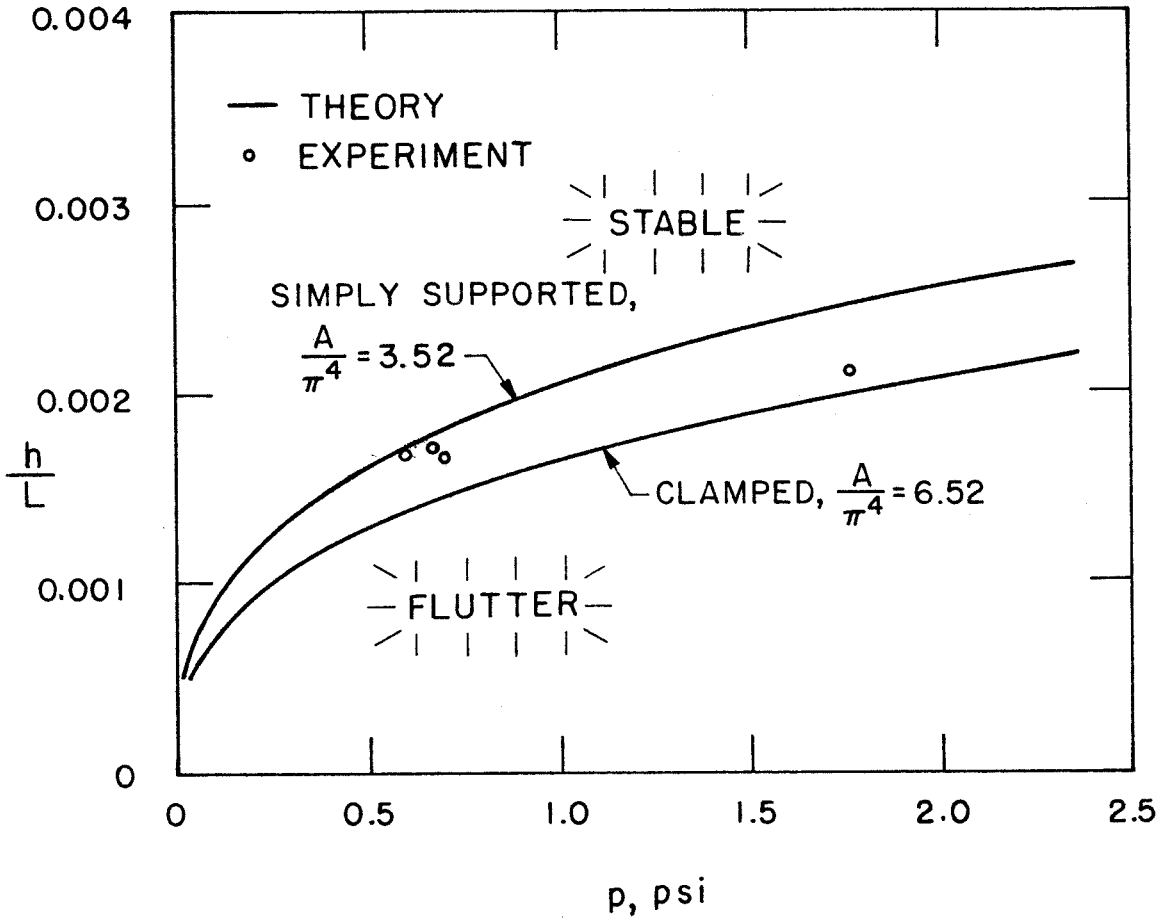


Fig. 7. Thickness Ratio Required to Prevent Flutter Versus Wind Tunnel Free-Stream Static Pressure. Two-Dimensional Flutter of Flat Panels, $M = 2.81$.

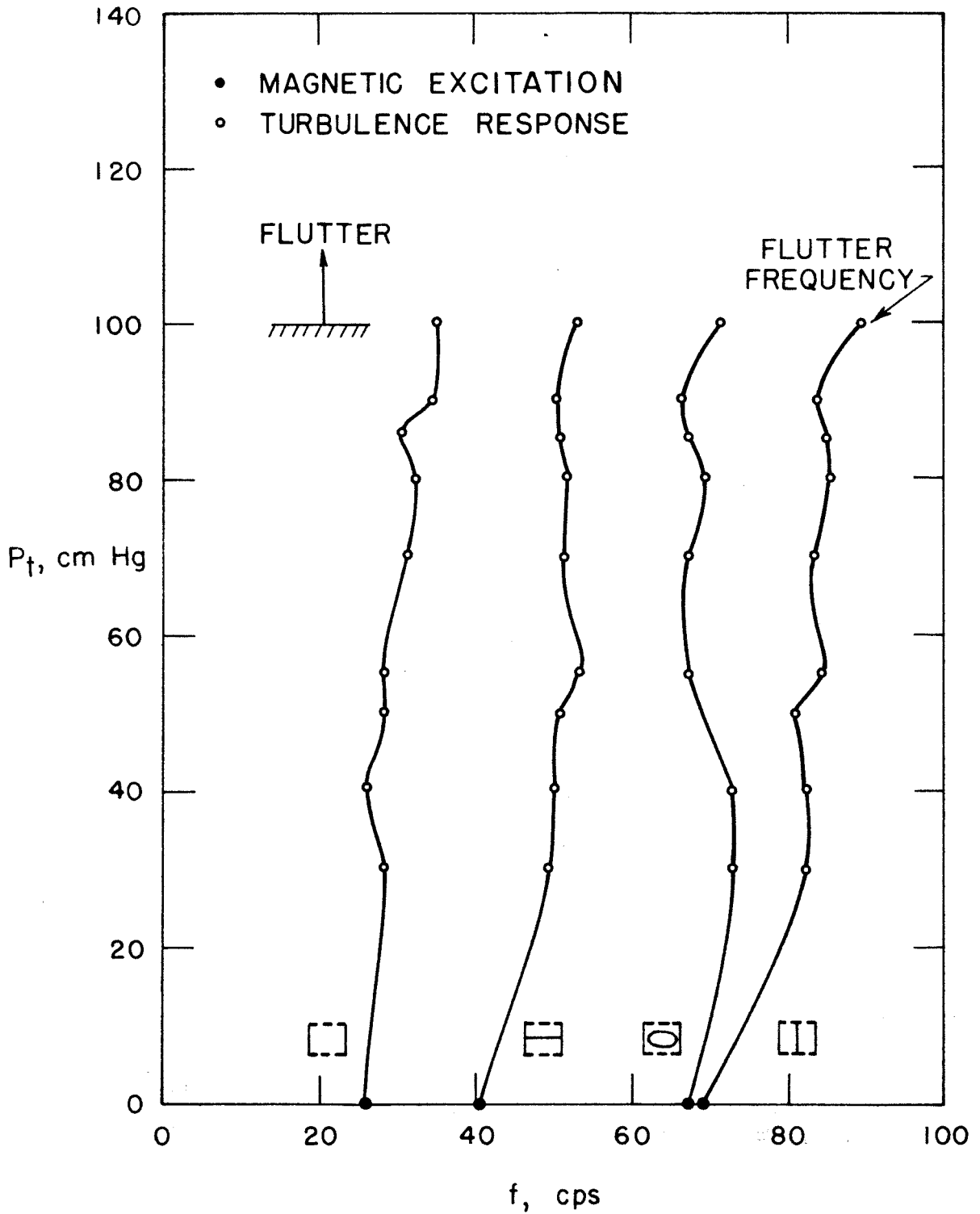


Fig. 8. Resonant Frequencies for a Flat Panel 0.0151" Thick. Two-Dimensional Flutter. 0.050" Diameter Wire Boundary Layer Trip.

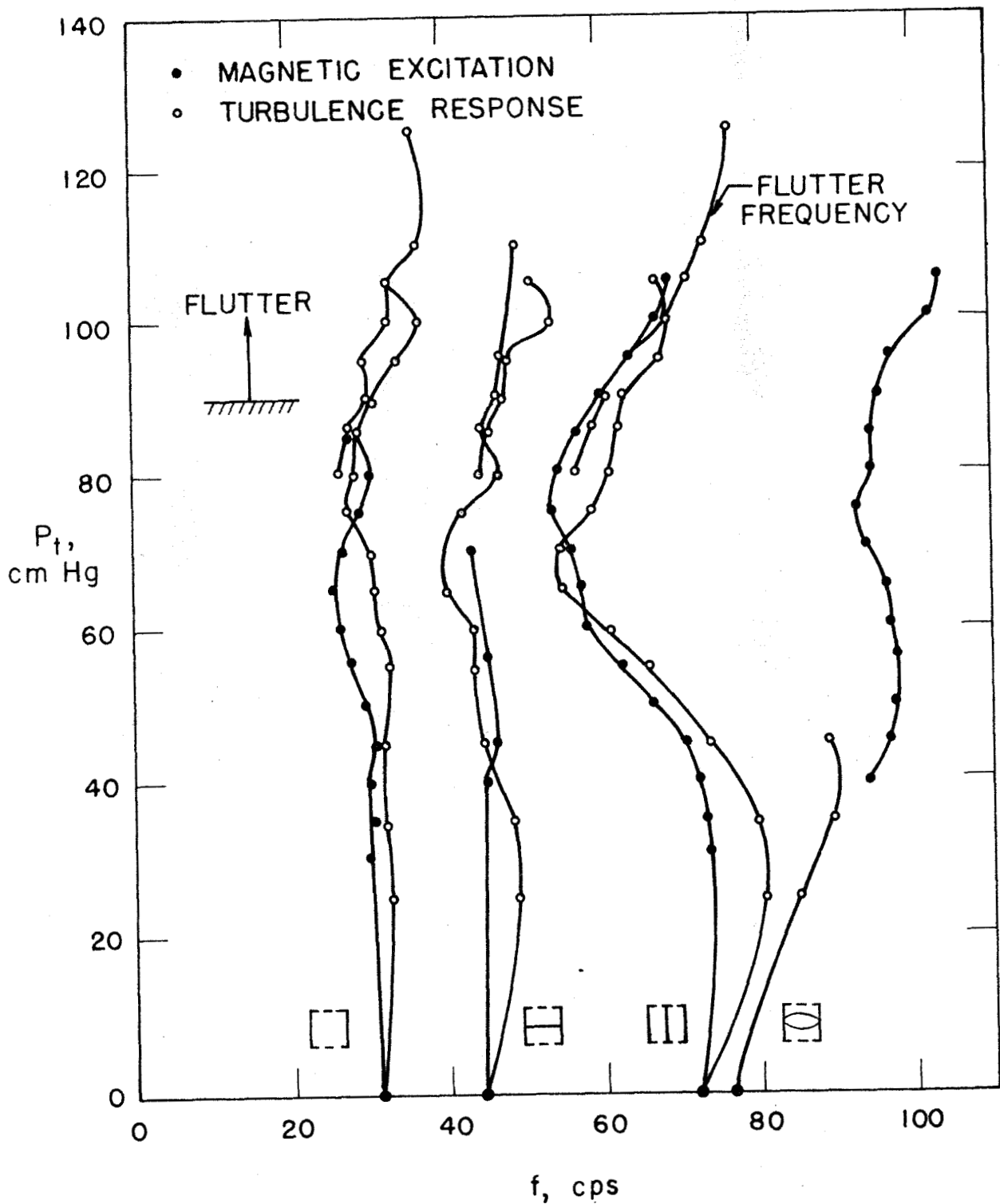


Fig. 9. Resonant Frequencies for a Flat Panel 0.0153" Thick.
Two-Dimensional Flutter.

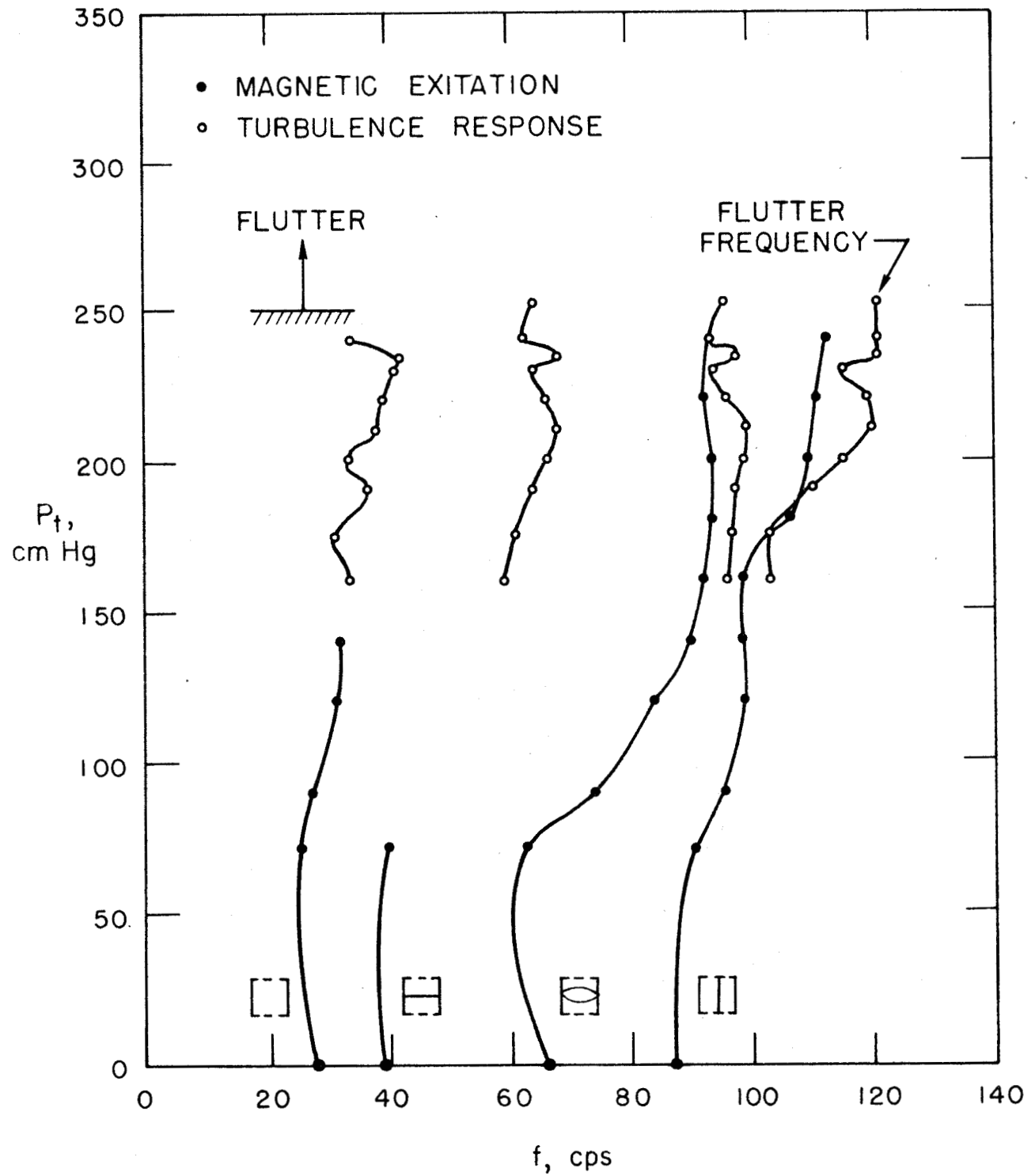


Fig. 10. Resonant Frequencies for a Flat Panel 0.0193" Thick. Two-Dimensional Flutter.

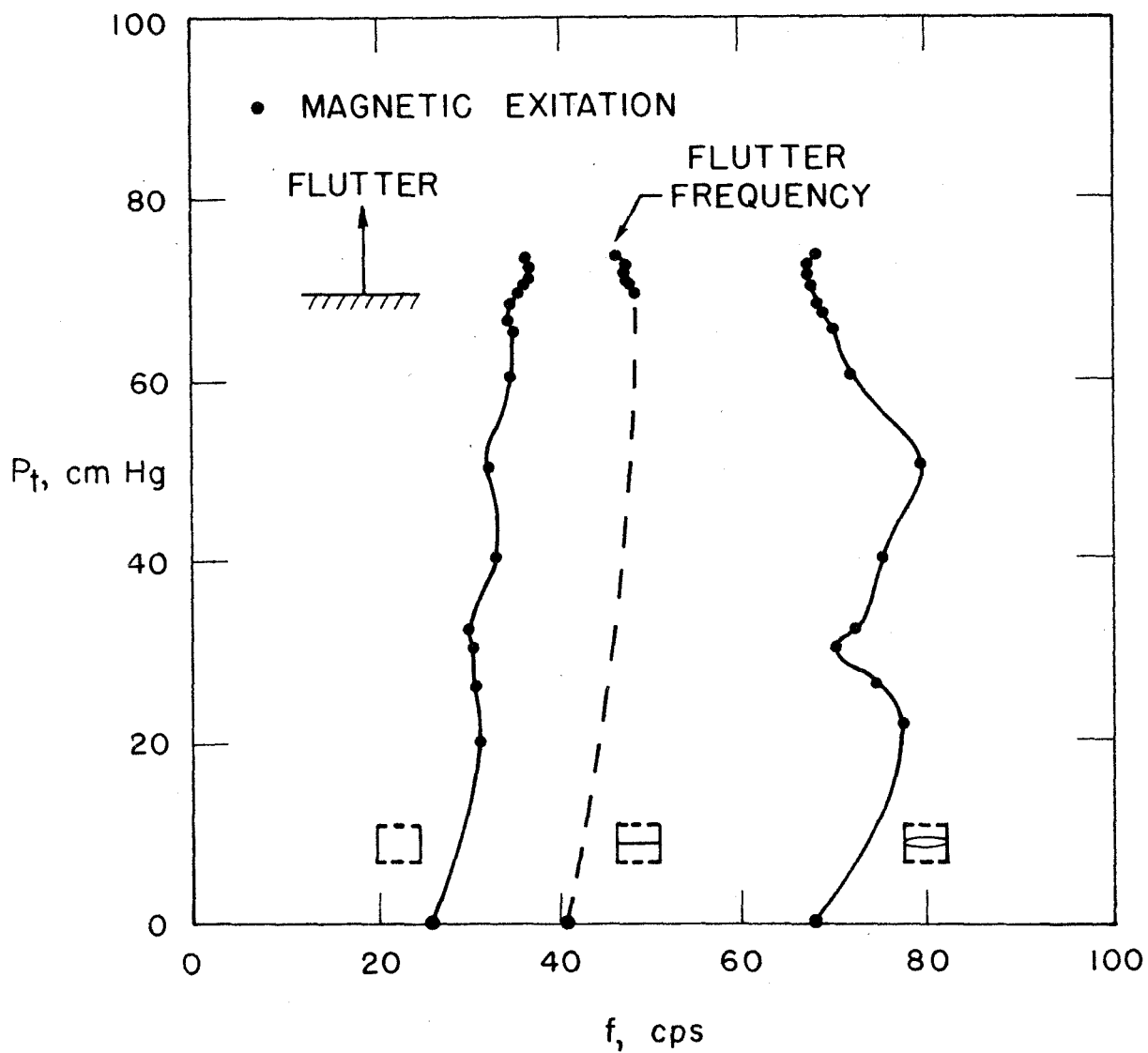
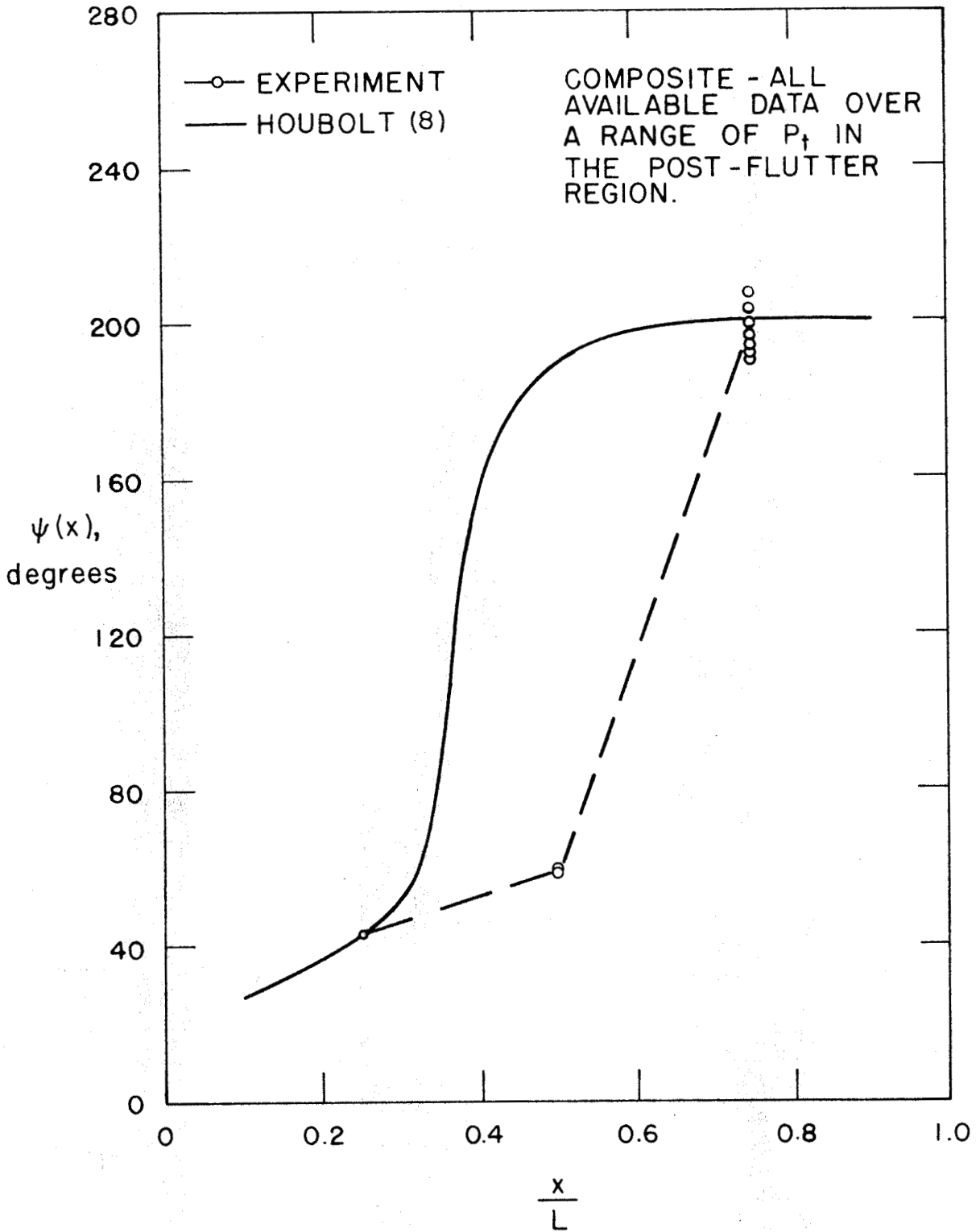


Fig. 11. Resonant Frequencies for a Flat Panel 0.0151" Thick. Three-Dimensional Flutter.



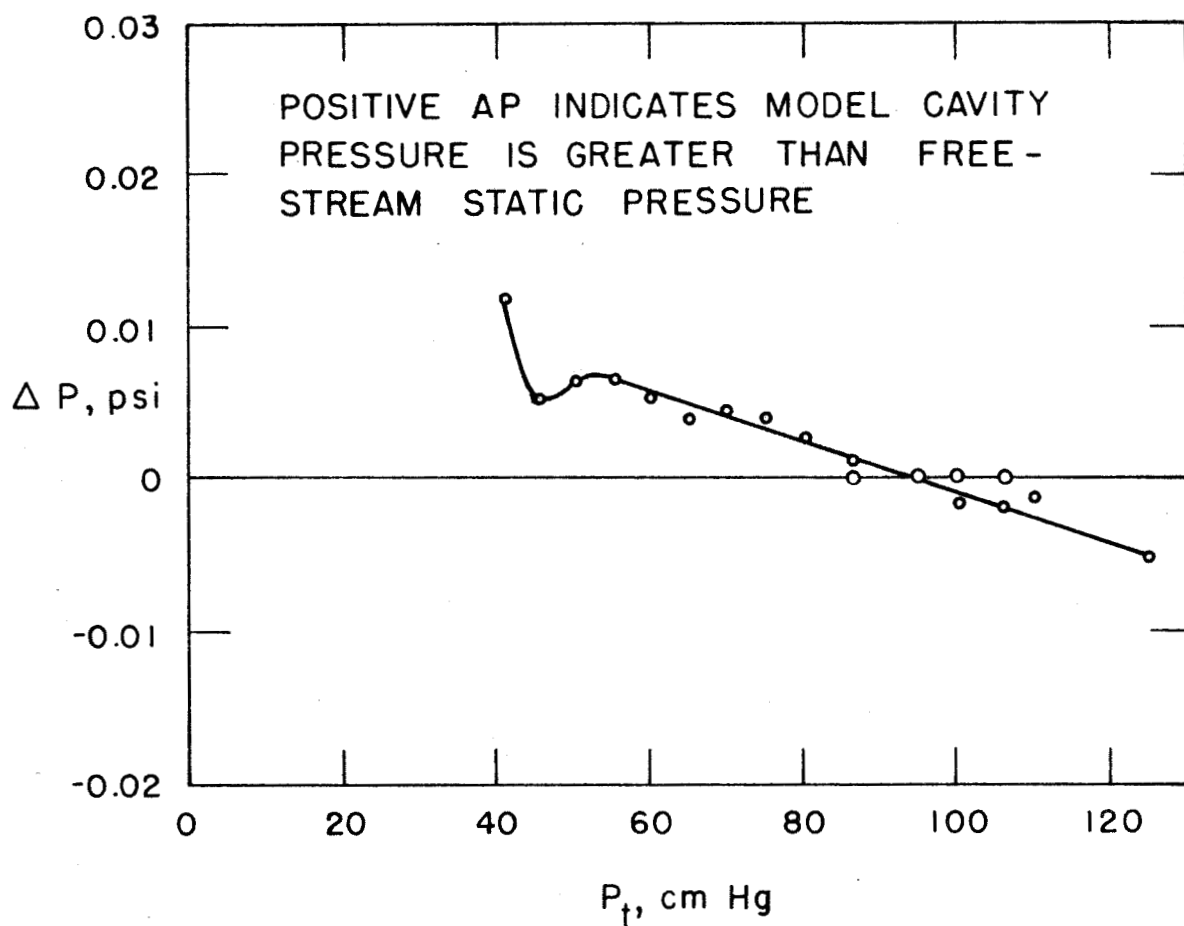


Fig. 13. Static Pressure Differential Between Model Cavity and Free Stream.

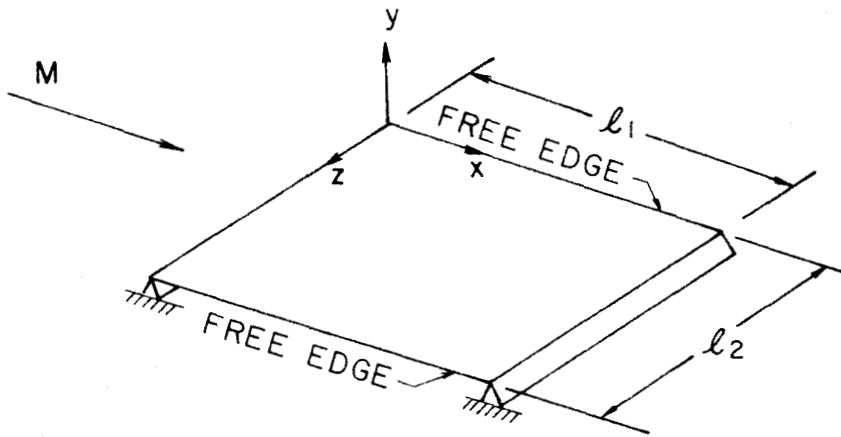


Fig. 14. Coordinate System for Three-Dimensional Flutter of a Simply-Supported Panel.

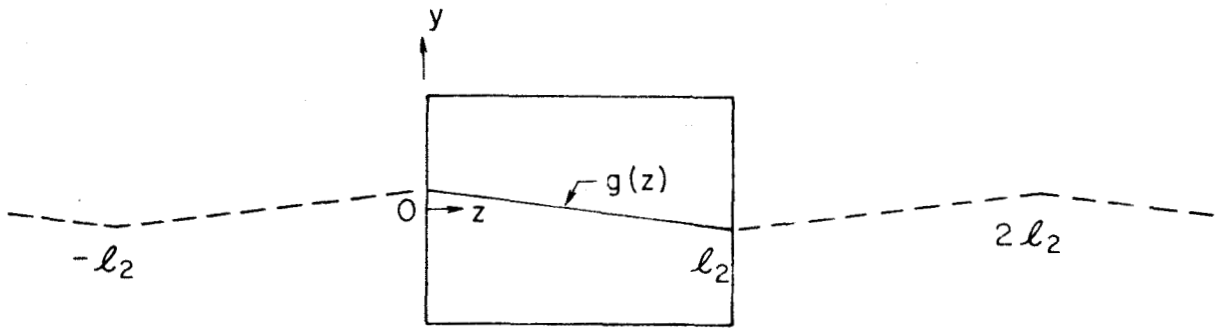


Fig. 15. Method of Images.

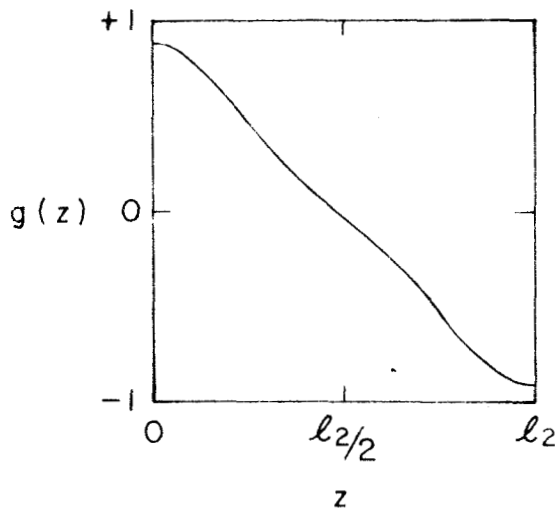


Fig. 16. Two-Term Fourier Series Representation of $g(z)$.

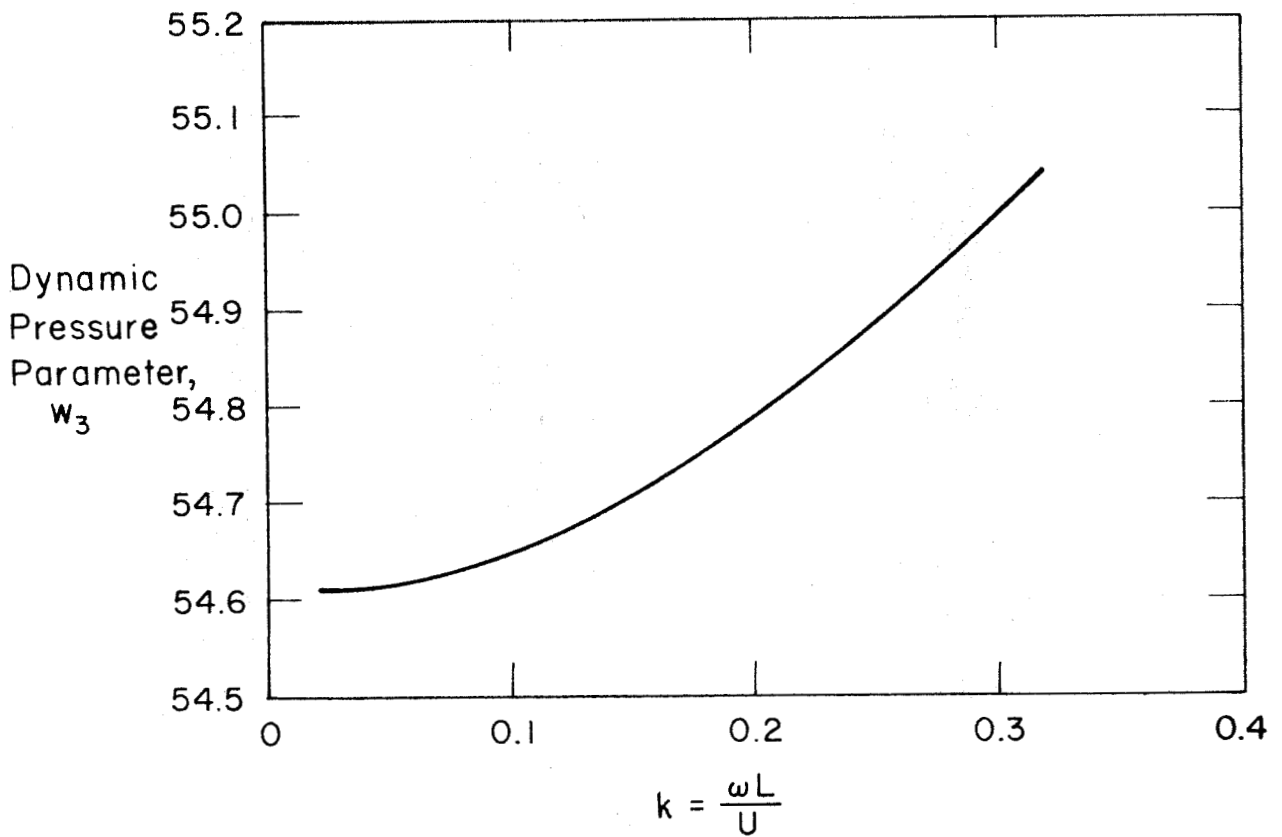
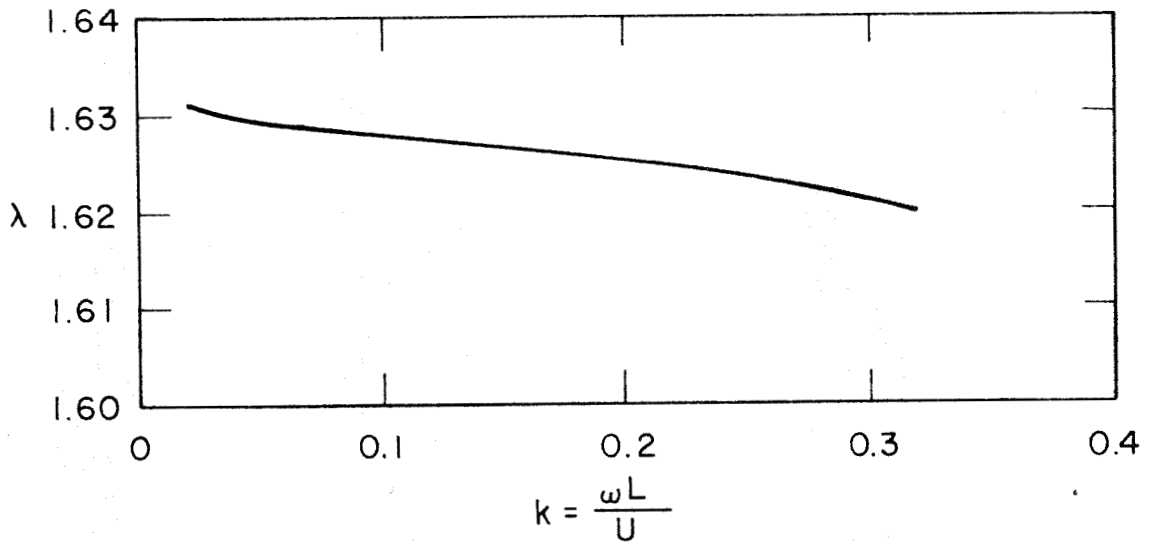


Fig. 17. Three-Dimensional Flutter Solution.
 $M = 2.81$, $\frac{l_1}{l_2} = 0.8555$, $\nu = 0.3$.

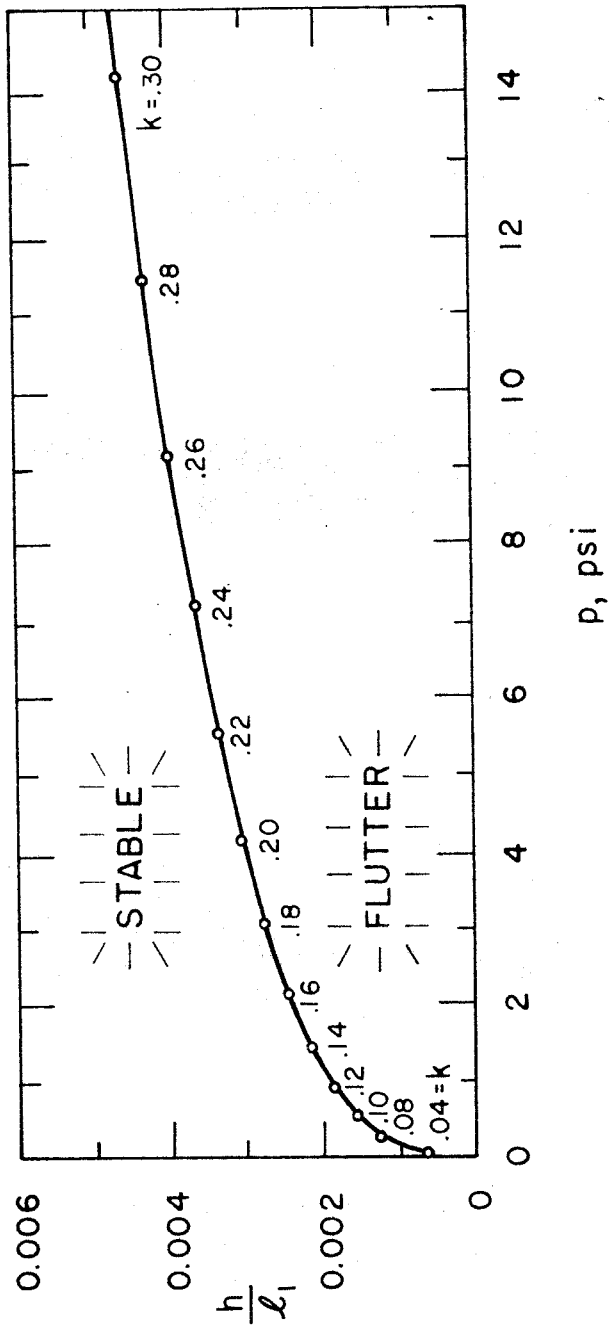


Fig. 18. Flutter Boundary for Three-Dimensional Case. Brass Panel at $T \approx 210^\circ\text{R}$.



Fig. 19. Wind Tunnel Model for Curved Panel Test.
(Panel No. 3 is Installed. The Discoloration
on the Panel is from the Baking Process
Used in Mounting the Panel.)



Fig. 20. Curved Panel Assembly, Inverted.

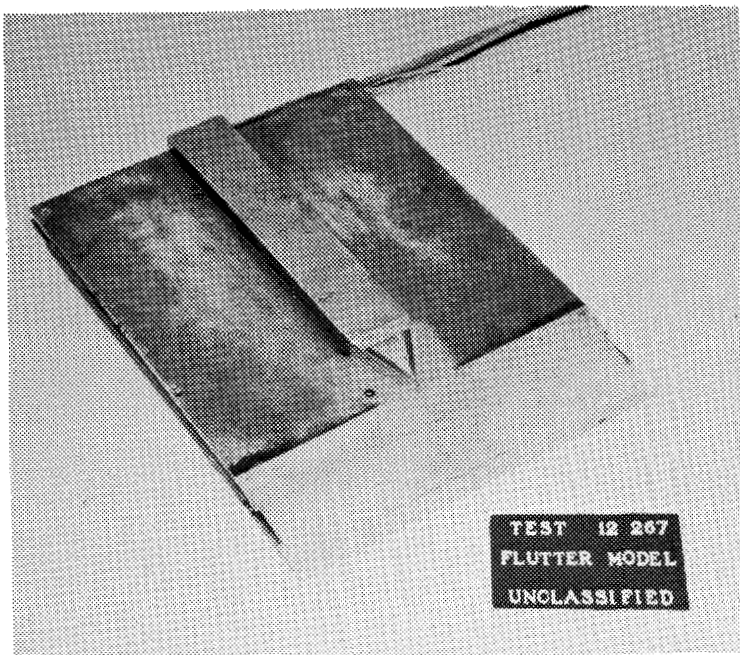


Fig. 21. Bottom View of Model.

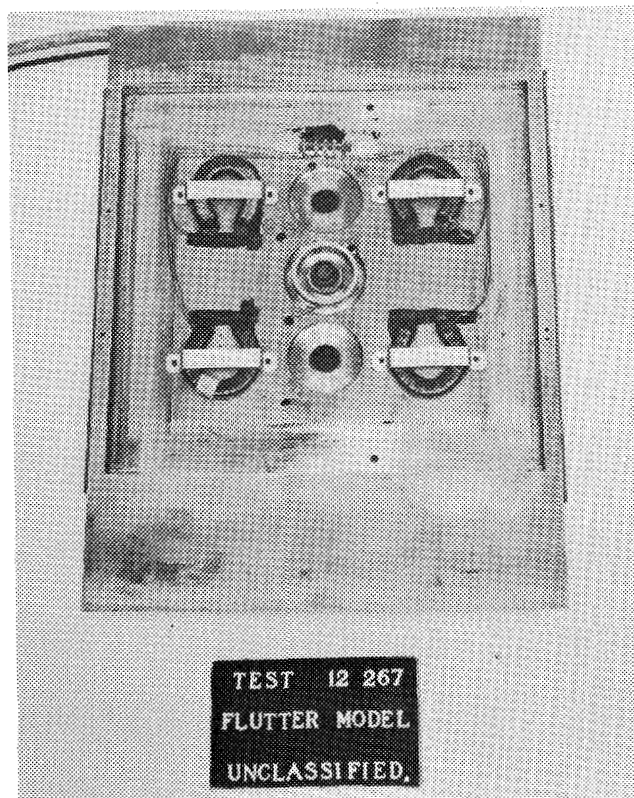


Fig. 22. View of Model Cavity. (Only One Pickup Installed)

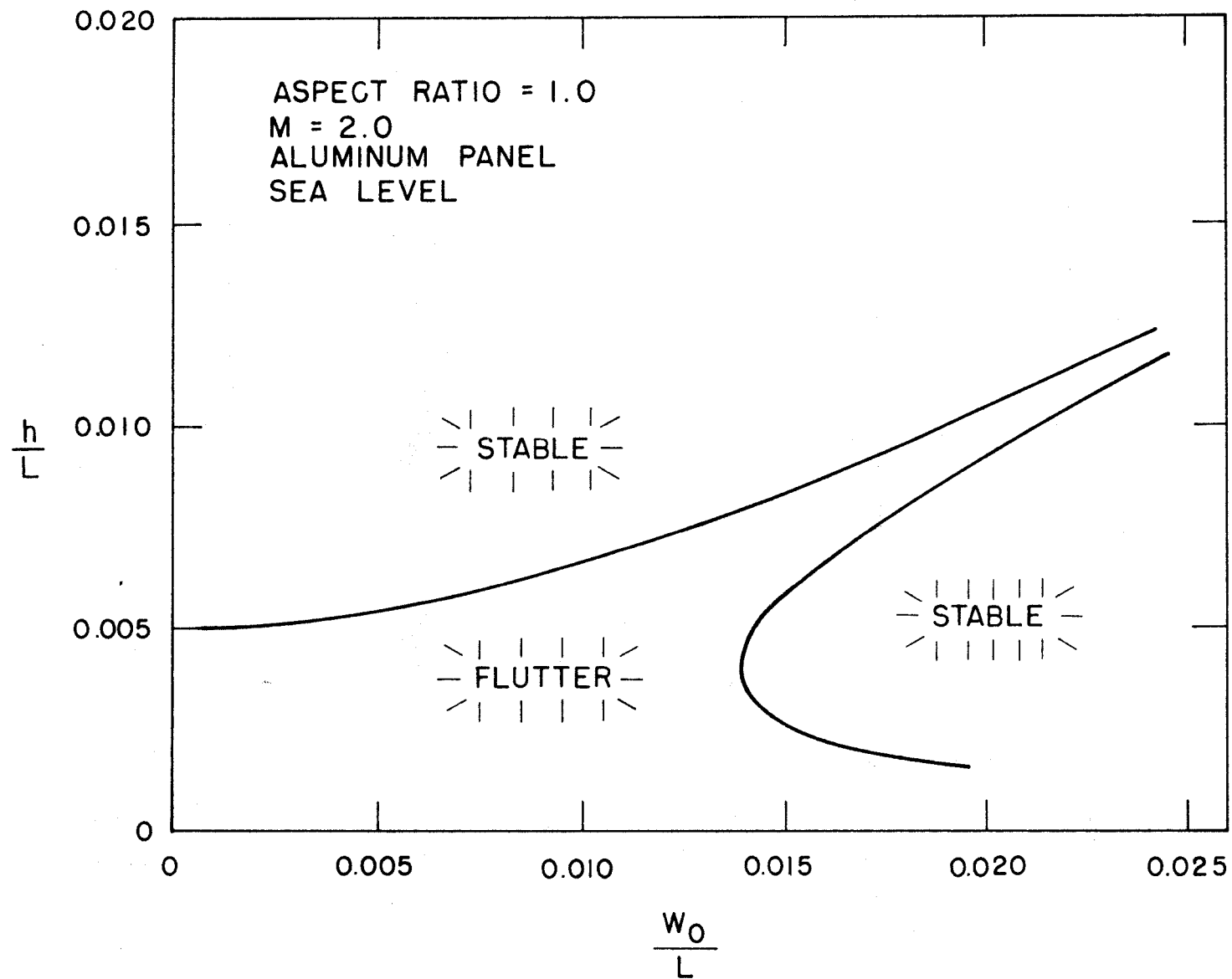


Fig. 23. Typical Theoretical Flutter Boundary for Curved Panels.
Yates and Zeijdel (Ref. 13).

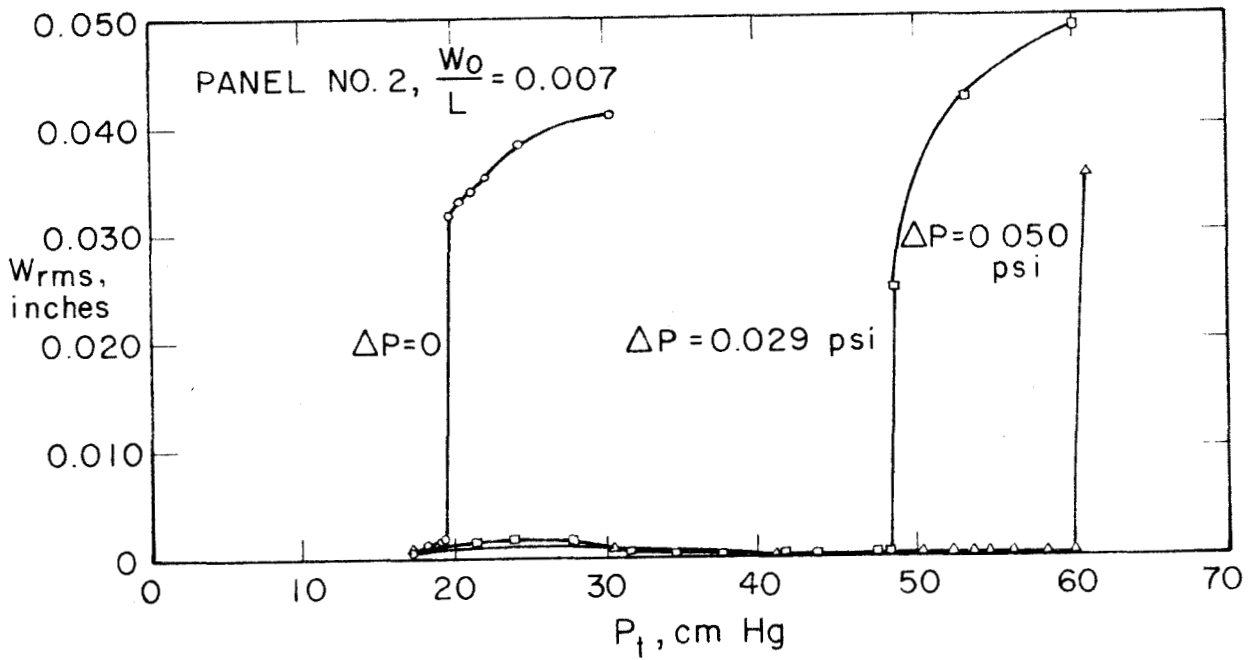
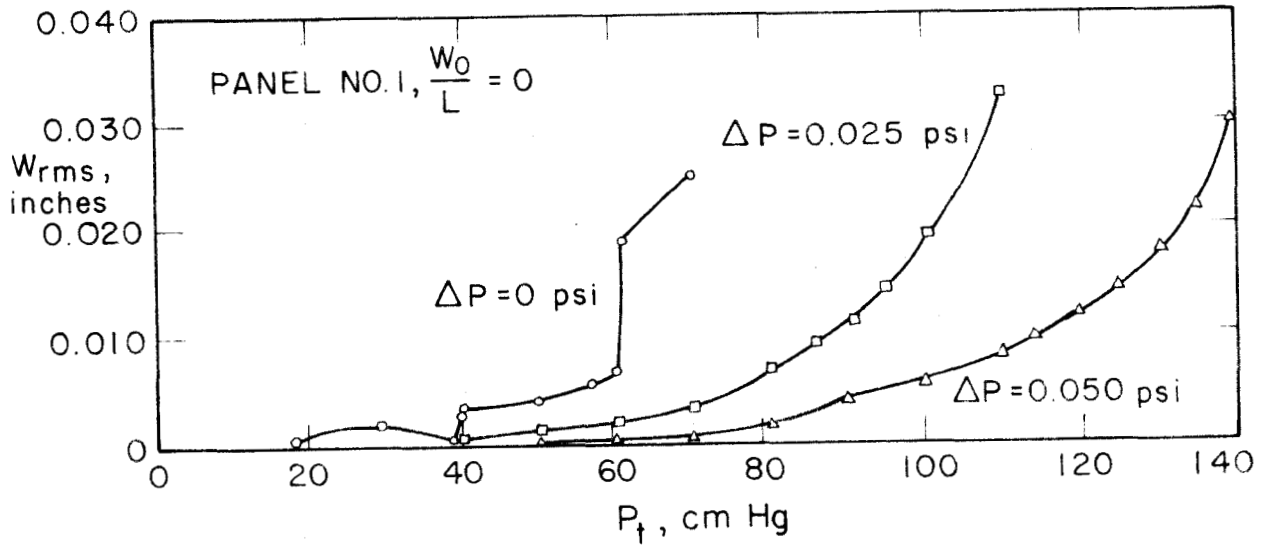


Fig. 24. Flutter Amplitudes for Slightly Curved Panels.

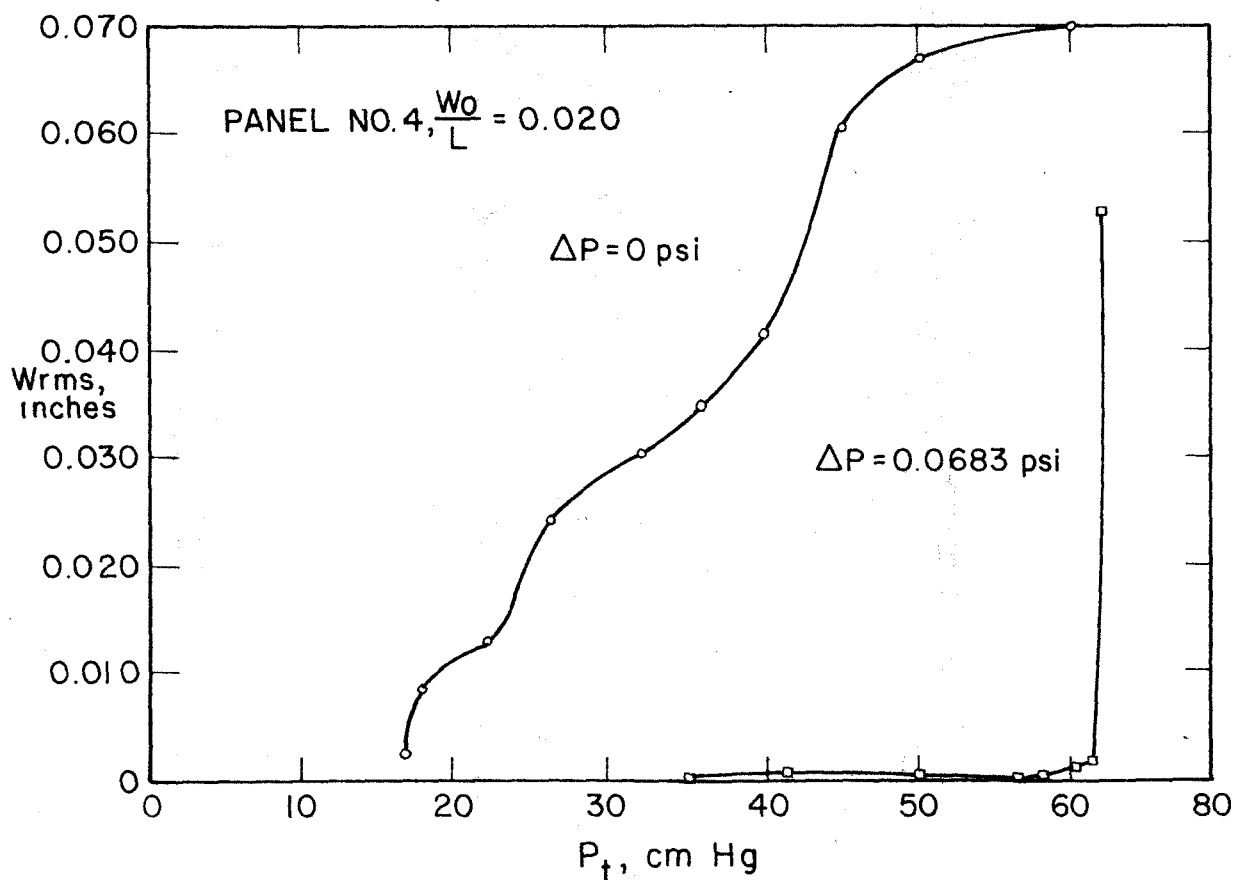
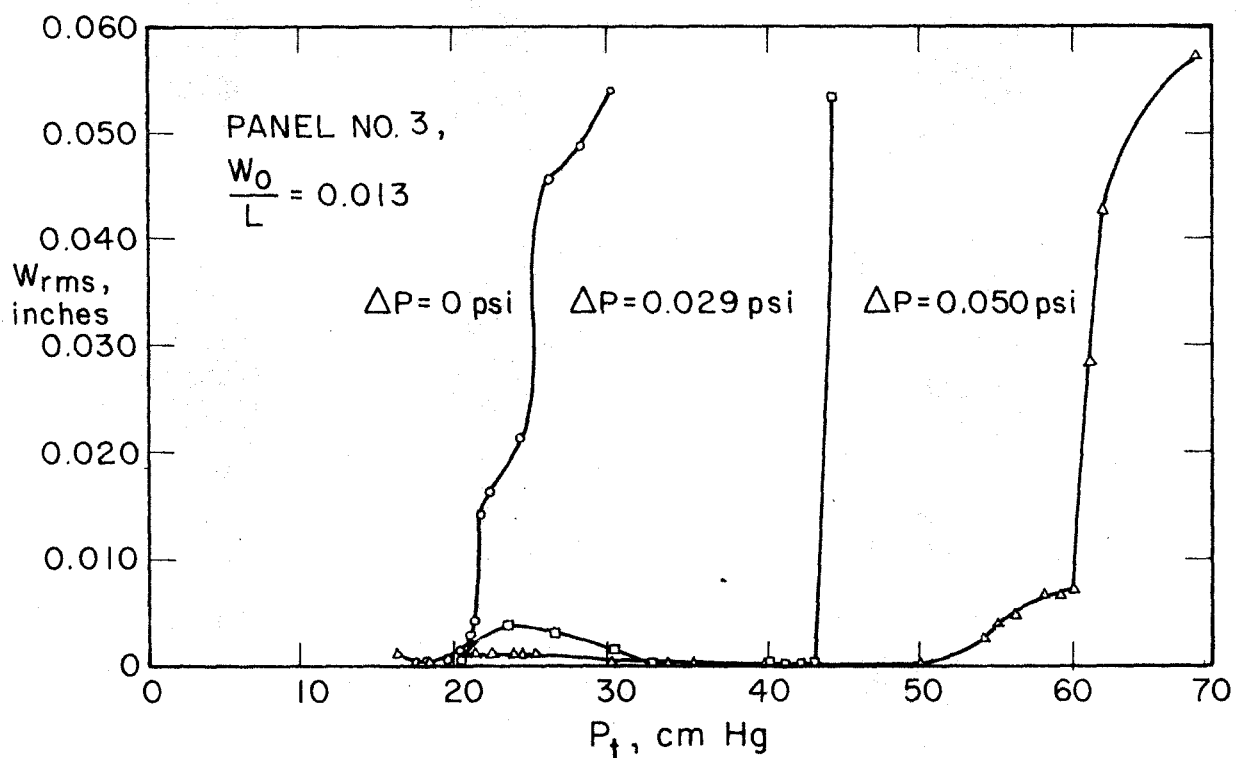


Fig. 25. Flutter Amplitudes for Slightly Curved Panels.

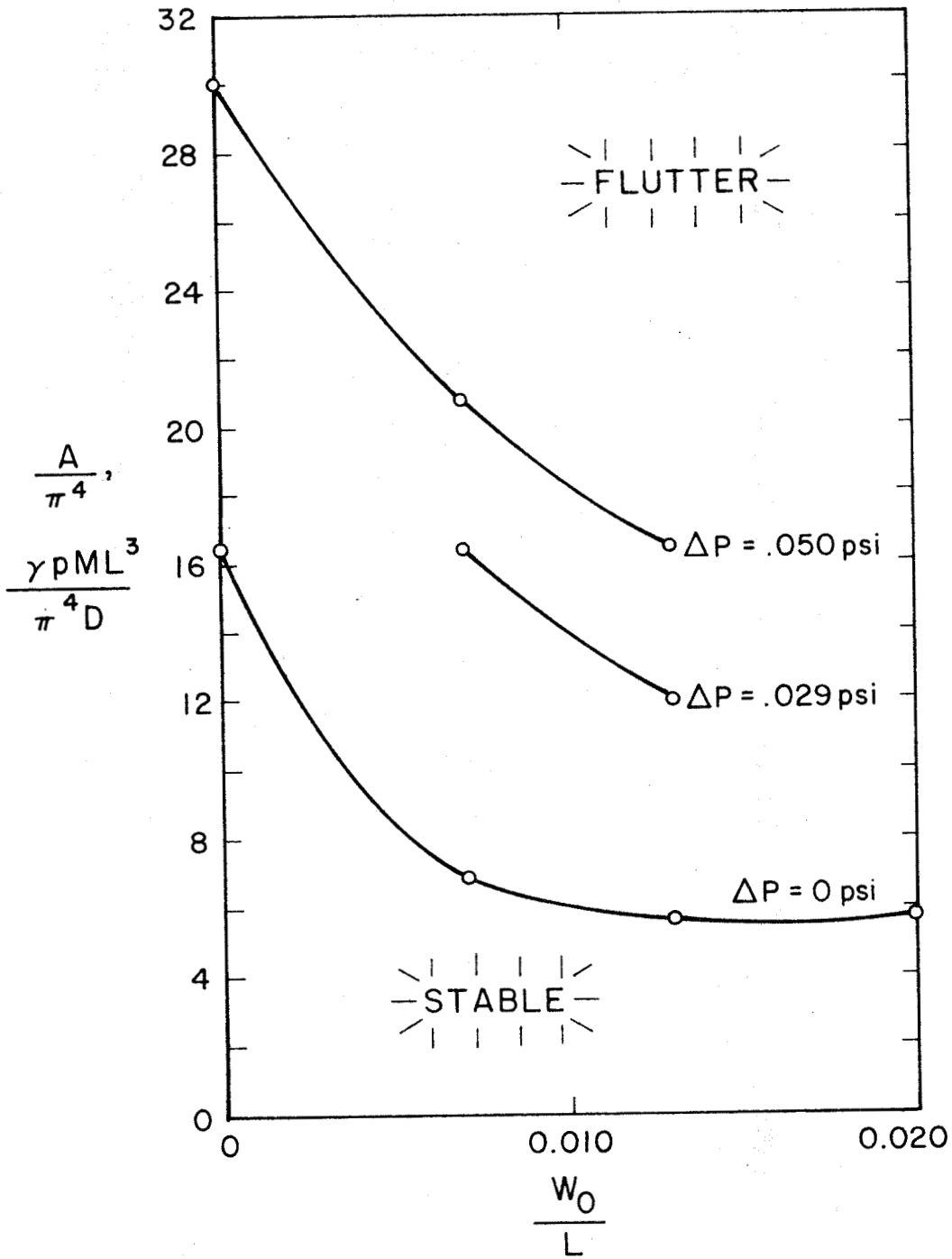


Fig. 26. Experimental Flutter Boundaries for Slightly Curved Panels.

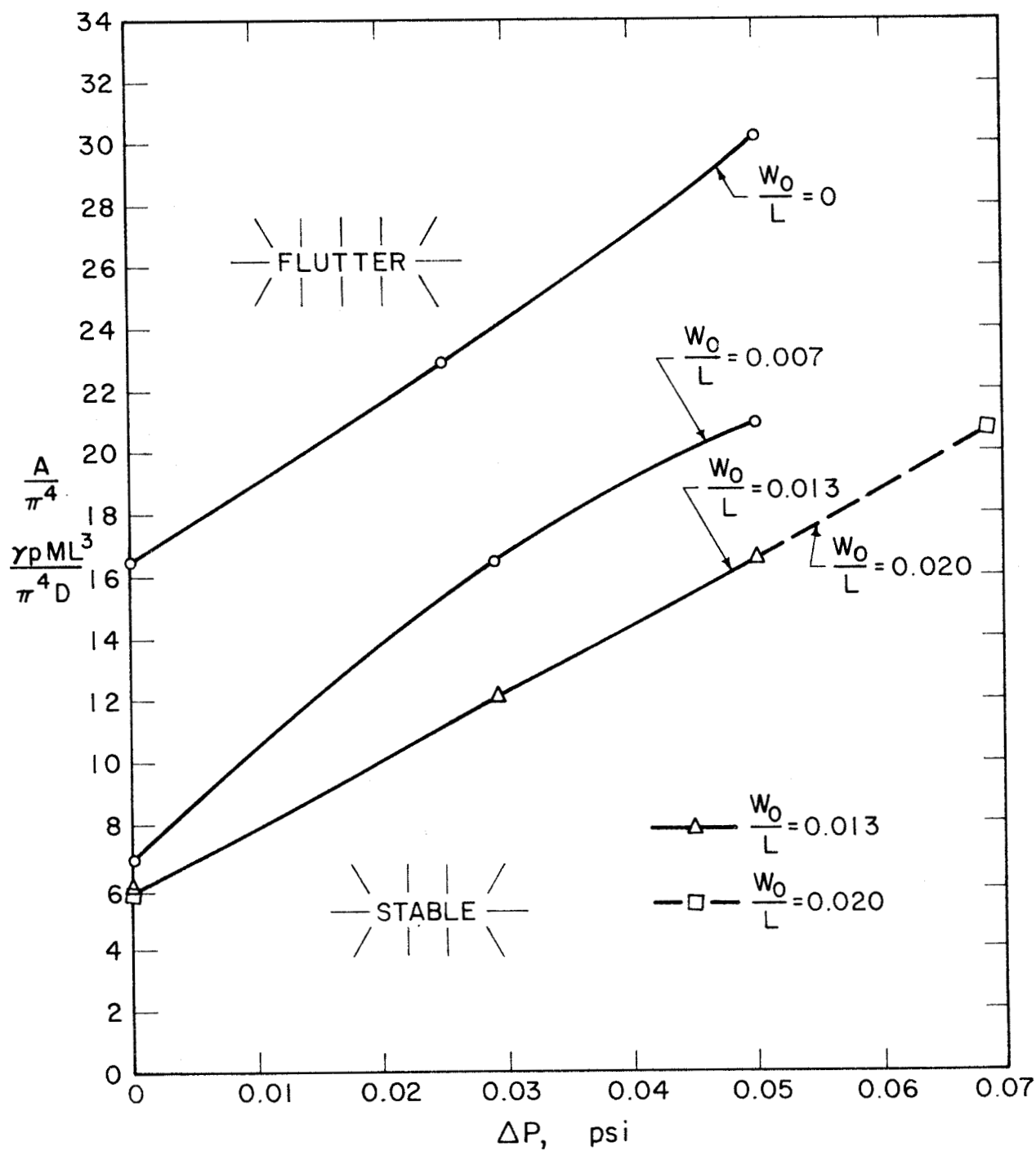


Fig. 27. Effect of Static Pressure Differential on the Flutter of Slightly Curved Panels.

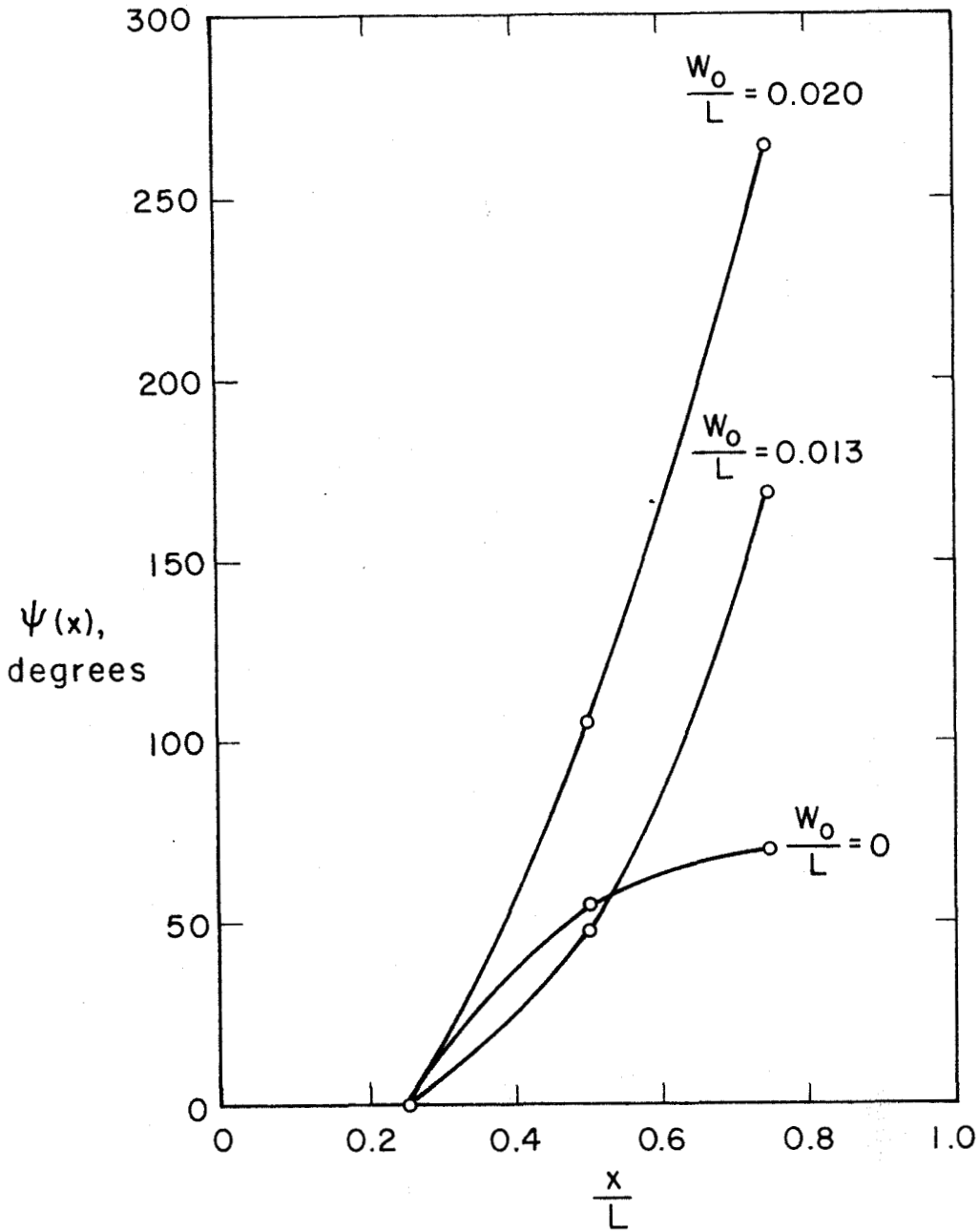


Fig. 28. Phase Lag at Initiation of Flutter, Curved Panels, $\Delta P = 0$.

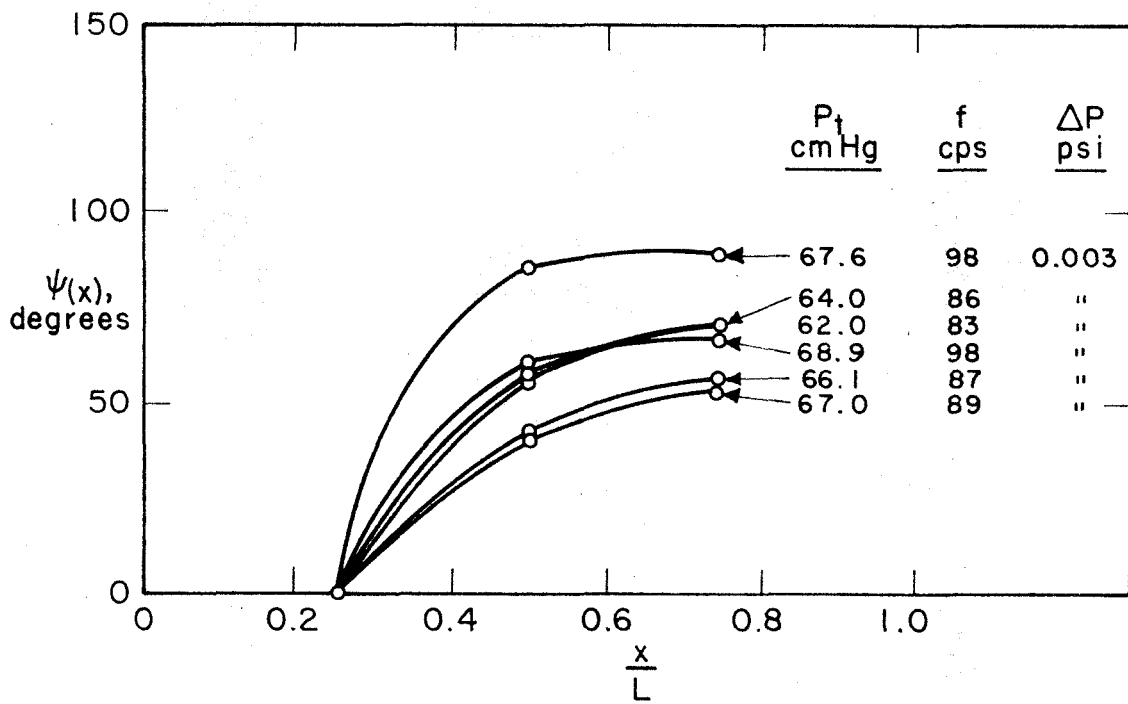


Fig. 29. Phase Lag for Curved Panel No. 1, $\frac{w_o}{L} = 0$.

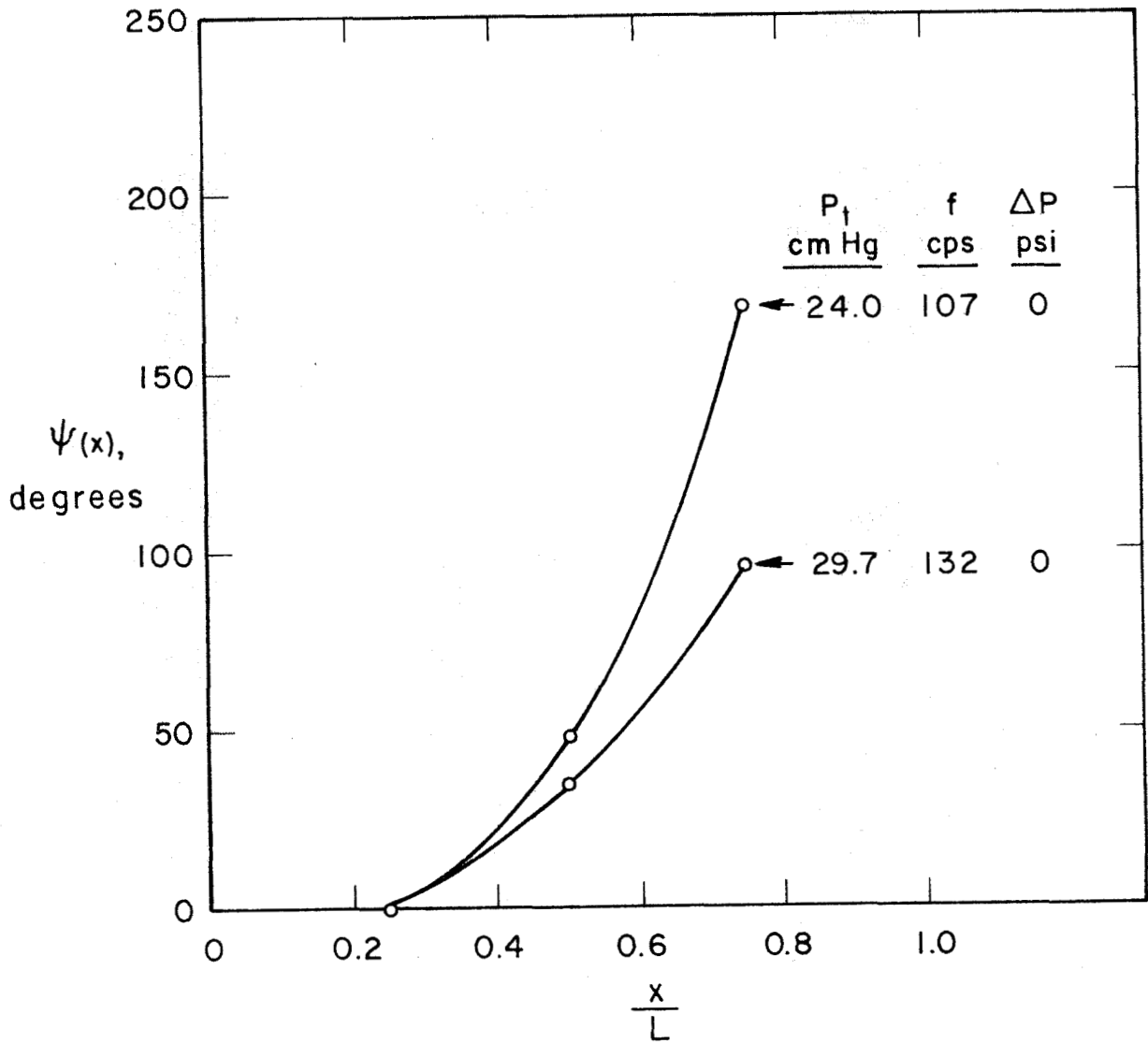


Fig. 30. Phase Lag for Curved Panel No. 3, $\frac{w_o}{L} = 0.013$

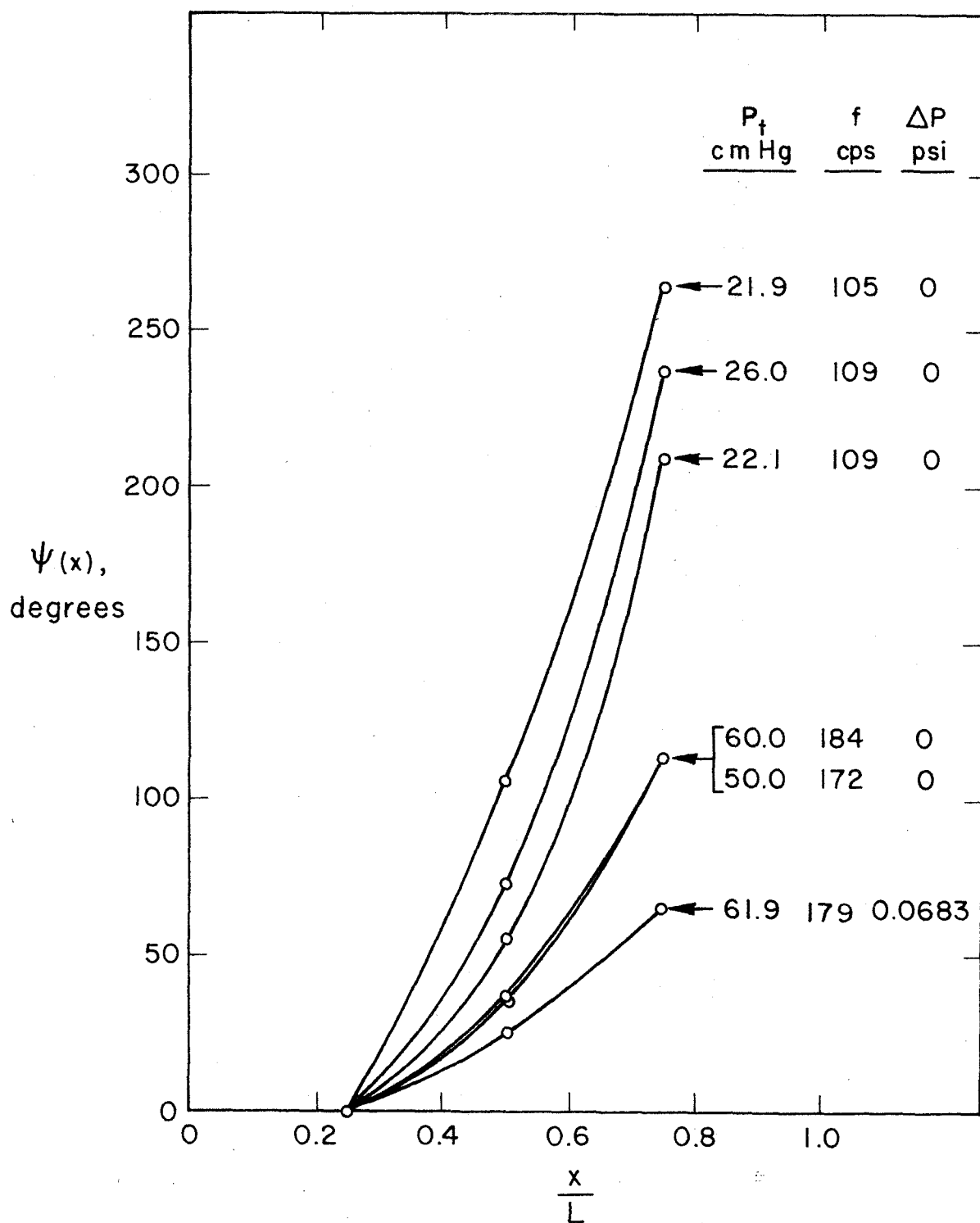


Fig. 31. Phase Lag for Curved Panel No. 4, $\frac{w_o}{L} = 0.020$.

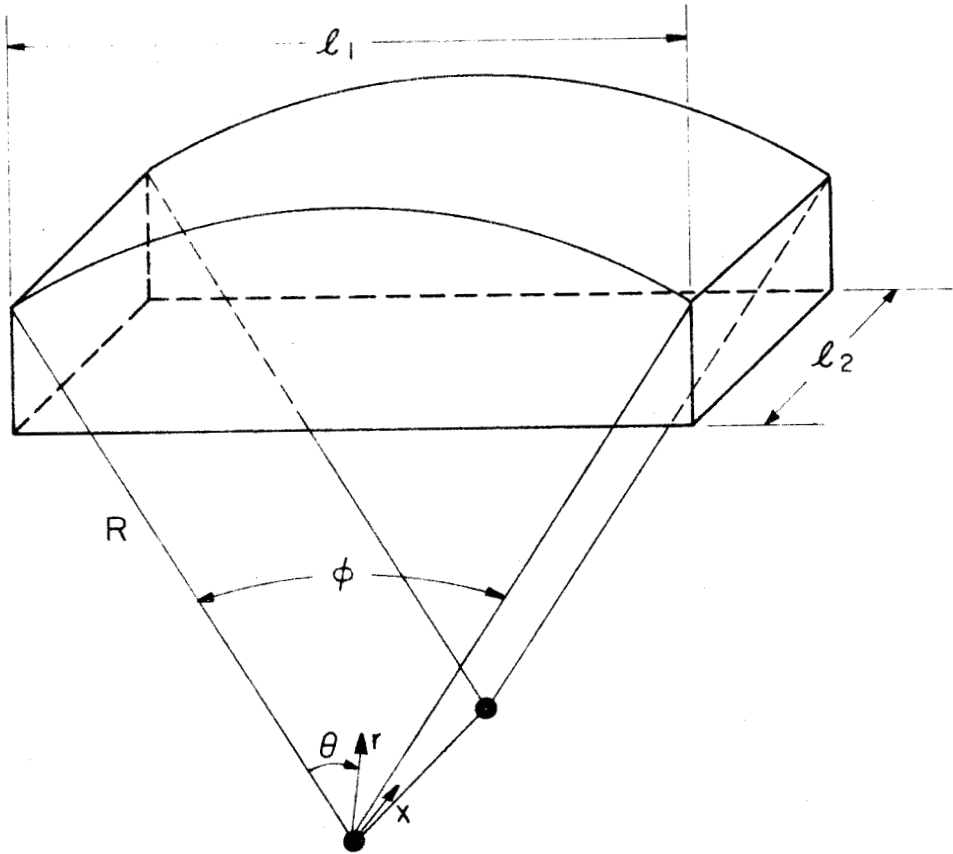


Fig. 32. Curved Panel over A Closed Cavity.



Fig. 33. Curved Panel in Initial and Deflected Positions.

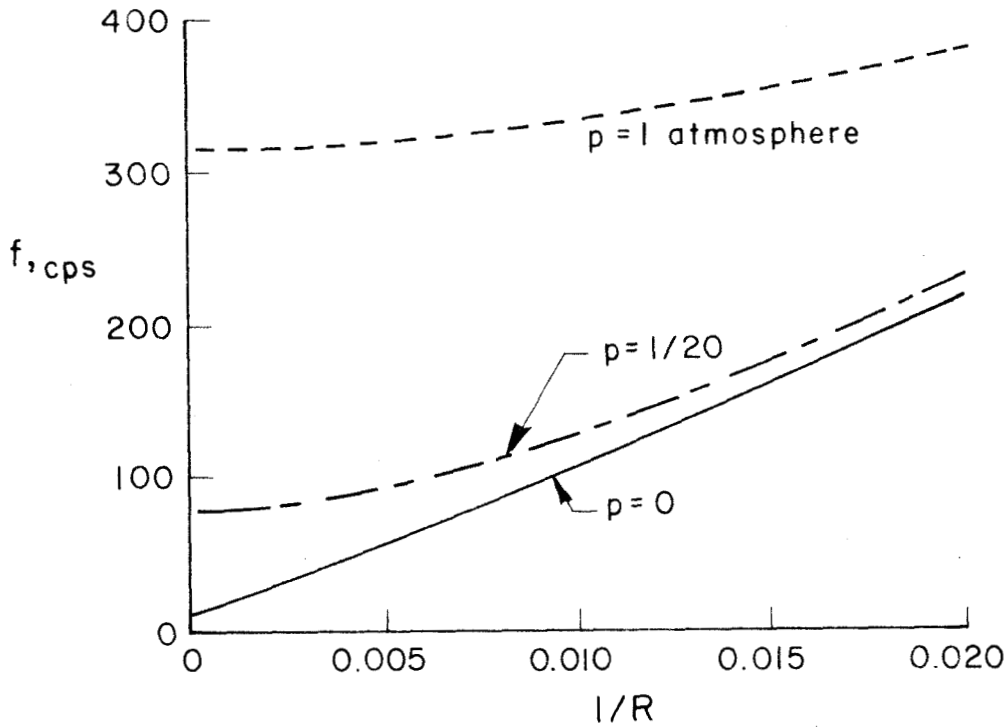


Fig. 34. Cavity Effect on Natural Frequencies of Curved Panels. "Simplest" Mode. (Predominant Term: $m = 1, n = 1$.)

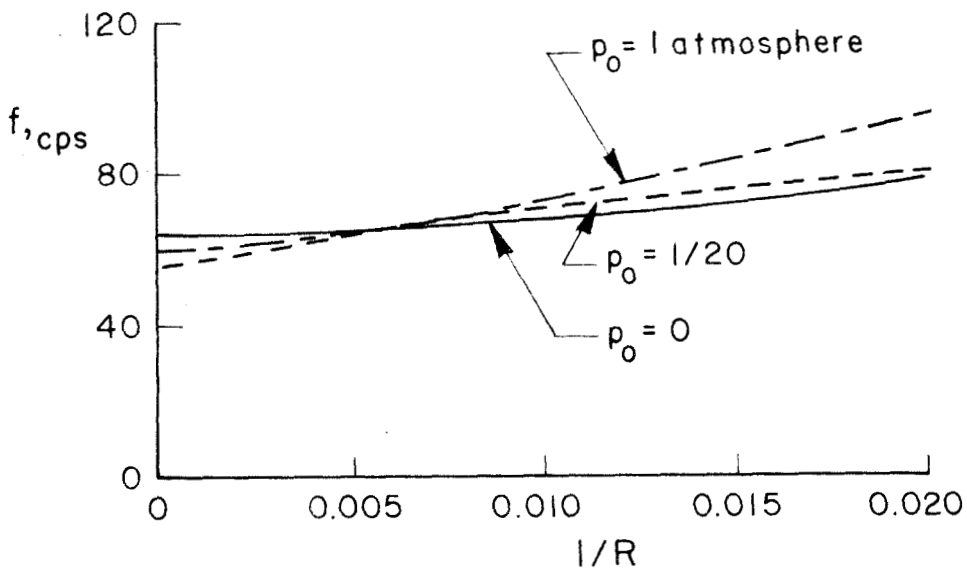


Fig. 35. Cavity Effect on Natural Frequencies of Curved Panels. Mode with Predominant Term: $m = 1, n = 3$.

II. CYLINDRICAL SHELLS WITH BOUNDARY LAYER

ABSTRACT

The effect of a boundary layer on the flutter of a cylindrical shell is studied. The aerodynamic forces are developed for a shell of infinite length. The boundary layer is idealized as an annular region of uniform subsonic flow surrounding the shell. This boundary layer is of constant thickness along the shell and has a constant velocity distribution through its thickness. The external supersonic flow is also taken to be of uniform velocity, resulting in a "stepped" velocity profile through the boundary layer. Small perturbation theory is used in the boundary layer region and linear piston theory is used for the supersonic flow.

In order to replace a physical boundary layer with an idealization for calculations, a procedure is developed for choosing the boundary layer parameters of velocity, pressure, etc. in a consistent way.

The forces which are found through this boundary layer theory are compared with those obtained using piston theory directly. It is found that the forces on a mode with many circumferential waves are much smaller than the forces given by piston theory -- a reduction in amplitude of 95 per cent is possible. Phase changes also occur. The effect of the boundary layer on axisymmetric modes is not so great.

Flutter boundaries are obtained for axisymmetric flutter under several conditions and illustrate the effect of boundary layer thickness and structural damping.

TABLE OF CONTENTS

PART II

Section	Page
Abstract	72
Table of Contents	73
List of Figures	74
List of Symbols	75
Introduction	79
1. Aerodynamic Forces on a Cylinder with an Idealized Boundary Layer	80
1.1. Surface Pressure for a Sinusoidal Upwash Distribution	81
1.1.1. Boundary Conditions	83
1.1.2. Solution	85
1.1.3. Surface Pressure	89
1.1.4. Interface Displacement	91
1.2. Surface Pressure for a System of Standing Waves	92
2. Choice of Parameters for the Idealized Boundary Layer	94
3. Comparison of Forces with Linear Piston Theory	98
4. Axisymmetric Flutter of a Finite Cylinder with Boundary Layer	102
5. Conclusions	111
References	113
Table	114

LIST OF FIGURES

Figure		Page
1	Coordinate System.	116
2	Effect of Circumferential Waves on Force Amplitudes.	117
3	Effect of Circumferential Waves on Force Phase Angles.	118
4	Effect of Circumferential Waves for Very Thin Boundary Layer.	119
5	Effect of Axial Waves on Force Amplitudes.	120
6	Effect of Axial Waves on Force Phase Angles.	121
7	Effect of Frequency on Force Amplitudes.	122
8	Effect of Frequency on Force Phase Angles.	123
9	Effect of Frequency on Force Amplitudes.	124
10	Effect of Frequency on Force Phase Angles.	125
11	Effect of the Choice of M_0 on Force Amplitudes.	126
12	Effect of the Choice of M_0 on Force Phase Angles.	127
13	Thickness Ratio Required to Prevent Flutter for a Copper Cylinder at Sea Level.	128
14	Thickness Ratio Required to Prevent Flutter for a Copper Cylinder at 50,000 feet.	129
15	Effect of Structural Damping in Addition to a Typical Boundary Layer.	130
16	Effect of the Choice of M_0 on a Typical Flutter Point.	131

LIST OF SYMBOLS

A	$\frac{\rho U^2 L^3}{MD}$
A_1, A_2	Force amplitudes, see equation 36
a, a_6	Speeds of sound for free stream and idealized boundary layer
B_1, B_2, C_1, C_2	Constants, see page 82
b, c, d	Constants in equation 10
D	Bending rigidity, $\frac{Eh^3}{12(1-\nu^2)}$
E	Modulus of elasticity of shell material
F_1, F_2	Constants, see page 88
g	Structural damping
h	Shell thickness
i	$\sqrt{-1}$
$J_m(x)$	Bessel function of the first kind
$K_1, K_2, \dots K_8$	Constants in equations 42 and 43
k	Reduced frequency, $\frac{\omega L}{U}$
k_6	Reduced frequency, $\frac{\omega L}{U_6}$
L	Cylinder length
M, M_6	Mach numbers
m	Number of axial half-waves
N	Number of modes used in flutter equations
N_x, N_θ	Membrane stress resultants, force per unit length

n	Number of circumferential waves
P	Flutter matrix
$\bar{p}(x, r, \theta, t)$	Perturbation pressure
$p^*(x, r, \theta, t)$	Perturbation pressure, see equation 21
p, p_0	Static pressures
R	Cylinder radius
R	Gas constant
r	Radial coordinate
T, T_0	Temperatures
T_x, T_θ	Dimensionless stresses, see equation 50
t	Time
U, U_0	Velocities
$u(x, t)$	Shell displacement in the x direction
$v(y)$	Velocity in the physical boundary layer
$w(x, r, \theta, t)$	Upwash
w_0	Constant
x	Axial coordinate
$Y_m(x)$	Bessel function of the second kind
y	$r - R$, distance from cylinder surface
$z(x, \theta, t)$	Shell displacement in the r direction, positive outward
z_0	Constant
$\bar{z}(x, \theta, t)$	Interface displacement in the r direction
$[\alpha_1]_{mn}, [\alpha_2]_{mn}$	Constants, see equations 22 and 23

β	$\sqrt{1 - M^2}$
$[\beta_1]_{mn}, [\beta_2]_{mn}$	Constants, see equations 24 and 25
Γ_{mn}, Δ_{mn}	Constants, see equations 29 and 30
γ	Ratio of specific heats
δ	Idealized boundary layer thickness
δ'	$\frac{M_\delta \delta}{\beta L}$
$\bar{\delta}$	Actual boundary layer thickness
δ_{ij}	Kronecker delta
$\epsilon(x)$	Error involved in Galerkin's method, equation 49
η	Transformed coordinate $\frac{M_\delta r}{\beta L}$
η_0	$\frac{M_\delta R}{\beta L}$
η_1	$\frac{M_\delta (R + \delta)}{\beta L}$
$\bar{\eta}_{qm}$	See equation 50
θ	Angular coordinate
Λ	Eigenvalue of the axisymmetric flutter equations
λ	$\frac{e_s h \omega^2 L^4}{D}$
λ_1, λ_2	Constants, see equation 11
μ_1, μ_2	Constants, page 82
ν	Poisson's ratio

ξ	Transformed coordinate, $\frac{M_\delta x}{\beta^2 L}$
e, e_δ	Air densities
e_s	Shell density
τ	Transformed coordinate, $\frac{U_\delta t}{L} + \frac{M_\delta^2 x}{\beta^2 L}$
$\phi(x, r, \theta, t)$	Velocity potential in the boundary layer region
ϕ_1, ϕ_2	Force phase angles, see equation 36
ψ_0	Constant in equation 9
ω	Frequency, radians per second

INTRODUCTION

One of the most interesting and current topics in the field of panel flutter is the flutter of cylindrical shells. It has been found that the thin outer skin of a missile will flutter when subjected to a supersonic flow of sufficient speed directed along the cylinder axis.

A number of theories have been advanced for cylinder flutter, but recent wind tunnel tests have shown that they are too conservative; i. e., they require that a cylinder be made stiffer than is actually necessary to prevent flutter.

One possible cause for the difference between experiment and theory is the viscous boundary layer, which has been neglected in the past, except for the work by Miles (Ref. 1). He considered the case of small wave length traveling waves on an infinite cylinder. Another possible source of error has been the omission of membrane inertia forces in the cylinder equations. Voss (Ref. 2) has studied the membrane inertia forces. He indicates that they may have a significant effect.

It was decided to investigate the effect of the boundary layer by starting with a simple theory. In this way it is possible to carry the problem through to the point where flutter boundaries are obtained. More refined theories may be developed in the future.

The boundary layer is idealized as an annular region of uniform subsonic flow surrounding the cylinder. Furthermore, it is assumed that the cylinder is infinitely long. In this way, the aerodynamic forces resulting from a system of standing waves on the cylinder surface can be found. Also, a procedure is developed for choosing the

the parameters M_δ , ρ_δ , U_δ , which characterize the idealized boundary layer.

Once the aerodynamic forces are obtained for an infinite cylinder, these results are applied as an approximation to the forces on a cylinder of finite length. Galerkin's method is used to set up the eigenvalue problem for the case of axisymmetric flutter. The effects of membrane inertia, membrane stresses, and structural damping are included.

Flutter boundaries are presented for the axisymmetric flutter of a cylinder with boundary layer and structural damping, but no numerical work is done on the effect of membrane inertia and membrane stresses.

1. Aerodynamic Forces on a Cylinder with an Idealized Boundary Layer

Consider an infinitely long cylinder of radius R immersed in a uniform supersonic flow along the cylinder axis. The boundary layer on the cylinder will be idealized as a subsonic layer of constant thickness δ and uniform velocity U_δ , as shown in figure 1.

A similar case has been worked out for the steady flow along an infinite axisymmetric body by Des Ciers and Chang (Ref. 3). We will consider the more general case where the cylinder surface oscillates harmonically in a sinusoidal standing wave pattern, with waves in both the axial and circumferential directions.

The fluid flow in the boundary layer is assumed to be inviscid and irrotational. Small perturbation theory will be used in this region.

With the restriction that disturbances at the cylinder wall must be small, the linearized equation for the velocity potential within the boundary layer is

$$\frac{1}{a_6^2} \frac{\partial^2 \phi_6}{\partial t^2} + 2 \frac{M_6}{a_6} \frac{\partial^2 \phi_6}{\partial x \partial t} - \beta^2 \frac{\partial^2 \phi_6}{\partial x^2} = \frac{\partial^2 \phi_6}{\partial r^2} + \frac{1}{r} \frac{\partial \phi_6}{\partial r} + \frac{1}{r^2} \frac{\partial^2 \phi_6}{\partial \theta^2} \quad (1)$$

where $\beta^2 = 1 - M_6^2$.

Linear piston theory will be used for the aerodynamic force on the outer surface of the interface at $r = R + \delta$.

1.1. Surface Pressure for a Sinusoidal Downwash Distribution

We will solve the problem corresponding to the upwash

$$w(x, R, \theta, t) = w_0 \sin \frac{m\pi x}{L} \cos n \theta e^{i\omega t} \quad (2)$$

When the aerodynamic force corresponding to this upwash is found, the force resulting from a cylinder oscillation of the form

$$z(x, \theta, t) = \sum_{m=1}^{\infty} \sum_{n=0}^{\infty} \left(a_{mn} \sin \frac{m\pi x}{L} + b_{mn} \cos \frac{m\pi x}{L} \right) \cos n \theta e^{i\omega t}$$

can be found by superposition.

Using the transformation

$$\tau = \frac{U_6}{L} t + \frac{M_6^2}{\beta^2} \frac{x}{L} \quad \xi = \frac{M_6}{\beta^2} \frac{x}{L} \quad \eta = \frac{M_6 t}{\beta L} \quad \theta = \theta ,$$

equation 1 becomes

$$\frac{\partial^2 \phi_6}{\partial \tau^2} = \frac{\partial^2 \phi_6}{\partial \xi^2} + \frac{\partial^2 \phi_6}{\partial \eta^2} + \frac{1}{\eta} \frac{\partial \phi_6}{\partial \eta} + \frac{1}{\eta^2} \frac{\partial^2 \phi_6}{\partial \theta^2} . \quad (3)$$

This equation has solutions of the form

$$\bar{\Phi}_6(\xi, \eta, \theta, \tau) = e^{ik_6 \tau} e^{\pm i\lambda \xi} \cos n \theta \begin{Bmatrix} J_n(\mu \eta) \\ Y_n(\mu \eta) \end{Bmatrix} ,$$

where $\mu^2 = k_6^2 - \lambda^2$ and where $J_n(\mu \eta)$ and $Y_n(\mu \eta)$ are Bessel functions of the 1st and 2nd kind.

It will be shown that the boundary conditions for the problem can be satisfied by the following choice of ϕ_6 :

$$\begin{aligned} \bar{\Phi}_6(\xi, \eta, \theta, \tau) = e^{ik_6 \tau} \cos n \theta & \left\{ e^{-i\lambda_1 \xi} \left[C_1 J_n(\mu_1 \eta) + B_1 Y_n(\mu_1 \eta) \right] \right. \\ & \left. - e^{i\lambda_2 \xi} \left[C_2 J_n(\mu_2 \eta) + B_2 Y_n(\mu_2 \eta) \right] \right\} \end{aligned}$$

where λ_1 and λ_2 are constants to be determined later and

$$\mu_1 = \sqrt{k_6^2 - \lambda_1^2} \quad \mu_2 = \sqrt{k_6^2 - \lambda_2^2} .$$

Returning to physical coordinates,

$$\Phi_6(x, r, \theta, t) = \bar{\Phi}_6(\xi(x), \eta(r), \theta, \tau(t, x)) = e^{i\omega t} \cos n \theta \left\{ e^{i(\lambda_1 - k_6 M_6)} \frac{M_6 x}{\beta^2 L} \left[C_1 J_n\left(\mu_1 \frac{M_6 r}{\beta L}\right) + B_1 Y_n\left(\mu_1 \frac{M_6 r}{\beta L}\right) \right] - e^{i(\lambda_2 + k_6 M_6)} \frac{M_6 x}{\beta^2 L} \left[C_2 J_n\left(\mu_2 \frac{M_6 r}{\beta L}\right) + B_2 Y_n\left(\mu_2 \frac{M_6 r}{\beta L}\right) \right] \right\} . \quad (4)$$

We will use the physical variables x, r, θ, t for the remainder of the problem.

1.1.1. Boundary Conditions

There are three boundary conditions. They will be applied at the mean positions of the cylinder wall and the interface. At the wall, the upwash condition is

$$\frac{\partial \Phi_6}{\partial r}(x, R, \theta, t) = w_0 \sin \frac{m\pi x}{L} \cos n \theta e^{i\omega t} . \quad (5)$$

The assumption of the existence of an interface implies the separation of the fluid particles in the two flow regions,

$$\frac{\partial \Phi_6}{\partial r}(x, R + \delta, \theta, t) = \frac{\partial \bar{\xi}(x, \theta, t)}{\partial t} + U_6 \frac{\partial \bar{\xi}(x, \theta, t)}{\partial x} . \quad (6)$$

It is also necessary that the pressure be continuous across the interface. Linear piston theory is used at the outer surface of the interface.

$$-e_6 \left[\frac{\partial \Phi_6}{\partial t}(x, R + \delta, \theta, t) + U_6 \frac{\partial \Phi_6}{\partial x}(x, R + \delta, \theta, t) \right] = \frac{\rho U}{M} \left[\frac{\partial \bar{\xi}(x, \theta, t)}{\partial t} + U \frac{\partial \bar{\xi}(x, \theta, t)}{\partial x} \right] \quad (7)$$

Equations 5, 6, and 7 constitute the boundary conditions. They can be written in more usable form if equation 6 is used to eliminate \bar{z} from equation 7. We will then have two equations expressing boundary conditions on ϕ_δ and one equation giving \bar{z} as a function of ϕ_δ .

If $\bar{z} \sim e^{i\omega t}$, then equation 6 becomes

$$\frac{\partial \phi_\delta}{\partial r}(x, R+\delta, \theta, t) = i\omega \bar{z}(x, \theta, t) + U_\delta \frac{\partial \bar{z}(x, \theta, t)}{\partial x} \quad (8)$$

We may solve for \bar{z} to get

$$\bar{z}(x, \theta, t) = \frac{1}{U_\delta} e^{-i\omega \frac{x}{U_\delta}} \int_{\psi_0}^x \frac{\partial \phi_\delta}{\partial r}(\psi, R+\delta, \theta, t) e^{i\omega \frac{\psi}{U_\delta}} d\psi \quad (9)$$

The integral is to be viewed as an integral of the complex variable ψ , with a complex constant ψ_0 which will be determined later. Since the explicit form of $\frac{\partial \phi_\delta}{\partial r}$ is known from equation 4, it can be seen that the integrand is an analytic function of ψ on the entire ψ plane.

Inserting equation 9 into equation 7, we have

$$\begin{aligned} \frac{\partial \phi_\delta}{\partial r}(x, R+\delta, \theta, t) + b \phi_\delta(x, R+\delta, \theta, t) + c \frac{\partial \phi_\delta}{\partial x}(x, R+\delta, \theta, t) \\ + d e^{-i\omega \frac{x}{U_\delta}} \int_{\psi_0}^x \frac{\partial \phi_\delta}{\partial r}(\psi, R+\delta, \theta, t) e^{i\omega \frac{\psi}{U_\delta}} d\psi = 0 \quad (10) \end{aligned}$$

where

$$b = i \left(\frac{\rho_6}{\rho} \right) M \left(\frac{U_6}{U} \right)^2 \frac{k_6}{L} ,$$

$$c = \frac{\rho_6}{\rho} \left(\frac{U_6}{U} \right)^2 M ,$$

and

$$d = i \left[\frac{U_6}{U} - 1 \right] \frac{k_6}{L} .$$

The problem has been resolved to the solution of the differential equation 1 under the boundary conditions 5 and 10. The interface displacement is given by equation 9.

1.1.2. Solution

Boundary condition 5 requires that

$$e^{-i(\lambda_1 - k_6 M_6) \frac{M_6 x}{\beta^2 L}} \cdot \mu_1 \left[C_1 J'_n \left(\mu_1 \frac{M_6 R}{\beta L} \right) + B_1 Y'_n \left(\mu_1 \frac{M_6 R}{\beta L} \right) \right] \quad (11)$$

$$- e^{-i(\lambda_2 + k_6 M_6) \frac{M_6 x}{\beta^2 L}} \cdot \mu_2 \left[C_2 J'_n \left(\mu_2 \frac{M_6 R}{\beta L} \right) + B_2 Y'_n \left(\mu_2 \frac{M_6 R}{\beta L} \right) \right] = \frac{w_0 \beta L}{M_6 2i} \left[e^{i \frac{m \pi x}{L}} - e^{-i \frac{m \pi x}{L}} \right] .$$

This is satisfied if we take

$$\lambda_1 = \frac{m \pi \beta^2}{M_6} + k_6 M_6 ,$$

$$\lambda_2 = \frac{m \pi \beta^2}{M_6} - k_6 M_6 ,$$

$$C_1 = \frac{1}{J'_n(\mu_1 \eta_0)} \left[\frac{w_0 \beta L i}{2 M_6 \mu_1} - B_1 Y'_n(\mu_1 \eta_0) \right] ,$$

and

$$C_2 = \frac{1}{J_n'(\mu_2 \eta_0)} \left[\frac{w_0 \beta L i}{2 M_6 \mu_2} - B_2 Y_n'(\mu_2 \eta_0) \right],$$

where $\eta_0 = \frac{M_6 R}{\beta L}$.

We may now rewrite ϕ_6 , redefining the arbitrary constants B_1 and B_2 .

$$\begin{aligned} \phi_6(x, r, \theta, t) = \frac{w_0 \beta L i}{2 M_6} e^{i \omega t} \cos n \theta & \left\{ \frac{e^{-i \frac{m \pi x}{L}}}{\mu_1 J_n'(\mu_1 \eta_0)} \left[J_n\left(\mu_1 \frac{M_6 r}{\beta L}\right) + B_1 \left(Y_n\left(\mu_1 \frac{M_6 r}{\beta L}\right) - \frac{Y_n'(\mu_1 \eta_0)}{J_n'(\mu_1 \eta_0)} J_n\left(\mu_1 \frac{M_6 r}{\beta L}\right) \right) \right] \right. \\ & \left. - \frac{e^{-i \frac{m \pi x}{L}}}{\mu_2 J_n'(\mu_2 \eta_0)} \left[J_n\left(\mu_2 \frac{M_6 r}{\beta L}\right) + B_2 \left(Y_n\left(\mu_2 \frac{M_6 r}{\beta L}\right) - \frac{Y_n'(\mu_2 \eta_0)}{J_n'(\mu_2 \eta_0)} J_n\left(\mu_2 \frac{M_6 r}{\beta L}\right) \right) \right] \right\} \end{aligned} \quad (12)$$

Boundary condition 10 may now be applied. Substituting ϕ_6 from equation 12 into equation 10, and cancelling a common factor

$\frac{w_0 \beta L i}{2 M_6} e^{i \omega t} \cos n \theta$, we obtain

$$\begin{aligned} e^{-i \frac{m \pi x}{L}} & \left\{ \frac{F_1}{J_n'(\mu_1 \eta_0)} \left[J_n'(\mu_1 \eta_1) + B_1 \left(Y_n'(\mu_1 \eta_1) - \frac{Y_n'(\mu_1 \eta_0)}{J_n'(\mu_1 \eta_0)} J_n'(\mu_1 \eta_1) \right) \right] + \frac{b - i \frac{m \pi c}{L}}{\mu_1 J_n'(\mu_1 \eta_0)} \left[J_n(\mu_1 \eta_1) + B_1 \left(Y_n(\mu_1 \eta_1) - \frac{Y_n'(\mu_1 \eta_0)}{J_n'(\mu_1 \eta_0)} J_n(\mu_1 \eta_1) \right) \right] \right\} \\ - e^{-i \frac{m \pi x}{L}} & \left\{ \frac{F_2}{J_n'(\mu_2 \eta_0)} \left[J_n'(\mu_2 \eta_1) + B_2 \left(Y_n'(\mu_2 \eta_1) - \frac{Y_n'(\mu_2 \eta_0)}{J_n'(\mu_2 \eta_0)} J_n'(\mu_2 \eta_1) \right) \right] + \frac{b + i \frac{m \pi c}{L}}{\mu_2 J_n'(\mu_2 \eta_0)} \left[J_n(\mu_2 \eta_1) + B_2 \left(Y_n(\mu_2 \eta_1) - \frac{Y_n'(\mu_2 \eta_0)}{J_n'(\mu_2 \eta_0)} J_n(\mu_2 \eta_1) \right) \right] \right\} \\ - d \frac{M_6}{\beta i} e^{-i \omega \left(\frac{x}{v_6} - \frac{\psi_0}{v_6} \right)} & \left\{ \frac{e^{-i \frac{m \pi \psi_0}{L}}}{(K_6 - m \pi) J_n'(\mu_1 \eta_0)} \left[J_n'(\mu_1 \eta_1) + B_1 \left(Y_n'(\mu_1 \eta_1) - \frac{Y_n'(\mu_1 \eta_0)}{J_n'(\mu_1 \eta_0)} J_n'(\mu_1 \eta_1) \right) \right] \right. \\ & \left. - \frac{e^{-i \frac{m \pi \psi_0}{L}}}{(K_6 + m \pi) J_n'(\mu_2 \eta_0)} \left[J_n'(\mu_2 \eta_1) + B_2 \left(Y_n'(\mu_2 \eta_1) - \frac{Y_n'(\mu_2 \eta_0)}{J_n'(\mu_2 \eta_0)} J_n'(\mu_2 \eta_1) \right) \right] \right\} = 0, \end{aligned} \quad (13)$$

where $\eta_1 = \frac{M_\delta (R + \delta)}{\beta L}$. Because of the linear independence of the functions $e^{-i \frac{m\pi x}{L}}$, $e^{i \frac{m\pi x}{L}}$, and $e^{-i\omega \frac{x}{U_\delta}}$, each of the coefficients of these functions must vanish. Hence

$$B_1 = - \frac{F_1 J_n'(\mu, \eta_1) + \frac{1}{\mu_1} \left(b - i \frac{m\pi c}{L} \right) J_n(\mu, \eta_1)}{F_1 \left[Y_n'(\mu, \eta_1) - \frac{Y_n'(\mu, \eta_0)}{J_n'(\mu, \eta_0)} J_n'(\mu, \eta_1) \right] + \frac{1}{\mu_1} \left(b - i \frac{m\pi c}{L} \right) \left[Y_n(\mu, \eta_1) - \frac{Y_n'(\mu, \eta_0)}{J_n'(\mu, \eta_0)} J_n(\mu, \eta_1) \right]}, \quad (14)$$

$$B_2 = - \frac{F_2 J_n'(\mu_2, \eta_1) + \frac{1}{\mu_2} \left(b + i \frac{m\pi c}{L} \right) J_n(\mu_2, \eta_1)}{F_2 \left[Y_n'(\mu_2, \eta_1) - \frac{Y_n'(\mu_2, \eta_0)}{J_n'(\mu_2, \eta_0)} J_n'(\mu_2, \eta_1) \right] + \frac{1}{\mu_2} \left(b + i \frac{m\pi c}{L} \right) \left[Y_n(\mu_2, \eta_1) - \frac{Y_n'(\mu_2, \eta_0)}{J_n'(\mu_2, \eta_0)} J_n(\mu_2, \eta_1) \right]}, \quad (15)$$

and

$$e^{i 2\pi m \frac{y_0}{L}} = \frac{(k_\delta + m\pi)}{(k_\delta - m\pi)} \frac{J_n'(\mu_2, \eta_0) \left[J_n'(\mu, \eta_1) + B_1 \left(Y_n'(\mu, \eta_1) - \frac{Y_n'(\mu, \eta_0)}{J_n'(\mu, \eta_0)} J_n'(\mu, \eta_1) \right) \right]}{J_n'(\mu, \eta_0) \left[J_n'(\mu_2, \eta_1) + B_2 \left(Y_n'(\mu_2, \eta_1) - \frac{Y_n'(\mu_2, \eta_0)}{J_n'(\mu_2, \eta_0)} J_n'(\mu_2, \eta_1) \right) \right]} \quad (16)$$

where

$$F_1 = \frac{M_\delta}{\beta L} + \frac{M_\delta d}{\beta i(k_\delta - m\pi)} = \frac{M_\delta}{\beta L} \frac{\left(\frac{U_\delta}{U} k_\delta - m\pi\right)}{(k_\delta - m\pi)}$$

and

$$F_2 = \frac{M_\delta}{\beta L} + \frac{M_\delta d}{\beta i(k_\delta + m\pi)} = \frac{M_\delta}{\beta L} \frac{\left(\frac{U_\delta}{U} k_\delta + m\pi\right)}{(k_\delta + m\pi)}$$

These expressions for B_1 , B_2 and ψ_0 can be simplified by expanding the Bessel functions in Taylor series and keeping only the linear terms. To do this, it is necessary to assume that

$$\begin{aligned} |\mu_1 \delta'| &<< 1 \\ |\mu_2 \delta'| &<< 1 \end{aligned} ,$$

where $\delta' = \frac{M_\delta \delta}{\beta L}$. When written out in full, these inequalities become

$$\begin{aligned} \left| \left[k_\delta^2 M_\delta^2 - m^2 \pi^2 \beta^2 - 2m\pi k_\delta M_\delta^2 \right]^{\frac{1}{2}} \left(\frac{\delta}{L} \right) \right| &<< 1 \\ \left| \left[k_\delta^2 M_\delta^2 - m^2 \pi^2 \beta^2 + 2m\pi k_\delta M_\delta^2 \right]^{\frac{1}{2}} \left(\frac{\delta}{L} \right) \right| &<< 1 \end{aligned} .$$

This puts a condition on the boundary layer thickness ratio, reduced frequency and number of axial waves allowed.

After expanding the Bessel functions, recurrence relations among the functions and their derivatives are used. We obtain

$$B_1 = - \frac{n \left[J_{n-1}(\mu_1 \eta_0) - J_{n+1}(\mu_1 \eta_0) \right] \left[F_1 \left(1 - \frac{\delta'}{\eta_0} \right) + \left(b - i \frac{m\pi c}{L} \right) \delta' \right] + \left[J_{n-1}(\mu_1 \eta_0) + J_{n+1}(\mu_1 \eta_0) \right] \left[F_1 \left(\frac{\delta'^2}{\eta_0^2} - \mu_1^2 \delta' \eta_0 \right) + \left(b - i \frac{m\pi c}{L} \right) \eta_0 \right]}{\left[\left(Y_{n-1}(\mu_1 \eta_0) + Y_{n+1}(\mu_1 \eta_0) \right) - \left(Y_{n-1}(\mu_1 \eta_0) - Y_{n+1}(\mu_1 \eta_0) \right) \frac{(J_{n-1}(\mu_1 \eta_0) + J_{n+1}(\mu_1 \eta_0))}{(J_{n-1}(\mu_1 \eta_0) - J_{n+1}(\mu_1 \eta_0))} \right] \left[F_1 \left(\frac{\delta'^2}{\eta_0^2} - \mu_1^2 \delta' \eta_0 \right) + \left(b - i \frac{m\pi c}{L} \right) \eta_0 \right]} \quad (17)$$

$$B_2 = - \frac{n \left[J_{n-1}(\mu_2 \eta_0) - J_{n+1}(\mu_2 \eta_0) \right] \left[F_2 \left(1 - \frac{\delta'}{\eta_0} \right) + \left(b + i \frac{m\pi c}{L} \right) \delta' \right] + \left[J_{n-1}(\mu_2 \eta_0) + J_{n+1}(\mu_2 \eta_0) \right] \left[F_2 \left(\frac{\delta'^2}{\eta_0^2} - \mu_2^2 \delta' \eta_0 \right) + \left(b + i \frac{m\pi c}{L} \right) \eta_0 \right]}{\left[\left(Y_{n-1}(\mu_2 \eta_0) + Y_{n+1}(\mu_2 \eta_0) \right) - \left(Y_{n-1}(\mu_2 \eta_0) - Y_{n+1}(\mu_2 \eta_0) \right) \frac{(J_{n-1}(\mu_2 \eta_0) + J_{n+1}(\mu_2 \eta_0))}{(J_{n-1}(\mu_2 \eta_0) - J_{n+1}(\mu_2 \eta_0))} \right] \left[F_2 \left(\frac{\delta'^2}{\eta_0^2} - \mu_2^2 \delta' \eta_0 \right) + \left(b + i \frac{m\pi c}{L} \right) \eta_0 \right]} \quad (18)$$

$$e^{i2\pi m \frac{\psi}{L}} = \frac{(k_\delta + m\pi) \left(b - i \frac{m\pi c}{L} \right) \left[\eta_0 - \delta' - \frac{\delta'^2 n^2}{\eta_0} + \mu_1^2 \delta'^2 \eta_0 \right] \left[F_2 \left(\frac{\delta'^2}{\eta_0^2} - \mu_2^2 \delta' \eta_0 \right) + \left(b + i \frac{m\pi c}{L} \right) \eta_0 \right]}{(k_\delta - m\pi) \left(b + i \frac{m\pi c}{L} \right) \left[\eta_0 - \delta' - \frac{\delta'^2 n^2}{\eta_0} + \mu_2^2 \delta'^2 \eta_0 \right] \left[F_1 \left(\frac{\delta'^2}{\eta_0^2} - \mu_1^2 \delta' \eta_0 \right) + \left(b - i \frac{m\pi c}{L} \right) \eta_0 \right]} \quad (19)$$

1.1.3. Surface Pressure

The pressure at the cylinder wall is given by

$$\bar{p}(x, R, \theta, t) = - \rho_\delta \left[\frac{\partial \Phi_\delta}{\partial t}(x, R, \theta, t) + U_\delta \frac{\partial \Phi_\delta}{\partial x}(x, R, \theta, t) \right]$$

Using p^* to denote the pressure field resulting from the upwash $w(x, R, \theta, t) = w_0 e^{i\omega t} \cos n\theta \sin \frac{mnx}{L}$, we can insert ϕ_s from equation 12 into the above equation to obtain

$$p^*(x, R, \theta, t) = \frac{w_0 \rho_s \beta U_s}{2 M_s} e^{i\omega t} \cos n\theta \left\{ e^{-i \frac{mnx}{L}} \frac{(K_s - mn)}{\mu J_n'(\mu_1 \eta_0)} \left[J_n(\mu_1 \eta_0) + B_1 \left(\chi_n(\mu_1 \eta_0) - \frac{Y_n'(\mu_1 \eta_0)}{J_n'(\mu_1 \eta_0)} J_n(\mu_1 \eta_0) \right) \right] - e^{-i \frac{mnx}{L}} \frac{(K_s + mn)}{\mu J_n'(\mu_2 \eta_0)} \left[J_n(\mu_2 \eta_0) + B_2 \left(\chi_n(\mu_2 \eta_0) - \frac{Y_n'(\mu_2 \eta_0)}{J_n'(\mu_2 \eta_0)} J_n(\mu_2 \eta_0) \right) \right] \right\} \quad (20)$$

This can be written

$$p^*(x, R, \theta, t) = \frac{w_0 \rho_s \beta U_s}{2 M_s} e^{i\omega t} \cos n\theta \left\{ [\alpha_1]_{mn} e^{i \frac{mnx}{L}} - [\alpha_2]_{mn} e^{i \frac{mnx}{L}} \right\} \quad (21)$$

The constants $[\alpha_1]_{mn}$ and $[\alpha_2]_{mn}$ are defined by equation 20. They may be simplified through the same expansion of the Bessel functions as was used earlier. Interestingly, all Bessel functions cancel out and we are left with

$$[\alpha_1]_{mn} = (K_s - mn) \frac{\left[F_1 \left(-\frac{\delta'}{\eta_0} \right) + \left(b - i \frac{mn c}{L} \right) \delta' \right]}{\left[F_1 s' \left(\mu^2 - \eta_0^2 \right) - \left(b - i \frac{mn c}{L} \right) \right]} \quad (22)$$

and

$$[\alpha_2]_{mn} = (k_8 + m\pi) \frac{\left[F_2 \left(1 - \frac{\delta'}{\eta_0} \right) + \left(b + i \frac{m\pi c}{L} \right) \delta' \right]}{\left[F_2 \delta' \left(\mu_2^2 - \frac{n^2}{\eta_0^2} \right) - \left(b + i \frac{m\pi c}{L} \right) \right]} \quad (23)$$

1.1.4. Interface Displacement

Let us now calculate the interface displacement $\bar{z}(x, \theta, t)$ using equation 9. After integration and much simplification, we have

$$\bar{z}(x, \theta, t) = \frac{w_0 L}{2 U_8} e^{i\omega t} \cos n \theta \left\{ [\beta_1]_{mn} e^{i \frac{m\pi x}{L}} - [\beta_2]_{mn} e^{i \frac{m\pi x}{L}} \right. \\ \left. - [\beta_1]_{mn} e^{-i \left[K_8 \frac{x}{L} - (K_8 - m\pi) \frac{\psi_0}{L} \right]} + [\beta_2]_{mn} e^{i \left[K_8 \frac{x}{L} - (K_8 + m\pi) \frac{\psi_0}{L} \right]} \right\}$$

where

$$[\beta_1]_{mn} = \frac{\left(b - i \frac{m\pi c}{L} \right) \left[\eta_0 - \delta' - \delta'^2 \frac{n^2}{\eta_0^2} + \delta'^2 \mu_2^2 \eta_0 \right]}{(K_8 - m\pi) \left[F_2 \delta' \left(\frac{n^2}{\eta_0^2} - \mu_2^2 \eta_0 \right) + \eta_0 \left(b - i \frac{m\pi c}{L} \right) \right]} \quad (24)$$

$$[\beta_2]_{mn} = \frac{\left(b + i \frac{m\pi c}{L} \right) \left[\eta_0 - \delta' - \delta'^2 \frac{n^2}{\eta_0^2} + \delta'^2 \mu_2^2 \eta_0 \right]}{(K_8 + m\pi) \left[F_2 \delta' \left(\frac{n^2}{\eta_0^2} - \mu_2^2 \eta_0 \right) + \eta_0 \left(b + i \frac{m\pi c}{L} \right) \right]} \quad (25)$$

Equation 16, which defines ψ_0 , can be written as

$$e^{i2m\pi\frac{\psi_0}{L}} = \frac{[\beta_1]_{mn}}{[\beta_2]_{mn}}.$$

The last two terms in $\bar{z}(x, \theta, t)$ cancel when this expression for ψ_0 is used, leaving

$$\bar{z}(x, \theta, t) = \frac{w_0 L}{2U_0} e^{i\omega t} \cos n \theta \left\{ [\beta_1]_{mn} \bar{e}^{i\frac{m\pi x}{L}} - [\beta_2]_{mn} e^{i\frac{m\pi x}{L}} \right\}. \quad (26)$$

This completes the problem for the case of a sinusoidal upwash distribution.

1.2. Surface Pressures for a System of Standing Waves

We will now find the surface pressure $\bar{p}(x, R, \theta, t)$ at the cylinder wall for a general system of standing waves by using superposition. In the preceding sections it was shown that an upwash $w(x, R, \theta, t) = w_0 e^{i\omega t} \cos n \theta \sin \frac{m\pi x}{L}$ caused a pressure $\bar{p}(x, r, \theta, t) = p^*(x, r, \theta, t)$. Because of the physical nature of the problem, shifting the upwash by an x distance of $\frac{L}{2m}$ merely shifts the pressure field by the same amount. Hence an upwash $w(x, R, \theta, t) = w_0 e^{i\omega t} \cos n \theta \sin \frac{m\pi}{L} (x + \frac{L}{2m})$ generates a pressure $\bar{p}(x, r, \theta, t) = p^*(x + \frac{L}{2m}, r, \theta, t)$.

If the deflection pattern is given as

$$z(x, \theta, t) = \sum_{m=1}^{\infty} \sum_{n=0}^{\infty} a_{mn} e^{i\omega t} \cos n \theta \sin \frac{m\pi x}{L},$$

the upwash at the surface of the shell is

$$w(x, R, \theta, t) = \frac{\partial z(x, \theta, t)}{\partial t} + U_\delta \frac{\partial z(x, \theta, t)}{\partial x} \quad (27)$$

$$= \sum_{m=1}^{\infty} \sum_{n=0}^{\infty} a_{mn} \left[\frac{i\omega}{w_0} (w_0 e^{i\omega t} \cos n \theta \sin \frac{m\pi x}{L}) + \frac{U_\delta m\pi}{L w_0} (w_0 e^{i\omega t} \cos n \theta \sin \frac{m\pi}{L} (x + \frac{L}{2m})) \right].$$

The identity $\cos \frac{m\pi x}{L} = \sin (\frac{m\pi x}{L} + \frac{\pi}{2})$ was used in the last equation.

The pressure corresponding to the upwash of equation 27 is therefore

$$\bar{p}(x, R, \theta, t) = \sum_{m=1}^{\infty} \sum_{n=0}^{\infty} a_{mn} \left[\frac{i\omega}{w_0} p^*(x, R, \theta, t) + \frac{U_\delta m\pi}{L w_0} p^*(x + \frac{L}{2m}, R, \theta, t) \right].$$

Introducing the expression for $p^*(x, R, \theta, t)$ from equation 21, we have

$$\bar{p}(x, R, \theta, t) = \sum_{m=1}^{\infty} \sum_{n=0}^{\infty} \frac{\rho U^2}{ML} a_{mn} e^{i\omega t} \cos n \theta \left[\Gamma_{mn} \cos \frac{m\pi x}{L} + \Delta_{mn} \sin \frac{m\pi x}{L} \right], \quad (28)$$

where

$$\Gamma_{mn} = \left[i [\alpha_1]_{mn} (k_\delta - m\pi) - i [\alpha_2]_{mn} (k_\delta + m\pi) \right] \left(\frac{\rho_\delta}{\rho} \right) \left(\frac{U_\delta}{U} \right)^2 \left(\frac{M}{M_\delta} \right) \frac{\beta}{2} \quad (29)$$

and

$$\Delta_{mn} = \left[[\alpha_1]_{mn}(k_\delta - mn) + [\alpha_2]_{mn}(k_\delta + mn) \right] \left(\frac{\rho_\delta}{e} \right) \left(\frac{U_\delta}{U} \right)^2 \left(\frac{M}{m_\delta} \right) \frac{\beta}{2} \quad (30)$$

Equation 28 will provide the aerodynamic loading to be used in the cylinder flutter equations of Part 4.

The dimensionless variables Γ_{mn} and Δ_{mn} are functions of $m, n, M, M_\delta, k_\delta, \left(\frac{U_\delta}{U}\right), \left(\frac{\rho_\delta}{e}\right), \left(\frac{R}{L}\right)$, and $\left(\frac{\delta}{R}\right)$.

2. Choice of Parameters for the Idealized Boundary Layer

In order to make use of the aerodynamic forces of the previous section, it is necessary to develop a scheme for replacing a physical boundary layer with an appropriate idealized boundary layer. At first glance it might appear that this would be a hopelessly arbitrary procedure. In addition to the fact that an idealized boundary layer of constant thickness has been chosen to represent a growing boundary layer, a number of parameters must be chosen. Although nothing can be done in this theory to allow boundary layer growth, it is possible to choose the idealized boundary layer parameters in a consistent way which helps to minimize arbitrariness.

All of the following work is based on steady, flat plate boundary layer theory. The small perturbations of $M_\delta, \rho_\delta, T_\delta, U_\delta$ and p_δ are negligible in comparison with the quantities themselves.

For clarity, assume that the physical problem has been defined. A cylinder of finite length and fixed geometry is exposed to a supersonic

flow of given M, U, ρ, T and p . Consider the case where the boundary layer is turbulent and where the ratio of boundary layer thickness to cylinder radius is small enough that flat plate boundary layer theory can be used. A typical cross section of the cylinder is chosen to represent the physical case. Let the boundary layer thickness at this cross section be called δ , where δ is defined as the distance from the cylinder surface at which the flow is 99 per cent of free stream velocity.

For the idealized boundary layer, the parameters $M_\delta, U_\delta, \rho_\delta, T_\delta, p_\delta$, and δ must be found. Five relations among the six variables can be prescribed using various physical arguments, leaving only one independent variable. It is convenient to let M_δ be the independent variable and solve for the others as functions of M_δ .

First of all, the equation of state and the isentropic speed of sound will be used in both regions

$$p = \rho R T \quad (31)$$

and

$$a = \frac{U}{M} = \sqrt{\gamma R T} \quad (32)$$

For a steady boundary layer which is thin and growing slowly we may take, according to reference 4,

$$p_\delta = p \quad (33)$$

A condition on U_δ can be found by requiring that the loss in volume flow through the idealized boundary layer be the same as the loss in volume flow through the actual boundary layer. If we define y as the distance from the wall and let $v(y)$ be the velocity distribution in the actual boundary layer, then

$$(U - U_\delta) \delta = \int_0^{\bar{\delta}} [U - v(y)] dy . \quad (34)$$

It should be noted that for the special case $U_\delta = 0$ and $\varrho =$ constant, δ becomes the familiar displacement boundary layer thickness. For a turbulent boundary layer on a flat plate, the velocity profile can be taken, according to reference 5, as

$$v(y) = U \left(\frac{y}{\delta} \right)^{\frac{1}{7}} ,$$

so that equation 34 becomes

$$\frac{U_\delta}{U} = 1 - \frac{1}{8} \frac{\bar{\delta}}{\delta} . \quad (34a)$$

Prescribing a condition on the temperature in the boundary layer is difficult. There seems to be no "averaging" law applicable to this case. Let us take T_δ to be equal to the adiabatic wall temperature, the hottest temperature obtained in the physical boundary layer. For a turbulent boundary layer with recovery factor of 0.89,

$$T_\delta = T_{aw} = T \left[1 + 0.89 \left(\frac{\gamma-1}{2} \right) M^2 \right] . \quad (35)$$

Taking $\gamma = 1.4$, this gives

$$\frac{T_6}{T} = [1 + 0.178 M^2] \quad .$$

Also,

$$\frac{M_6}{M} = \frac{U_6}{U} \sqrt{\frac{T}{T_6}} = \left(1 - \frac{1}{8} \frac{\bar{\delta}}{\delta}\right) \frac{1}{\sqrt{1 + 0.178 M^2}} \quad .$$

Solving for $\frac{\bar{\delta}}{\delta}$, we have

$$\frac{\bar{\delta}}{\delta} = 8 \left[1 - \frac{M_6}{M} \sqrt{1 + 0.178 M^2} \right] \quad .$$

Knowing $\frac{\bar{\delta}}{\delta}$ as a function of M and M_6 , we can rewrite equation 34a as

$$\frac{U_6}{U} = \frac{M_6}{M} \sqrt{1 + 0.178 M^2} \quad .$$

The equation of state gives

$$\frac{\rho_6}{\rho} = \frac{p_6 T}{p T_6} = \frac{T}{T_6} = \frac{1}{[1 + 0.178 M^2]} \quad .$$

All parameters have been determined as functions of M and M_6 .

In summary, given a turbulent, thin, slowly growing boundary layer on a cylinder in a supersonic flow of Mach number M , we may construct an idealized boundary layer through the following steps:

a) Arbitrarily choose a subsonic M_6

b) $\frac{p_6}{p} = 1$

c) $\frac{T_6}{T} = 1 + 0.178 M^2$

$$d) \quad \frac{p_6}{p} = \frac{1}{1 + 0.178 M^2}$$

$$e) \quad \frac{U_6}{U} = \frac{M_6}{M} \sqrt{1 + 0.178 M^2}$$

$$f) \quad \frac{\delta}{\bar{\delta}} = \frac{1}{8 \left[1 - \frac{M_6}{M} \sqrt{1 + 0.178 M^2} \right]}$$

The effect of the choice of M_6 can be studied by constructing several different idealized boundary layers to represent the same physical case. This will be done in the next section.

As soon as M_6 is chosen, the representation scheme is fixed. When data are given in the following sections, for instance the flutter boundary curves, the value M_6 is held constant for all data points. This is only one possible way to compare data at different M and $\frac{\bar{\delta}}{R}$. More generally, M_6 might be taken as a function of M and $\frac{\bar{\delta}}{R}$.

3. Comparison of Forces with Linear Piston Theory

Before using the boundary layer theory in flutter equations, it is of interest to study the forces generated by this theory and to compare them with linear piston theory. This comparison is particularly useful because much of the research on cylinder flutter has been carried out using linear piston theory. It also provides a check on the present results due to the use of linear piston theory as the force at the interface.

Given a cylinder wall displacement

$$z = z_0 e^{i\omega t} \cos n \theta \sin \frac{m\pi x}{L} ,$$

boundary layer theory gives a surface pressure as in equation 28. This may be rewritten as

$$\bar{p}(x, \theta, t) = \frac{z_0 \rho U^2}{ML} \cos n \theta \left[A_1 e^{i(\omega t + \phi_1)} \cos \frac{m\pi x}{L} + A_2 e^{i(\omega t + \phi_2)} \sin \frac{m\pi x}{L} \right] , \quad (36)$$

where Γ_{mn} and Δ_{mn} have been written in polar form as

$$\Gamma_{mn} = A_1 e^{i\phi_1}$$

$$\Delta_{mn} = A_2 e^{i\phi_2}$$

For a cylinder with no boundary layer and the same wall displacement as above, piston theory gives

$$\bar{p}(x, \theta, t) = \frac{z_0 \rho U^2}{ML} \cos n \theta \left[m\pi e^{i\omega t} \cos \frac{m\pi x}{L} + k e^{i(\omega t + \frac{\pi}{2})} \sin \frac{m\pi x}{L} \right] . \quad (37)$$

We can now compare the surface forces on a cylinder with and without a boundary layer, using equations 36 and 37.

The constants A_1 , A_2 , ϕ_1 , and ϕ_2 could be written as functions of $m, n, M, M_\delta, k, \frac{R}{L}, \frac{\delta}{R}, \frac{U_\delta}{U}$, and $\frac{e_\delta}{e}$; however, using the results of the idealization scheme, we can express them as functions of

the seven variables $m, n, M, M_\delta, k, \frac{R}{L}$, and $\frac{\bar{\delta}}{R}$. This is still such an imposing list of variables that we will restrict ourselves to the case where

$$M = 3.5,$$

$$M_\delta = 0.5,$$

$$\frac{R}{L} = 0.5.$$

(Let us observe at this time that we are actually carrying one redundant variable. The axial wave length of the cylinder deflection pattern could have been fully defined by using L as the wave length. In this way, m would not have been needed. However, for convenience, we will consider L to be a fixed length and use the index m to indicate the number of axial half waves contained in that length. This approach is advantageous in the formulation of the flutter problem to be carried out later.)

We will now look at the changes in the forces on the shell as the parameters m, n, k , and $\frac{\bar{\delta}}{R}$ are varied. The effect of the circumferential wave number n is perhaps the simplest. Figures 2, 3, and 4 show that increasing the number of circumferential waves essentially intensifies the boundary layer thickness effect, causing the same results for a thinner boundary layer. These figures are given for $m = 1$. When m is higher, increasing the number of circumferential waves has a similar effect. The reduction in amplitude of the forces is very apparent for the case $n = 22$.

Increasing the axial wave number m also tends to increase the boundary layer effect, as is seen in figures 5 and 6. Again, a large reduction in forces is possible. The case shown is for $n = 0$, i. e. an axisymmetric mode.

The role played by frequency is rather complicated. Figures 7, 8, 9, and 10 show that the boundary layer effect is not as large at higher frequencies as it is at low frequencies. For this reason, the boundary layer will probably have less effect on axisymmetric flutter than on flutter with many circumferential waves, the latter usually occurring at a lower frequency.

In all cases above, it should be noted that as $\frac{\bar{\delta}}{R} \rightarrow 0$, the forces become identical with linear piston theory. Since piston theory was used at the outer surface of the interface, this is a reasonable result. It is also possible to see that the piston theory forces are recovered as $\frac{\bar{\delta}}{R} \rightarrow 0$ directly from equation 36 and the definitions of Γ_{mn} and Δ_{mn} . These constants are continuous functions of $\frac{\bar{\delta}}{R}$. If $\frac{\bar{\delta}}{R} \rightarrow 0$ for a given idealization scheme, then $\frac{\delta}{R} \rightarrow 0$ also, and

$$\lim_{\frac{\delta}{R} \rightarrow 0} \Gamma_{mn} = m\pi \quad ,$$

$$\lim_{\frac{\delta}{R} \rightarrow 0} \Delta_{mn} = ik \quad .$$

As a result, equation 36 becomes identical with equation 37.

Finally, let us consider the effect of the arbitrary choice of M_δ . Forces for several different modes are plotted in figures 11 and 12. Unfortunately, varying M_δ causes large changes in the forces for the cases where $m = 10$. It was hoped that the boundary layer idealization scheme would prevent this. For $m = 1$ the results look

better, however. In the next section, flutter work will be done for the axisymmetric case, $n = 0$. Ten modes will be used, i. e. $m = 1$ through 10. Hence, it is expected that the flutter results will depend on the choice of M_8 .

4. Axisymmetric Flutter of a Finite Cylinder with Boundary Layer

The aerodynamic forces developed in the previous sections are for an infinitely long cylinder. Let us consider the flutter of an unstiffened cylinder of constant thickness and finite length L and use the boundary layer theory as an approximation to the aerodynamic forces.

There are several possible ways in which a cylinder may flutter. Let us consider only axisymmetric flutter. The case of axisymmetric flutter of a cylinder with no boundary layer has been solved by Krumhaar (Ref. 6). He uses linear piston theory for aerodynamics and finds an exact solution of the stability problem. His work provides reliable flutter boundaries for comparison and his comments on the number of modes necessary for convergence are useful for the application of Galerkin's method.

We will use Timoshenko's equations of equilibrium (Ref. 7). These equations are specialized to the case of axisymmetric displacements and inertial, aerodynamic, and structural damping forces are added. Since harmonic oscillations are considered, the structural damping force is taken as η times the elastic restoring force.

$$(1+ig) \left[\frac{\partial^2 u}{\partial x^2} + \frac{\nu}{R} \frac{\partial z}{\partial x} - N_0 \frac{(1-\nu^2)}{EhR} \frac{\partial z}{\partial x} \right] - \frac{(1-\nu^2)}{Eh} e_{sh} \frac{\partial^2 u}{\partial t^2} = 0 \quad (38)$$

$$(1+ig) \left[\nu \frac{\partial u}{\partial x} + \frac{z}{R} + \frac{Rh^2}{12} \frac{\partial^4 z}{\partial x^4} - \frac{R(1-\nu^2)}{Eh} N_x \frac{\partial^2 z}{\partial x^2} \right] + \frac{R(1-\nu^2)}{Eh} \left[e_{sh} \frac{\partial^2 z}{\partial t^2} + \bar{p}(x,t) \right] = 0 \quad (39)$$

The cylinder will be assumed to be freely supported at $x = 0$ and $x = L$. For an axisymmetric displacement, the boundary conditions are

$$z(0,t) = z(L,t) = \frac{\partial^2 z}{\partial x^2}(0,t) = \frac{\partial^2 z}{\partial x^2}(L,t) = 0 \quad (40)$$

and

$$\frac{\partial u}{\partial x}(0,t) = \frac{\partial u}{\partial x}(L,t) = 0 \quad (41)$$

Assume that $z \sim e^{i\omega t}$ and $u \sim e^{i\omega t}$ and let a prime denote differentiation with respect to x . Equations 38 and 39 become

$$K_1 u'' + K_2 u + K_3 z' = 0 \quad (42)$$

and

$$K_4 \bar{z}^{IV} + K_5 \bar{z}'' + K_6 \bar{z} + K_7 u' + K_8 \bar{p}(x, t) = 0, \quad (43)$$

where

$$\begin{aligned} K_1 &= 1 + ig \\ K_2 &= \frac{1-\nu^2}{Eh} \rho_s h \omega^2 \\ K_3 &= (1+ig) \left(\frac{\nu}{R} - \frac{N_0 (1-\nu^2)}{EhR} \right) \\ K_4 &= (1+ig) \frac{Rh^2}{12} \\ K_5 &= -(1+ig) \frac{R(1-\nu^2)}{Eh} N_x \\ K_6 &= (1+ig) \frac{1}{R} - \rho_s h \omega^2 \frac{R(1-\nu^2)}{Eh} \\ K_7 &= \nu(1+ig) \\ K_8 &= \frac{R(1-\nu^2)}{Eh} \end{aligned}$$

Equations 42 and 43 with the boundary conditions 40 and 41 define the eigenvalue problem. An approximate solution will be done using Galerkin's method.

We will search for a neutrally stable solution, i. e., a displacement which has a harmonic time dependence. Assume

$$z(x, t) = \sum_{m=1}^N a_m e^{i\omega t} \sin \frac{m\pi x}{L}. \quad (44)$$

This series satisfies the boundary conditions for $z(x, t)$. When it is substituted into the equation of equilibrium in the x direction, we have

$$u'' + \frac{K_2}{K_1} u = - \frac{K_3}{K_1} e^{i\omega t} \sum_{m=1}^N a_m \frac{m\pi}{L} \cos \frac{m\pi x}{L} \quad (45)$$

The particular solution to this equation is

$$u(x,t) = e^{i\omega t} \sum_{m=1}^N \frac{\left(\frac{m\pi}{L}\right) K_3 a_m \cos \frac{m\pi x}{L}}{\left[K_1 \left(\frac{m\pi}{L}\right)^2 - K_2\right]} \quad (46)$$

For the homogeneous solution to equation 45, there are two cases resulting from the inclusion or exclusion of membrane inertia effects:

$$K_2 \neq 0 \quad u = G_1(t) \sin \sqrt{\frac{K_2}{K_1}} x + G_2(t) \cos \sqrt{\frac{K_2}{K_1}} x \quad (47)$$

and

$$K_2 = 0 \quad u = G_3(t) x + G_4(t) \quad (48)$$

It is easily seen that the particular solution satisfies the boundary conditions and the homogeneous solutions do not; therefore, equation 46 gives the proper solution for $u(x,t)$.

We now have functions $z(x,t)$ and $u(x,t)$ which satisfy all boundary conditions and satisfy the equation of equilibrium in the x direction. The equation of equilibrium in the radial direction, equation

43, will now be satisfied approximately. Inserting the series representations for z and u into equation 43, and using the aerodynamic force as developed in equation 28, we have

$$\sum_{m=1}^N a_m \left\{ \left[\frac{K_3 K_7 \left(\frac{m\pi}{L} \right)^2}{\left[K_2 - \left(\frac{m\pi}{L} \right)^2 K_1 \right]} + K_6 + K_4 \left(\frac{m\pi}{L} \right)^4 - K_5 \left(\frac{m\pi}{L} \right)^2 + \frac{K_8 e U^2}{ML} \Delta_{m0} \right] \sin \frac{m\pi x}{L} + \frac{K_8 e U^2}{ML} \Gamma_{m0} \cos \frac{m\pi x}{L} \right\} = \epsilon(x) \quad (49)$$

The function $\epsilon(x)$ is merely the error involved in the approximation of the displacements and is minimized by requiring that

$$\int_0^L \epsilon(x) \sin \frac{q\pi x}{L} dx = 0 \quad (q = 1, 2, \dots, N) .$$

This yields the equations

$$\begin{aligned} \sum_{m=1}^N a_m \left[(m\pi)^2 (1+ig) \left\{ \left[12(1-\nu^2)(1+ig) \left(\frac{h}{L} \right)^2 \left(\frac{L}{R} \right)^2 + \nu(1+ig) T_\theta \left(\frac{L}{R} \right)^2 + (m\pi)^4 (1+ig) \right. \right. \right. \\ \left. \left. + (m\pi)^2 (1+ig) T_x + A \Delta_{m0} \right] \delta_{qm} + A \Gamma_{m0} \bar{\eta}_{qm} \right\} \\ - \lambda \left\{ (1+ig) \left(\frac{(m\pi)^4}{12} \left(\frac{h}{L} \right)^2 + \frac{(m\pi)^2}{12} T_x \left(\frac{h}{L} \right)^2 + (m\pi)^2 + \left(\frac{L}{R} \right)^2 \right) + \frac{1}{12} A \left(\frac{h}{L} \right)^2 \Delta_{m0} \right\} \delta_{qm} \\ \left. + \frac{A}{12} \left(\frac{h}{L} \right)^2 \Gamma_{m0} \bar{\eta}_{qm} \right\} + \lambda^2 \left\{ \frac{1}{12} \left(\frac{h}{L} \right)^2 \delta_{qm} \right\} \right] = 0 \quad (q = 1, 2, \dots, N) , \end{aligned} \quad (50)$$

where

$$\lambda = \frac{\rho_s h \omega^2 L^4}{D} = 12(1-\nu^2)M^2 \left(\frac{\rho_s a^2}{E} \right) \left(\frac{R}{h} \right)^2 \left(\frac{L}{R} \right)^2 K^2$$

$$T_x = \frac{N_x L^2}{D}$$

$$T_\theta = \frac{N_\theta L^2}{D}$$

$$\delta_{qm} = \begin{cases} 0 & q \neq m \\ 1 & q = m \end{cases}$$

$$\bar{\eta}_{qm} = \begin{cases} 0 & \text{if } (q+m) \text{ is even} \\ \frac{4q}{\pi(q-m)(q+m)} & \text{if } (q+m) \text{ is odd} \end{cases}$$

$$A = \frac{\rho U^2 L^3}{MD} = 12(1-\nu^2)M \left(\frac{\rho a^2}{E} \right) \left(\frac{R}{h} \right)^3 \left(\frac{L}{R} \right)^3$$

For the case where membrane inertia is ignored, the equations simplify to

$$\sum_{m=1}^N a_m \left[\left\{ (1+ig) \left[12(1-\nu^2) \left(\frac{L}{h} \right)^2 \left(\frac{L}{R} \right)^2 + (mn)^4 + \nu T_\theta \left(\frac{L}{R} \right)^2 + (mn)^2 T_x \right] + A \Delta_{mo} - \lambda \right\} \delta_{qm} \right. \\ \left. + A \Gamma_{mo} \bar{\eta}_{qm} \right] = 0 \quad (q = 1, 2, \dots, N) \quad (51)$$

We are now at a point where we can proceed with numerical work. Let us neglect membrane inertia and use equations 51. There are several ways that the eigenvalue problem can be formulated; however, we will define the eigenvalue Λ as

$$\Lambda = \frac{12(1-\nu^2)M^2 c_s^2 a^2}{E} \left(\frac{R}{h}\right)^2 \left(\frac{L}{R}\right)^2 k^2 - (1+iq) \left[12(1-\nu^2) \left(\frac{R}{h}\right)^2 \left(\frac{L}{R}\right)^4 + \nu T_0 \left(\frac{L}{R}\right)^2 \right] \quad (52)$$

Equation 51 becomes

$$\sum_{m=1}^N a_m \left[\left\{ (1+iq) \left[(m\pi)^4 + (m\pi)^2 T_x \right] + A \Delta_{m0} - \Lambda \right\} \delta_{qm} + A \Gamma_{m0} \bar{\eta}_{qm} \right] = 0 \quad (q = 1, 2, \dots, N) \quad (53)$$

If the coefficients of the a_m are arranged in a matrix P , the condition that a non-trivial solution exists for the a_m is that

$$\text{Det}(P - \Lambda E) = 0 \quad (54)$$

Searching for eigenvalues is somewhat cumbersome when flutter points for a specific shell at a standard altitude are desired. There are 14 independent variables in the problem. Five of these, $M, M_0, k, \left(\frac{\delta}{R}\right)$, and $\left(\frac{R}{L}\right)$, must be specified in order to calculate the aerodynamic terms. Values for three more, g, T_x , and A , must be chosen in order to form the matrix P . Standard altitude conditions set the values for e and a , and the choice of a copper shell with given internal pressurization sets the values for ν, E, c_s , and T_0 . Therefore, all variables are specified, and a solution for Λ from equation 54 is not a true eigenvalue unless it also satisfies equation 52. Because equation 52 is complex, there are actually two constraining conditions. If we write

$$\Lambda = \Lambda_R + i\Lambda_I, \text{ then}$$

$$\Lambda_R = \frac{12(1-\nu^2)M^2e_s a^2}{E} \left(\frac{R}{h}\right)^2 \left(\frac{L}{R}\right)^2 k^2 - 12(1-\nu^2) \left(\frac{R}{h}\right)^2 \left(\frac{L}{R}\right)^4 - \nu T_\theta \left(\frac{L}{R}\right)^2 \quad (55)$$

$$\Lambda_I = -g \left[12(1-\nu^2) \left(\frac{R}{h}\right)^2 \left(\frac{L}{R}\right)^4 + \nu T_\theta \left(\frac{L}{R}\right)^2 \right] \quad (56)$$

In actual practice, the constraining equations were rewritten.

If F and g_o are defined as

$$F(A,k) = \left[\frac{12(1-\nu^2)M^2e_s a^2}{E} \left(\frac{R}{h}\right)^2 \left(\frac{L}{R}\right)^2 k^2 - 12(1-\nu^2) \left(\frac{R}{h}\right)^2 \left(\frac{L}{R}\right)^4 - \nu T_\theta \left(\frac{L}{R}\right)^2 \right] - \Lambda_R$$

and

$$g_o(A,k) = - \frac{\Lambda_I}{\left[12(1-\nu^2) \left(\frac{R}{h}\right)^2 \left(\frac{L}{R}\right)^4 + \nu T_\theta \left(\frac{L}{R}\right)^2 \right]}$$

then equations 55 and 56 become

$$F(A,k) = 0 \quad (57)$$

$$g_o(A,k) = g \quad (58)$$

For a given selection of the other 12 variables, k and A are varied until one of the eigenvalues from equation 54 also satisfies equations 57 and 58. This establishes a flutter point. The critical value of $\left(\frac{h}{R}\right)$ is found through the definition of A as

$$\frac{h}{R} = \left(\frac{L}{R}\right) \left[12(1-\nu^2) \frac{\rho U^2}{EM} \frac{1}{A} \right]^{\frac{1}{3}} .$$

Calculations were carried out on the IBM 7090 digital computer for unpressurized copper cylinders with $\frac{R}{L} = 0.5$. The following constants were used:

$$M_6 = 0.5$$

$$E = 1.3 \times 10^7 \text{ lb/in}^2$$

$$\nu = 0.33$$

$$\rho_s = 0.0008333 \frac{\text{lb sec}^2}{\text{in}^4}$$

All flutter boundaries were calculated using 10 modes. It was felt that 10 modes was the maximum number allowable because of the round-off error inherent in currently available eigenvalue subroutines for complex matrices. The expansion of the Bessel functions used earlier also becomes poorer as more modes are taken (as m becomes larger).

The curves of thickness ratio required to prevent flutter at sea level and 50,000 feet (figures 13 and 14) indicate that the boundary layer is slightly destabilizing. Even a very thin boundary layer has an effect; however, raising the thickness from $\frac{\delta}{R} = 0.0625$ to $\frac{\delta}{R} = 0.125$ causes little change. The convergence is only fair at low values of $\frac{h}{R}$ as can be seen in comparison with the exact work of Krumhaar. It is necessary to have such a comparison available because of the lack of convergence theorems for Galerkin's method when applied to a non-self-adjoint problem such as this.

Figure 15 shows the effect of structural damping in addition to a typical boundary layer. It is interesting to note that the boundary layer is stabilizing when structural damping is present. It is realized that the flutter boundaries for $\frac{h}{R} < 0.001$ are not accurate because of poor convergence; however, they still reveal trends.

The effect of the choice of M_6 is shown in figure 16. The choice of $M_6 = 0.5$ for the calculation of the flutter boundaries appears to have led to a slightly higher thickness ratios than might be obtained with a different choice.

Some of the flutter points are given in Table I. The values of A and k at flutter can be found in this table.

5. Conclusions

It has been found that a simplified boundary layer has a significant effect on the forces developed on an oscillating cylinder. This effect is especially pronounced for modes with many circumferential waves and at low frequencies. A case was given where the force amplitudes were only 5 per cent as large as those given by linear piston theory. This may mean that flutter with many circumferential waves will occur at higher dynamic pressures than current theories indicate.

The flutter boundaries which were calculated for axisymmetric flutter are not greatly different from the flutter boundaries obtained with no boundary layer. The results indicate that when structural damping is present, the boundary layer is stabilizing.

It is possible that the choice of M_0 for this simplified theory could be fixed by a matching process with a more exact boundary layer theory.

It should be mentioned that the case of a two-dimensional flat plate with boundary layer has also been worked out. The results are similar to those presented here. The equations for pressure and interface displacement for the two-dimensional flat plate may be obtained from the cylinder equations by taking $n = 0$ and letting $\frac{R}{L} \rightarrow \infty$.

Cylinder flutter with many circumferential waves is of sufficient interest that flutter boundaries will be calculated for this case in the near future.

REFERENCES

1. Miles, J. W.: On Panel Flutter in the Presence of a Boundary Layer. *Journal of Aero. Sciences*, Vol. 26, No. 2, pp. 81-93, (February 1959).
2. Voss, H. M.: The effect of an External Flow on the Vibration Characteristics of Thin Cylindrical Shells. *Journal of Aero. Sciences*, Vol. 28, No. 12, pp. 945-956 (December 1961).
3. Des Ciers, B. and Chang, C.: On Some Problems in Linearized Axially Symmetric Flow. *Journal of Aero. Sciences*, Vol. 18, No. 2, pp. 127-138 (1951).
4. Liepmann, H. and Roshko, A.: Elements of Gasdynamics. John Wiley and Sons, Inc., New York, p. 218 (1957).
5. Schlichting, H.: Boundary Layer Theory. McGraw-Hill Book Co., Inc., New York, pp. 430-440 (1955).
6. Krumhaar, H.: Supersonic Flutter of a Cylindrical Shell of Finite Length in an Axisymmetric Mode. Air Force Office of Scientific Research Report No. 1574, California Institute of Technology, (October 1961).
7. Timoshenko, S.: Theory of Plates and Shells. McGraw-Hill Book Co., Inc., New York, p. 440 (1940).

TABLE I

AXISYMMETRIC FLUTTER POINTS

Altitude feet	M	M _δ	g	$\frac{\bar{\delta}}{R}$	A	k	$\frac{h}{R}$
0	2.0	0.5	0	0	11,620	9.34	0.00285
0	3.5	0.5	0	0	3,910	5.33	0.00494
0	5.0	0.5	0	0	1,895	3.73	0.00709
0	2.0	0.5	0	0.0100	6,200	9.36	0.00353
0	3.5	0.5	0	0.0100	2,540	5.33	0.00574
0	5.0	0.5	0	0.0100	1,175	3.73	0.00823
0	2.0	0.5	0	0.0625	5,840	9.33	0.00360
0	3.5	0.5	0	0.0625	1,906	5.33	0.00626
0	5.0	0.5	0	0.0625	1,005	3.74	0.00877
0	2.0	0.5	0	0.1250	5,993	9.33	0.00355
0	3.5	0.5	0	0.1250	1,908	5.33	0.00628
0	5.0	0.5	0	0.1250	1,168	3.78	0.00837
50,000	2.0	0.5	0	0	12,200	10.75	0.00136
50,000	3.5	0.5	0	0	5,250	6.14	0.00218
50,000	5.0	0.5	0	0	2,601	4.29	0.00310
50,000	2.0	0.5	0	0.0100	9,850	10.74	0.00146
50,000	3.5	0.5	0	0.0100	3,600	6.14	0.00248
50,000	5.0	0.5	0	0.0100	1,680	4.29	0.00357
50,000	2.0	0.5	0	0.0625	7,915	10.74	0.00158
50,000	3.5	0.5	0	0.0625	2,562	6.13	0.00277

TABLE I (contd.)

AXISYMMETRIC FLUTTER POINTS

Altitude feet	M	M _δ	g	$\frac{\bar{\delta}}{R}$	A	k	$\frac{h}{R}$
50,000	5.0	0.5	0	0.0625	1,252	4.29	0.00396
50,000	2.0	0.5	0	0.1250	8,108	10.73	0.00156
50,000	3.5	0.5	0	0.1250	2,482	6.13	0.00279
50,000	5.0	0.5	0	0.1250	1,295	4.29	0.00391
50,000	2.0	0.5	0.001	0.0625	59,500	10.74	0.000805
50,000	3.5	0.5	0.001	0.0625	44,000	6.13	0.00107
50,000	5.0	0.5	0.001	0.0625	66,200	4.30	0.00105
50,000	2.0	0.5	0.002	0.0625	640,000	10.72	0.000364
50,000	3.5	0.5	0.002	0.0625	405,000	6.12	0.000516
50,000	5.0	0.5	0.002	0.0625	582,000	4.27	0.000510
50,000	3.5	0.1	0	0.0625	6,500	6.13	0.00205
50,000	3.5	0.25	0	0.0625	3,790	6.14	0.00243
50,000	3.5	0.8	0	0.0625	3,078	6.13	0.00261

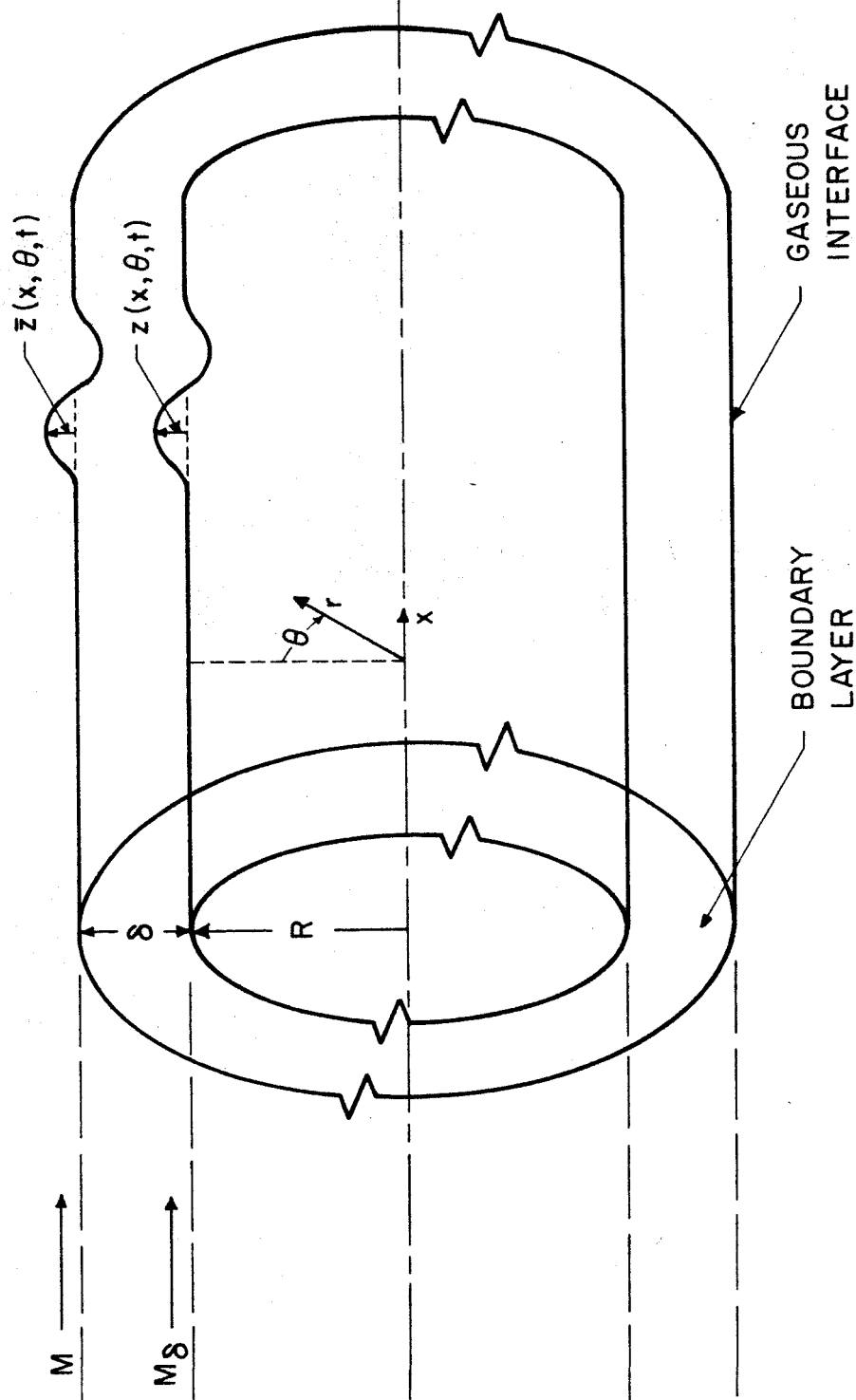


Fig. 1. Coordinate System.

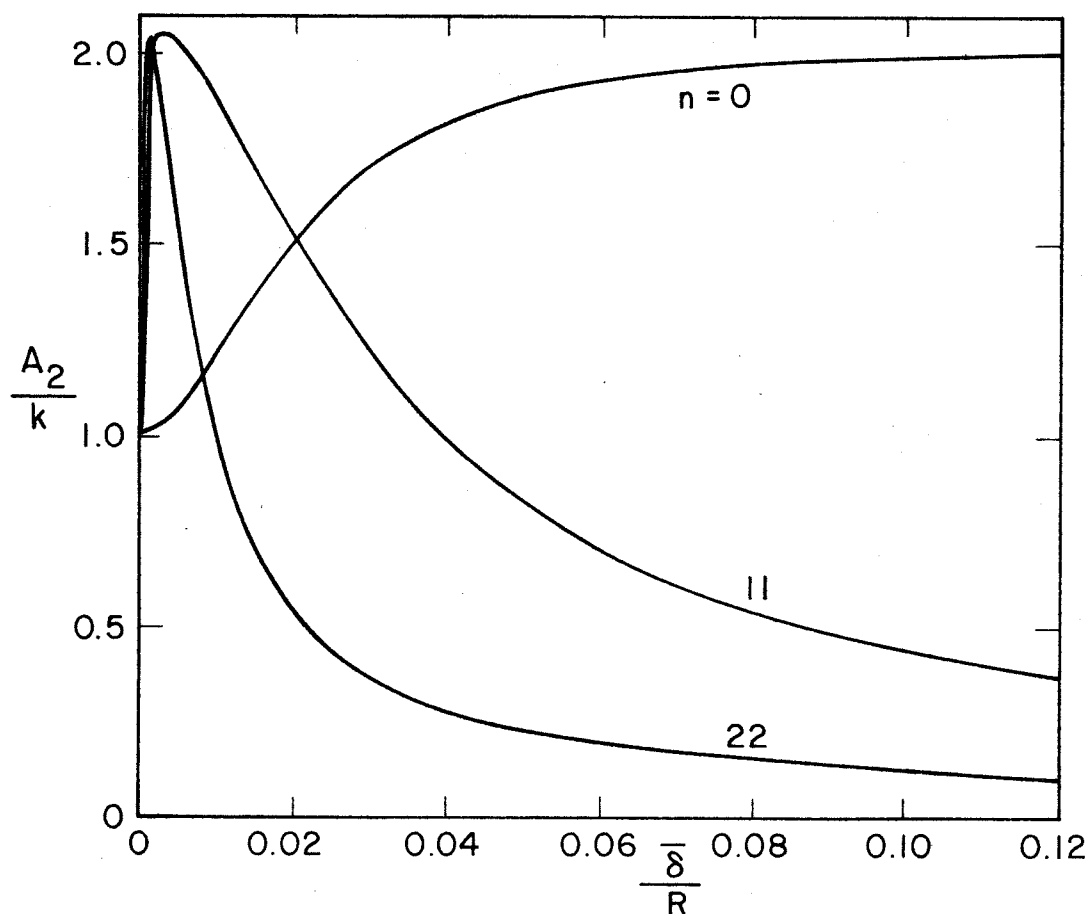
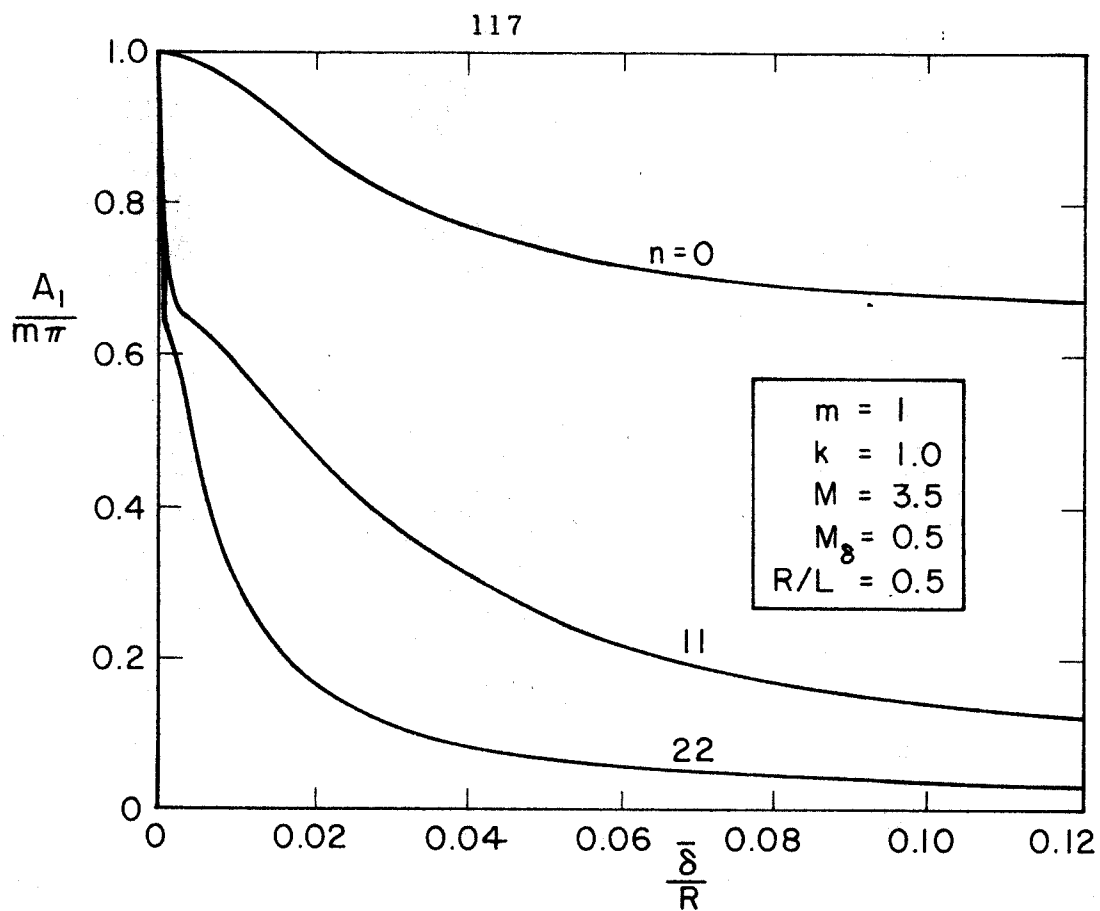


Fig. 2. Effect of Circumferential Waves on Force Amplitudes.

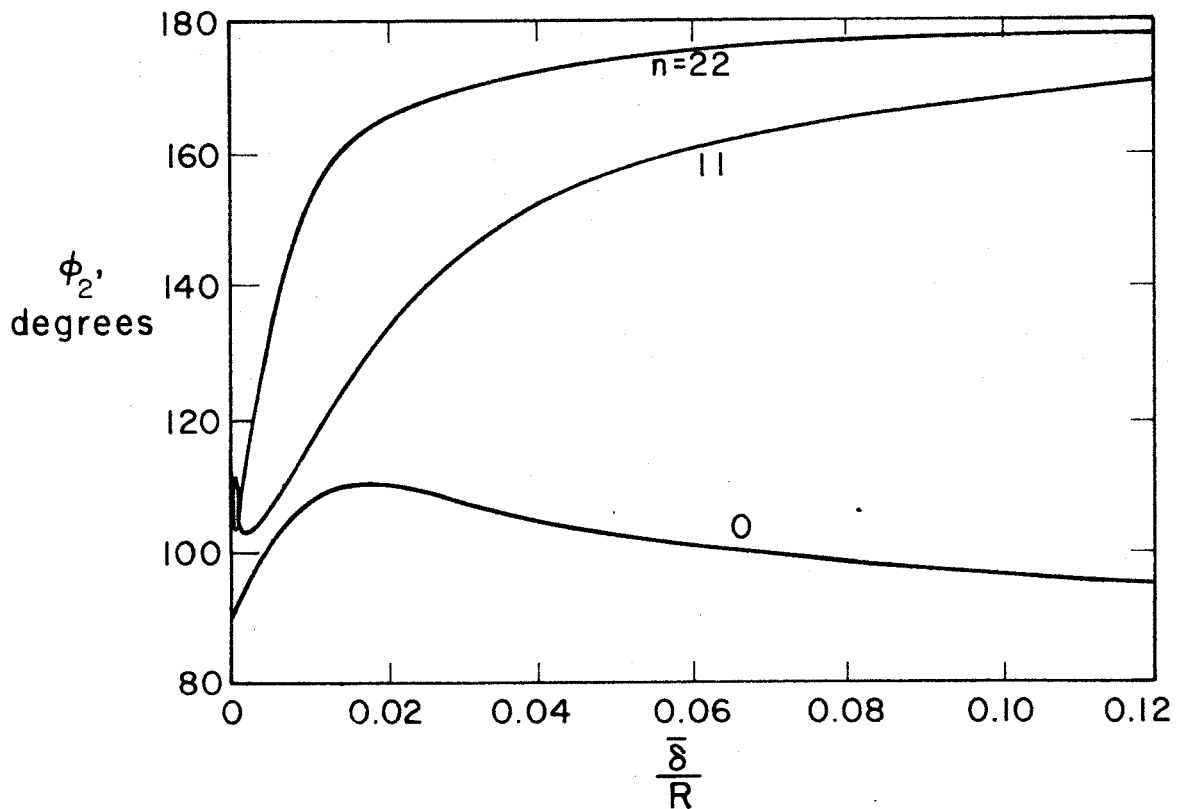
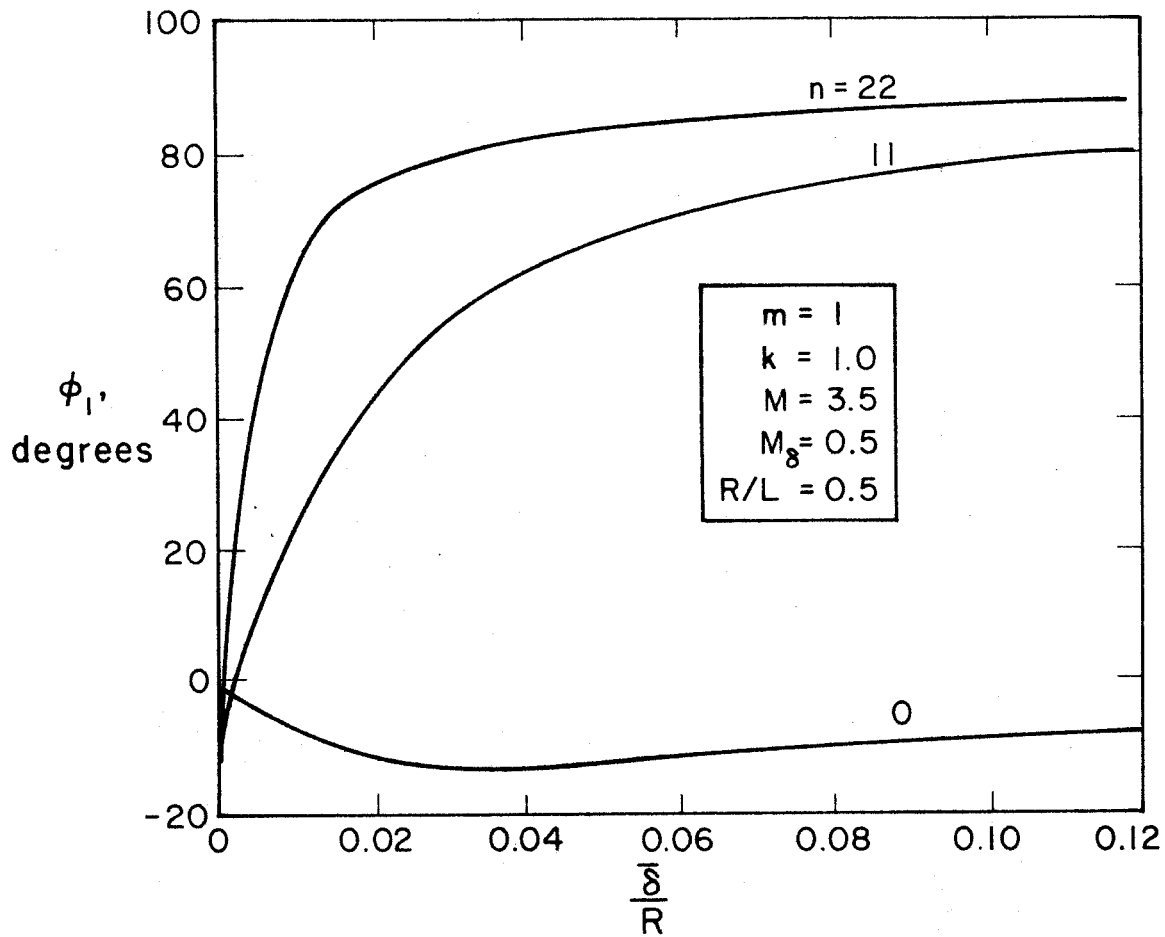


Fig. 3. Effect of Circumferential Waves on Force Phase Angles.

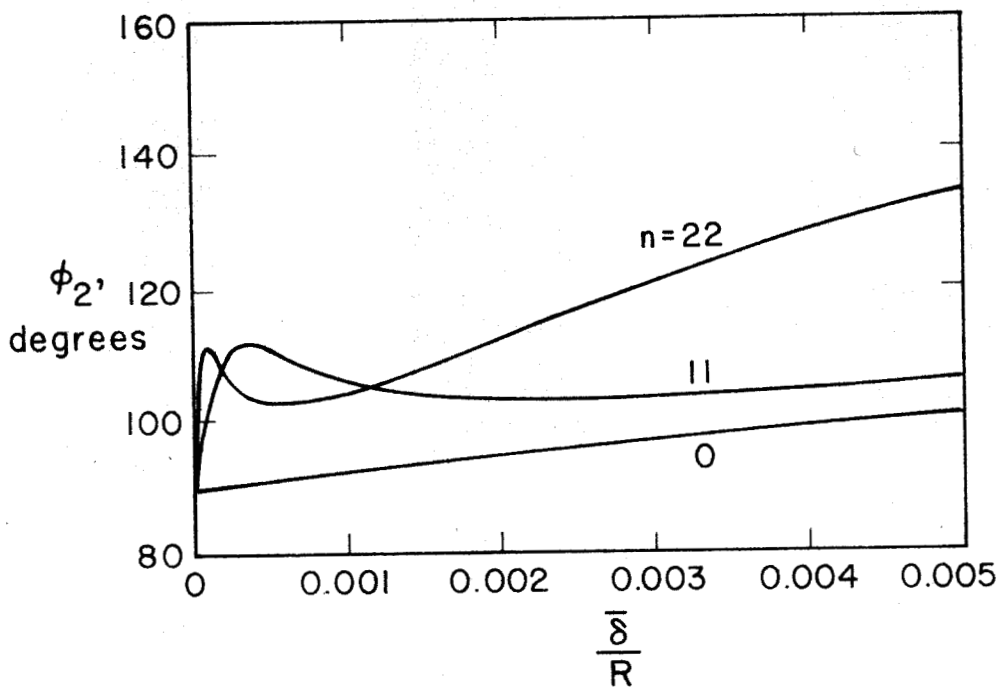
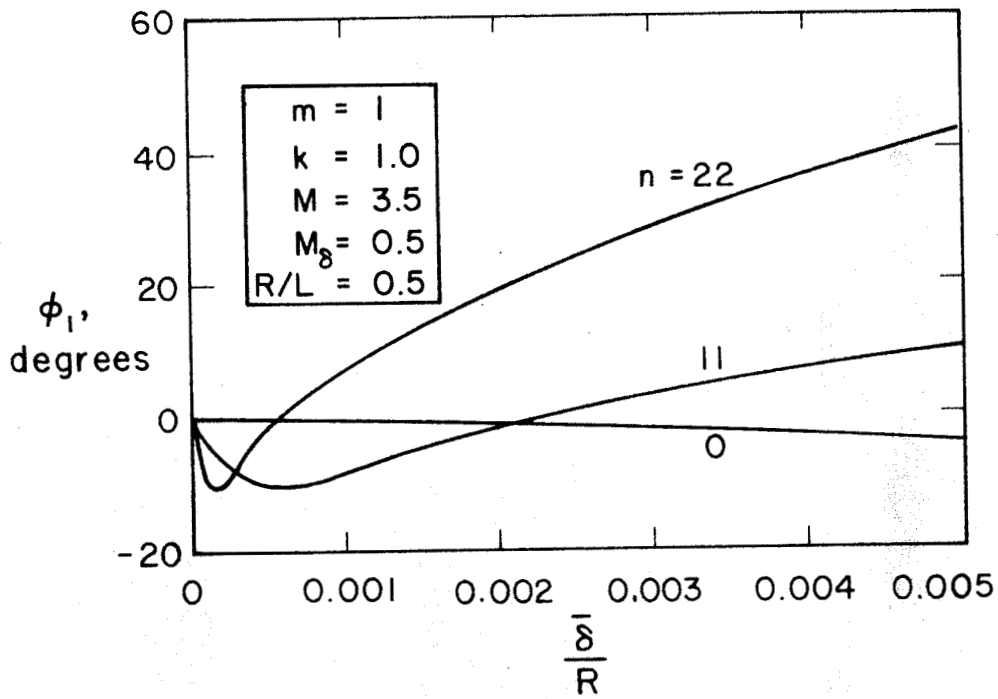


Fig. 4. Effect of Circumferential Waves for Very Thin Boundary Layer. (Enlargement of Origin in Fig. 3.)

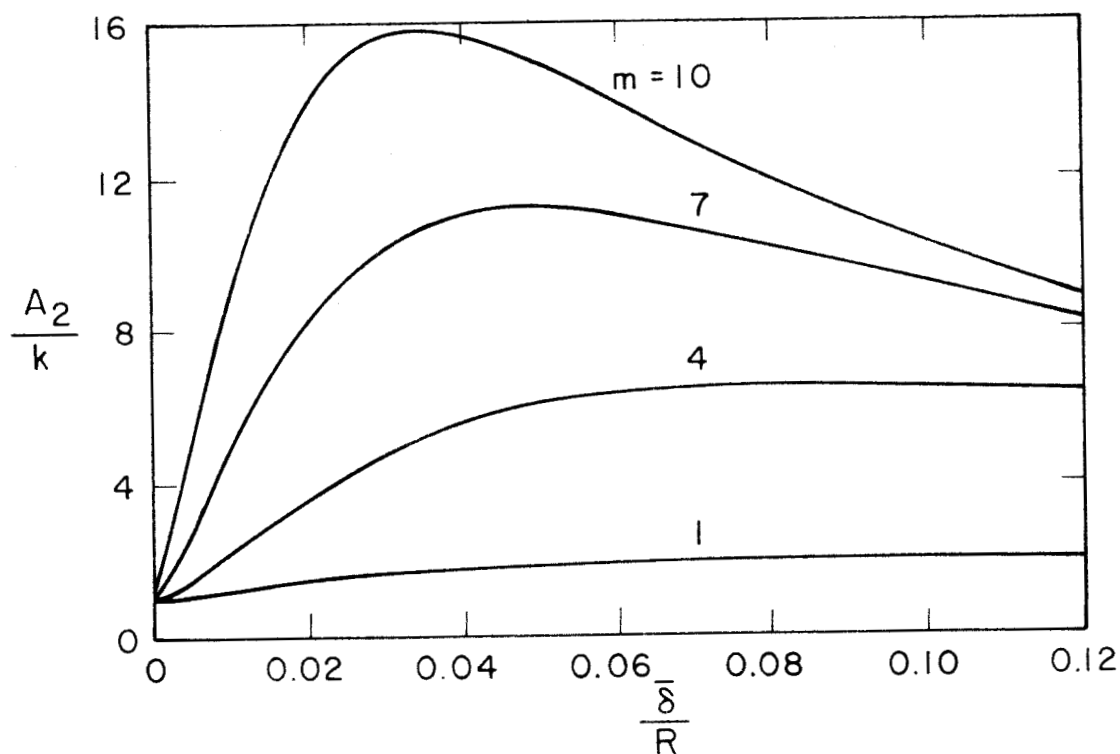
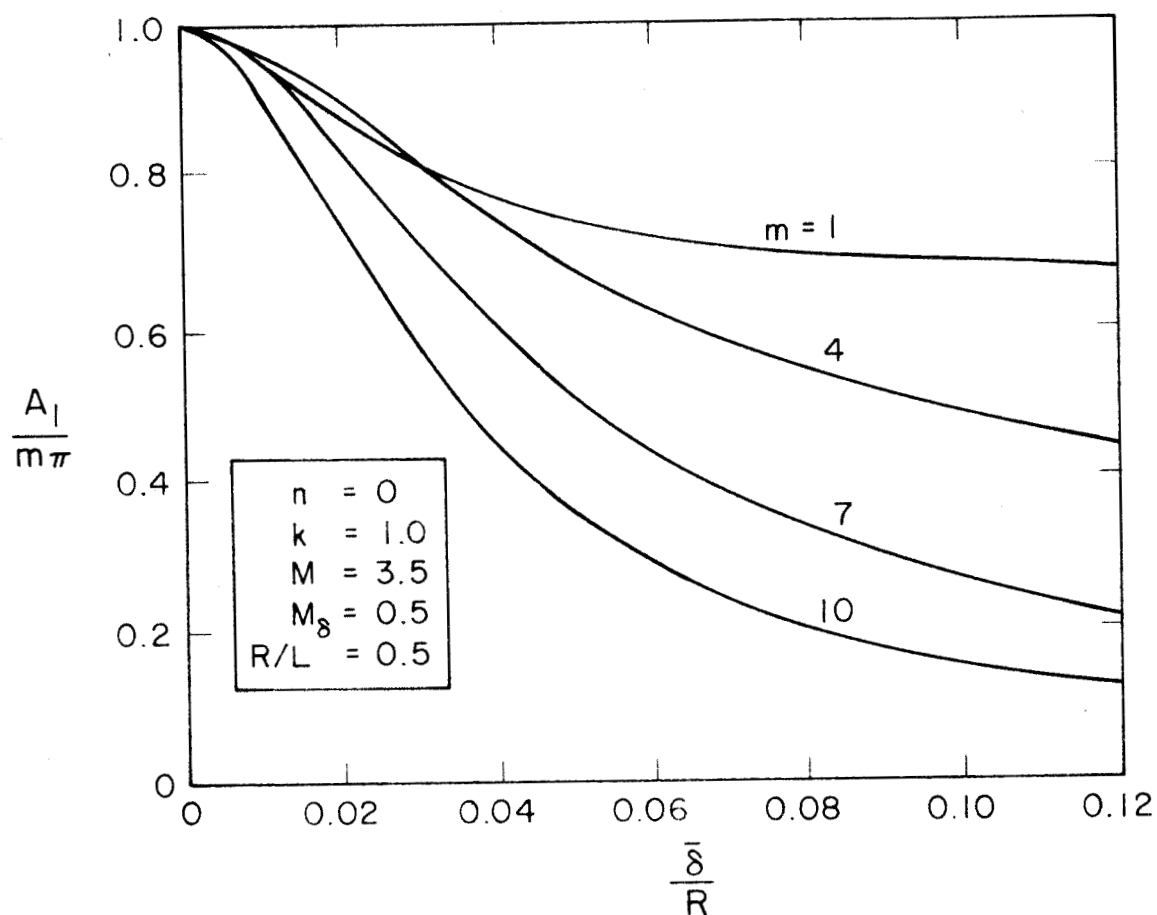


Fig. 5. Effect of Axial Waves on Force Amplitudes.

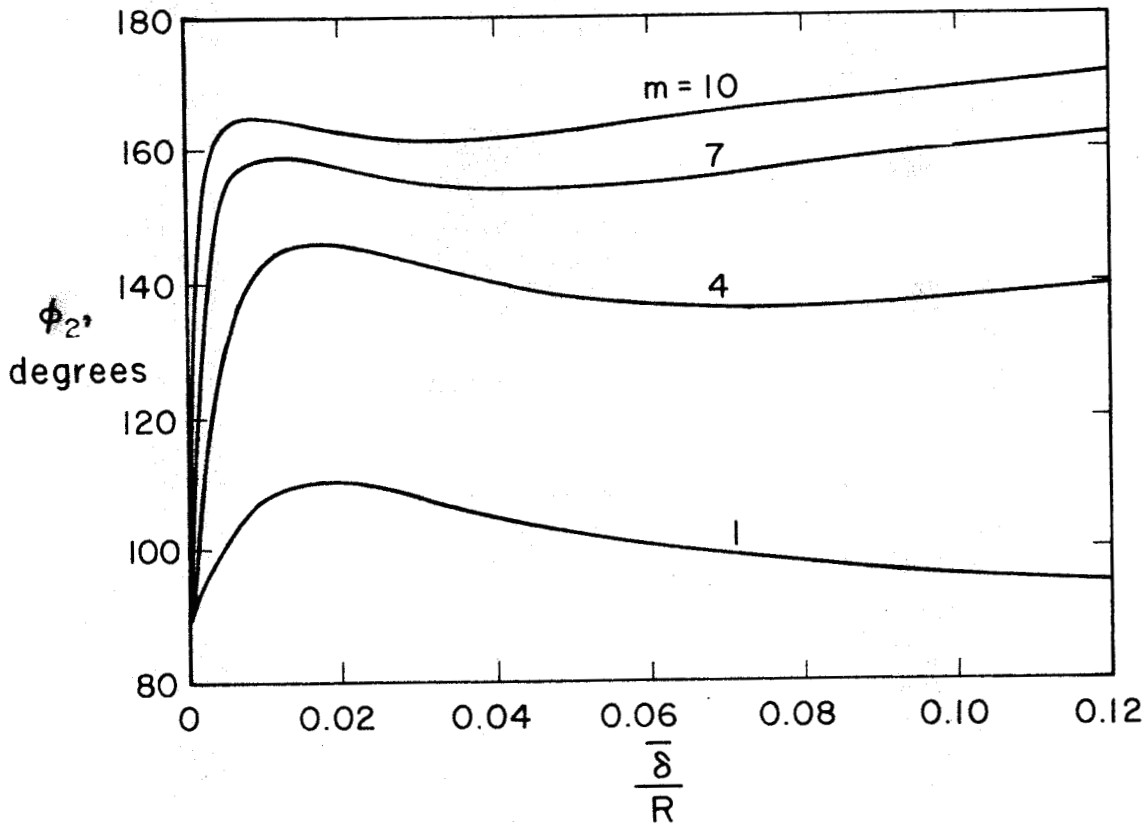
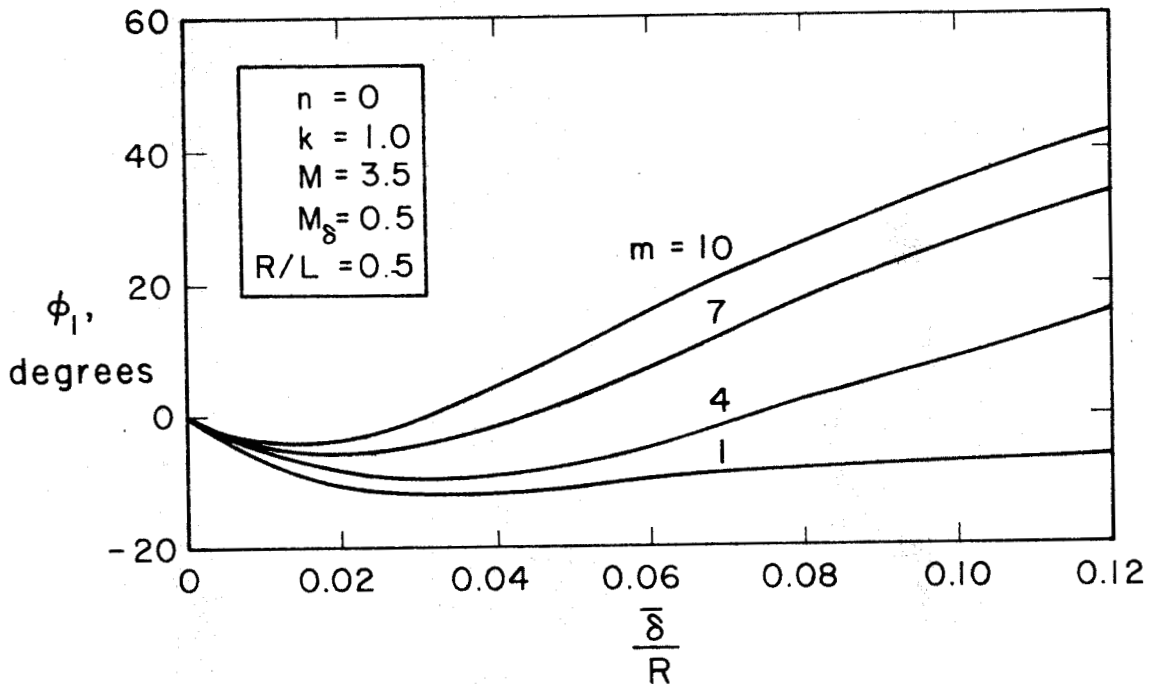


Fig. 6. Effect of Axial Waves on Force Phase Angles.

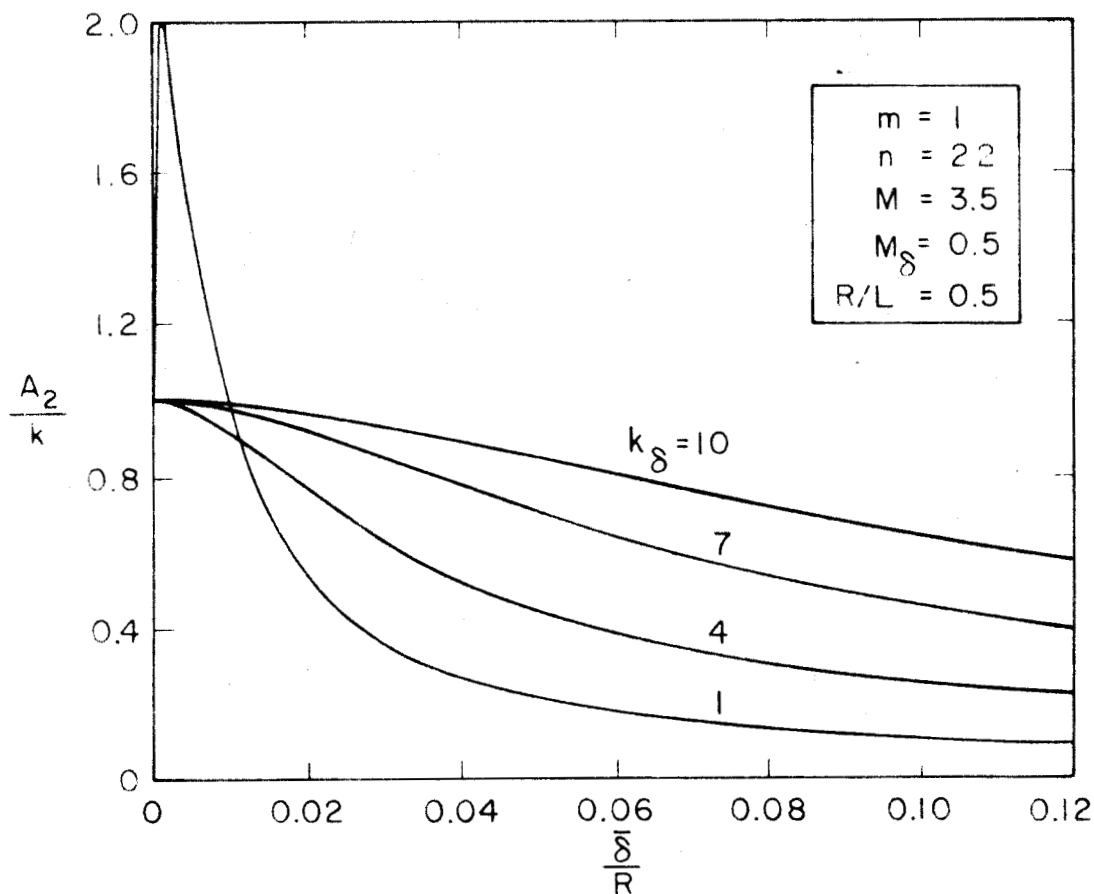
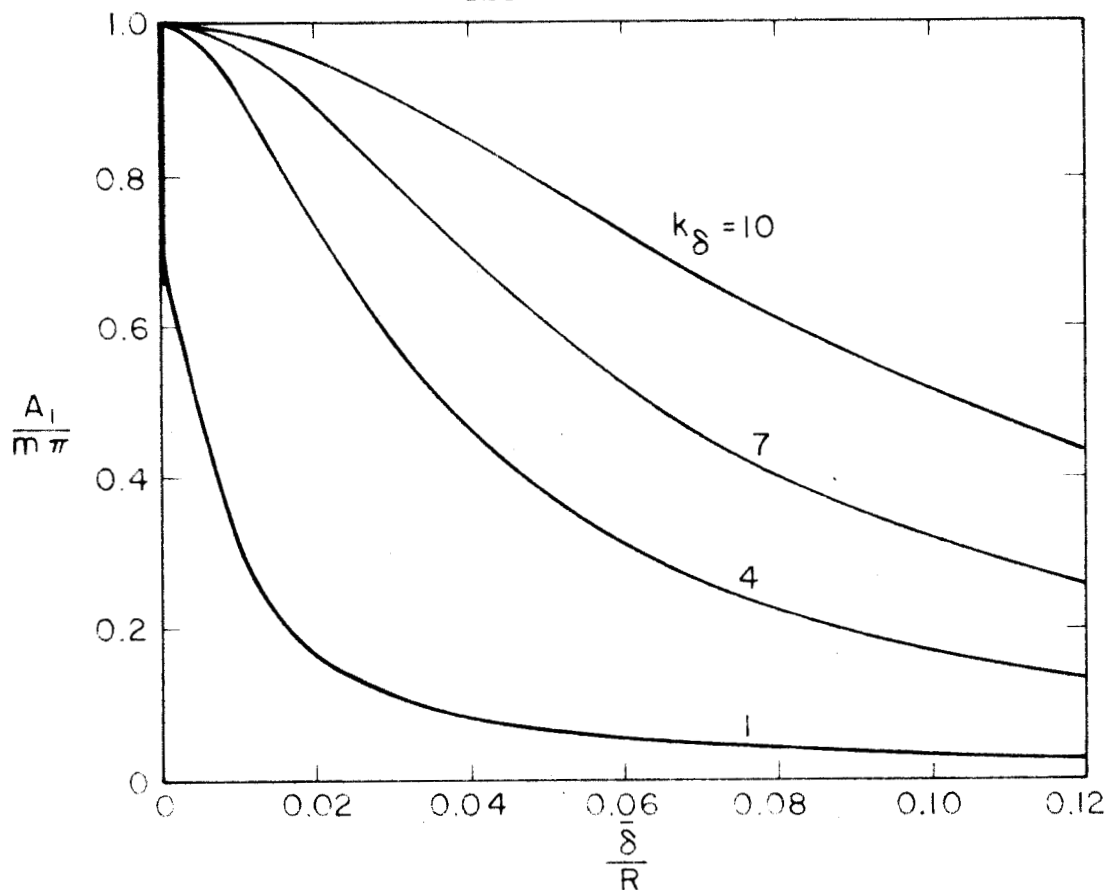


Fig. 7. Effect of Frequency on Force Amplitudes. Many Circumferential Waves ($n = 22$).

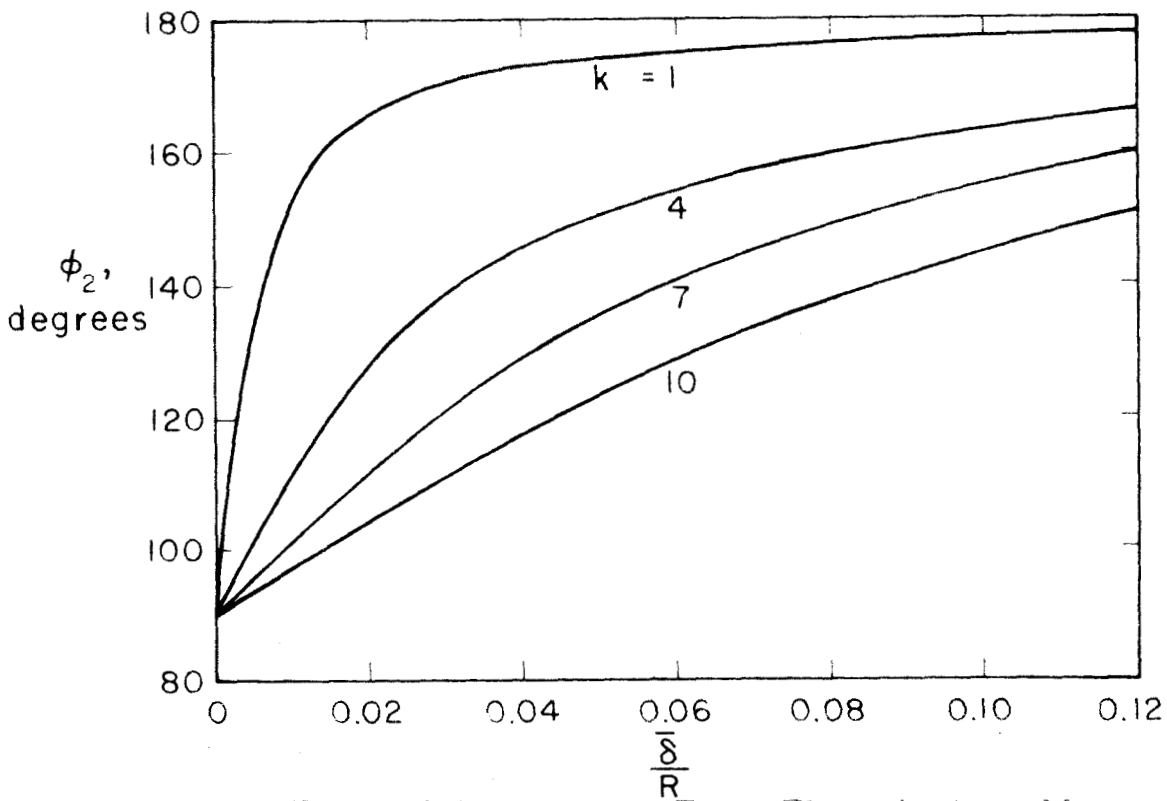
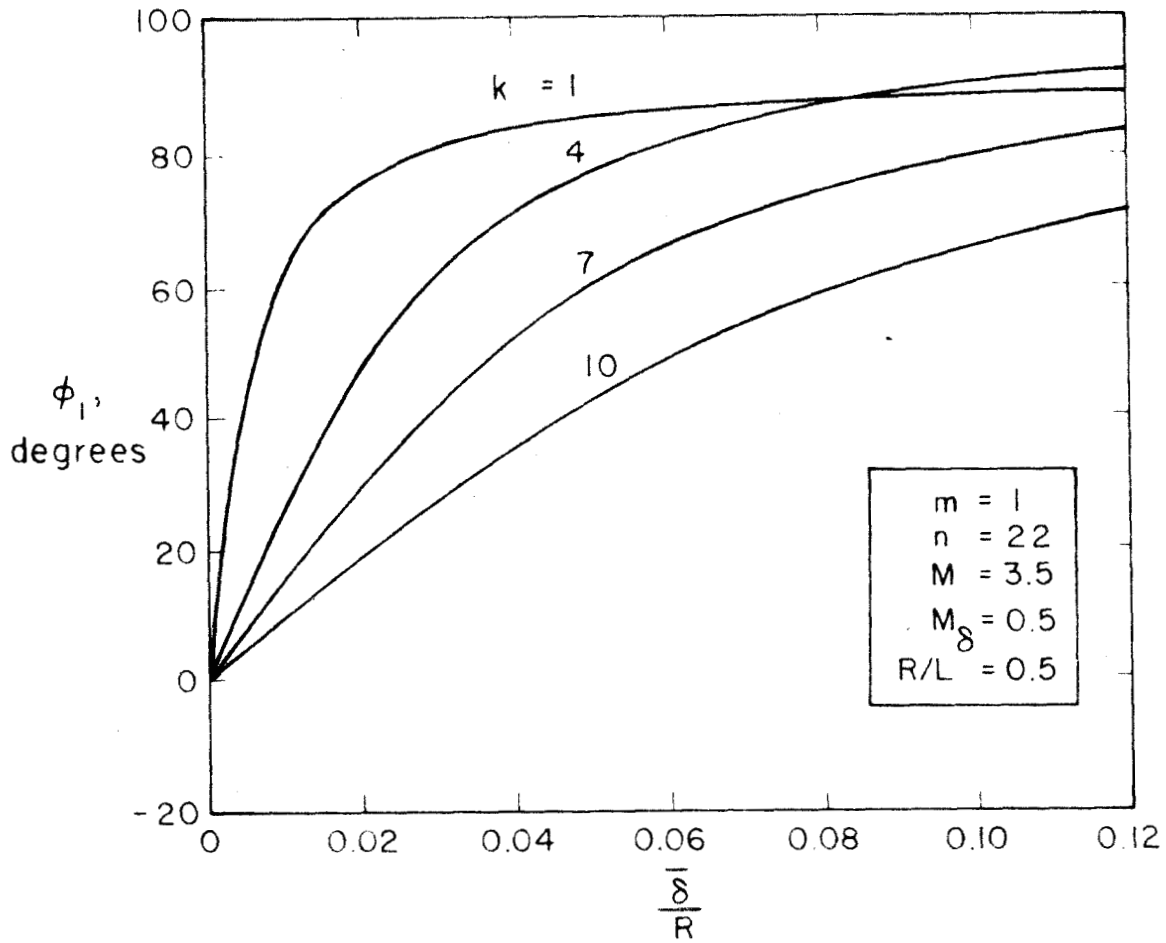


Fig. 8. Effect of Frequency on Force Phase Angles. Many Circumferential Waves ($n = 22$).

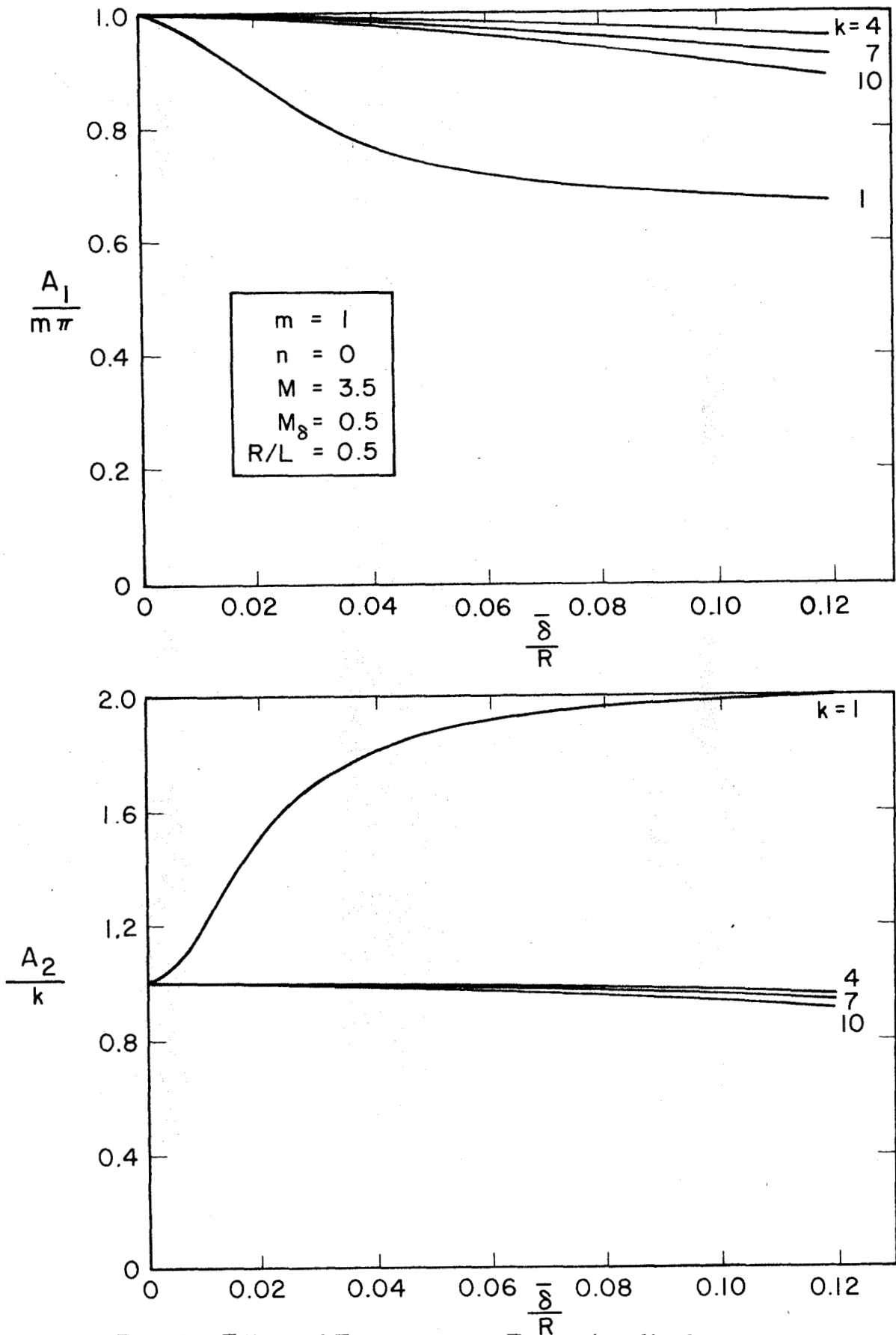


Fig. 9. Effect of Frequency on Force Amplitudes.
Axisymmetric Case ($n = 0$).

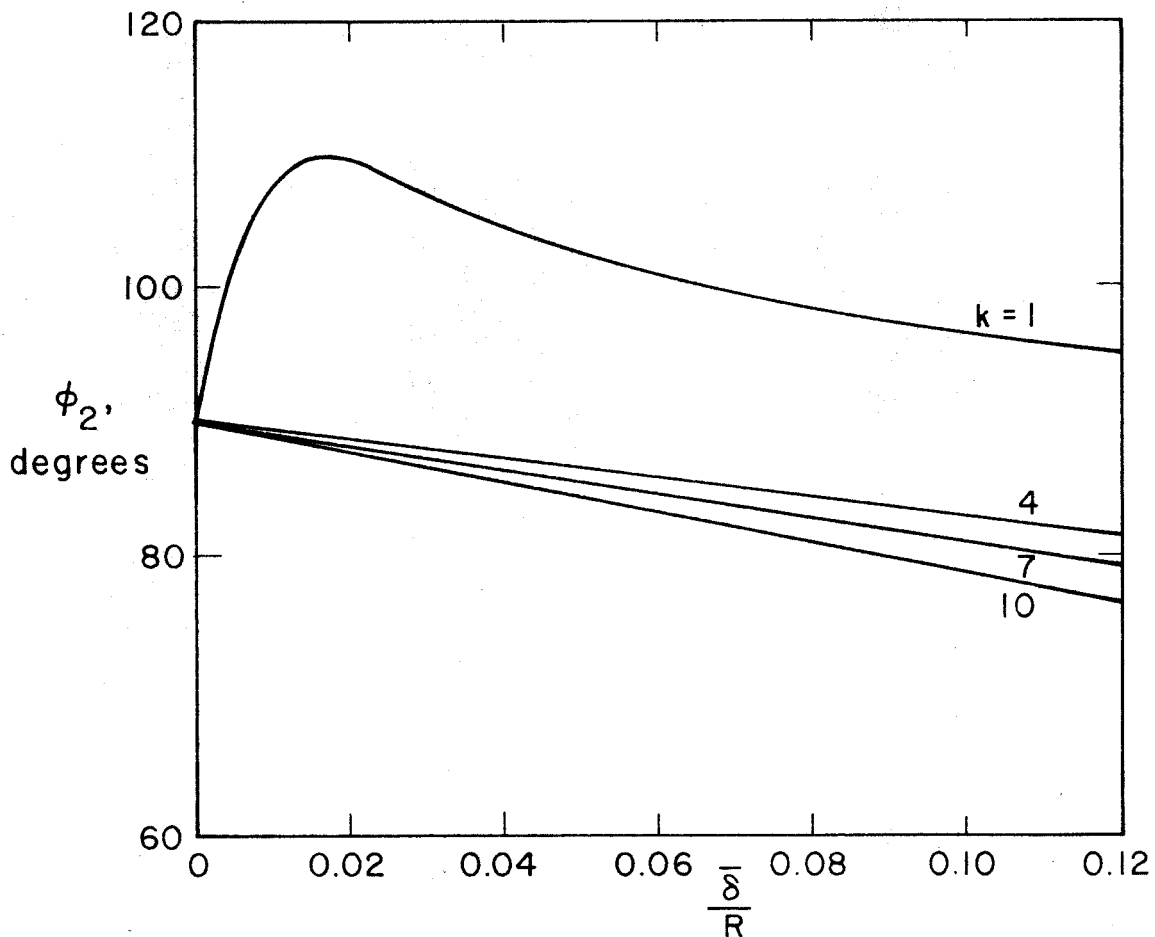
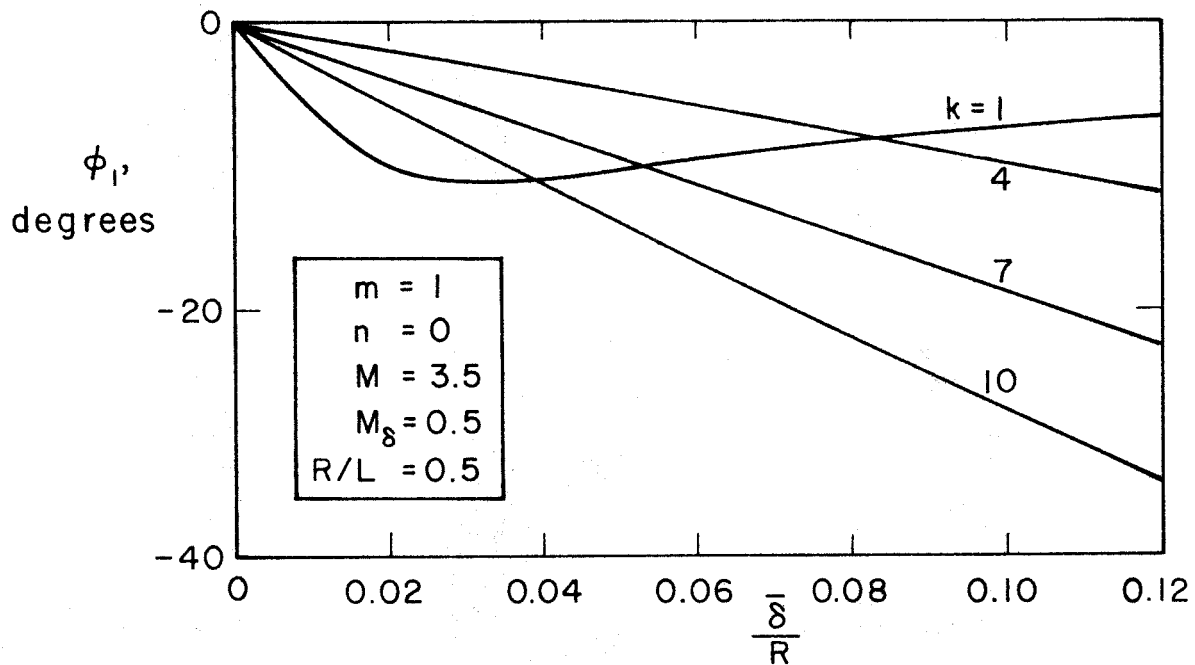


Fig. 10. Effect of Frequency on Force Phase Angles.
Axisymmetric Case ($n = 0$).

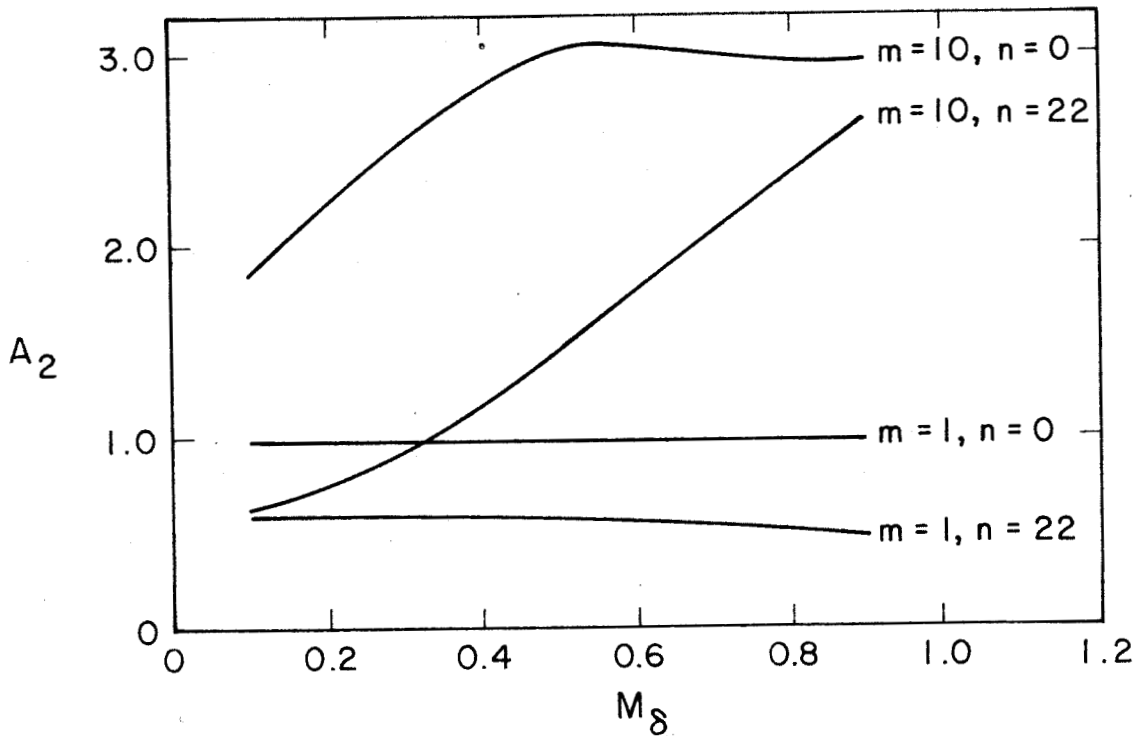
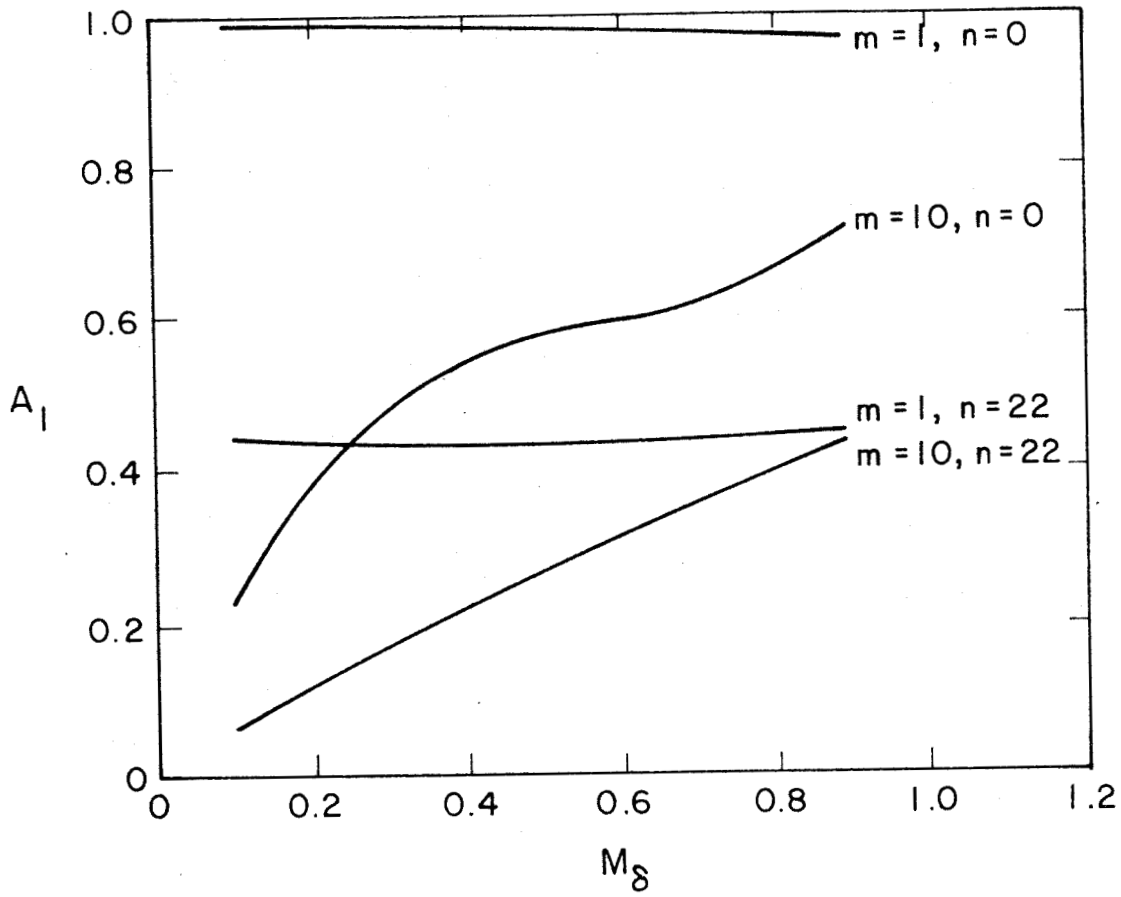


Fig. 11. Effect of the Choice of M_δ on Force Amplitudes.
 $k = 6.0$

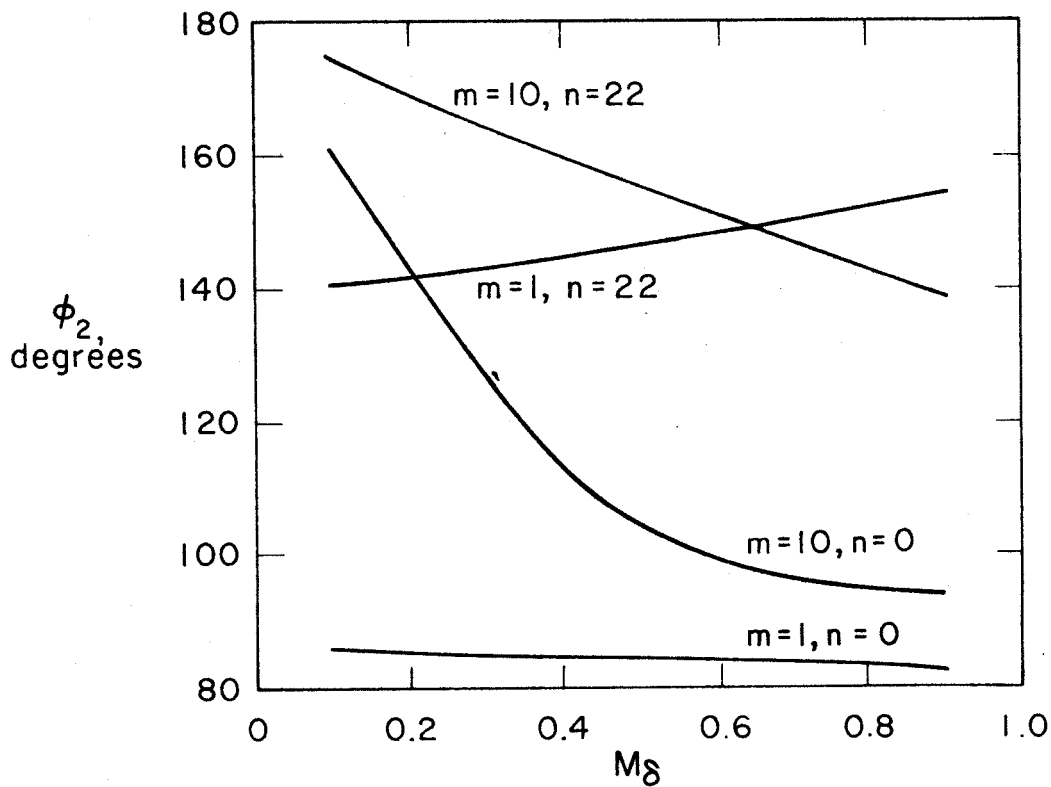
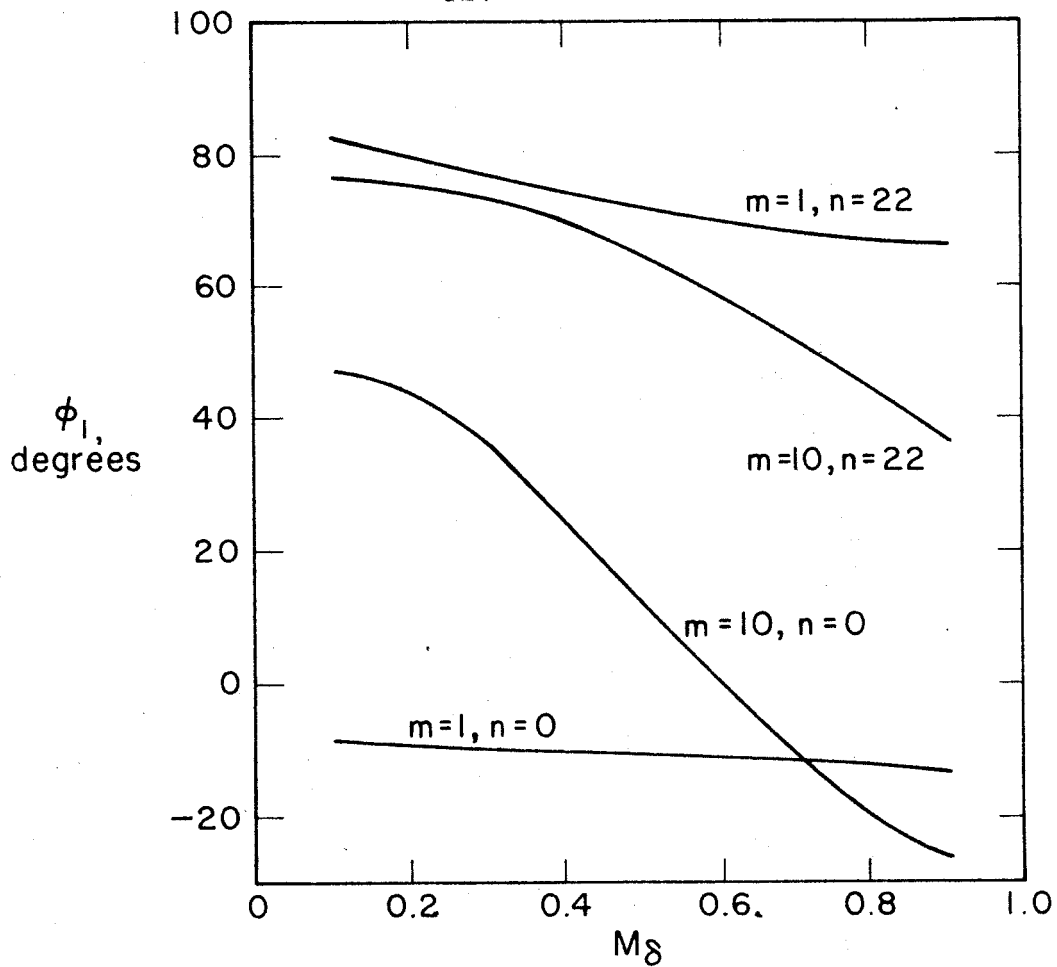


Fig. 12. Effect of the Choice of M_δ on Force Phase Angles.
 $k = 6.0$

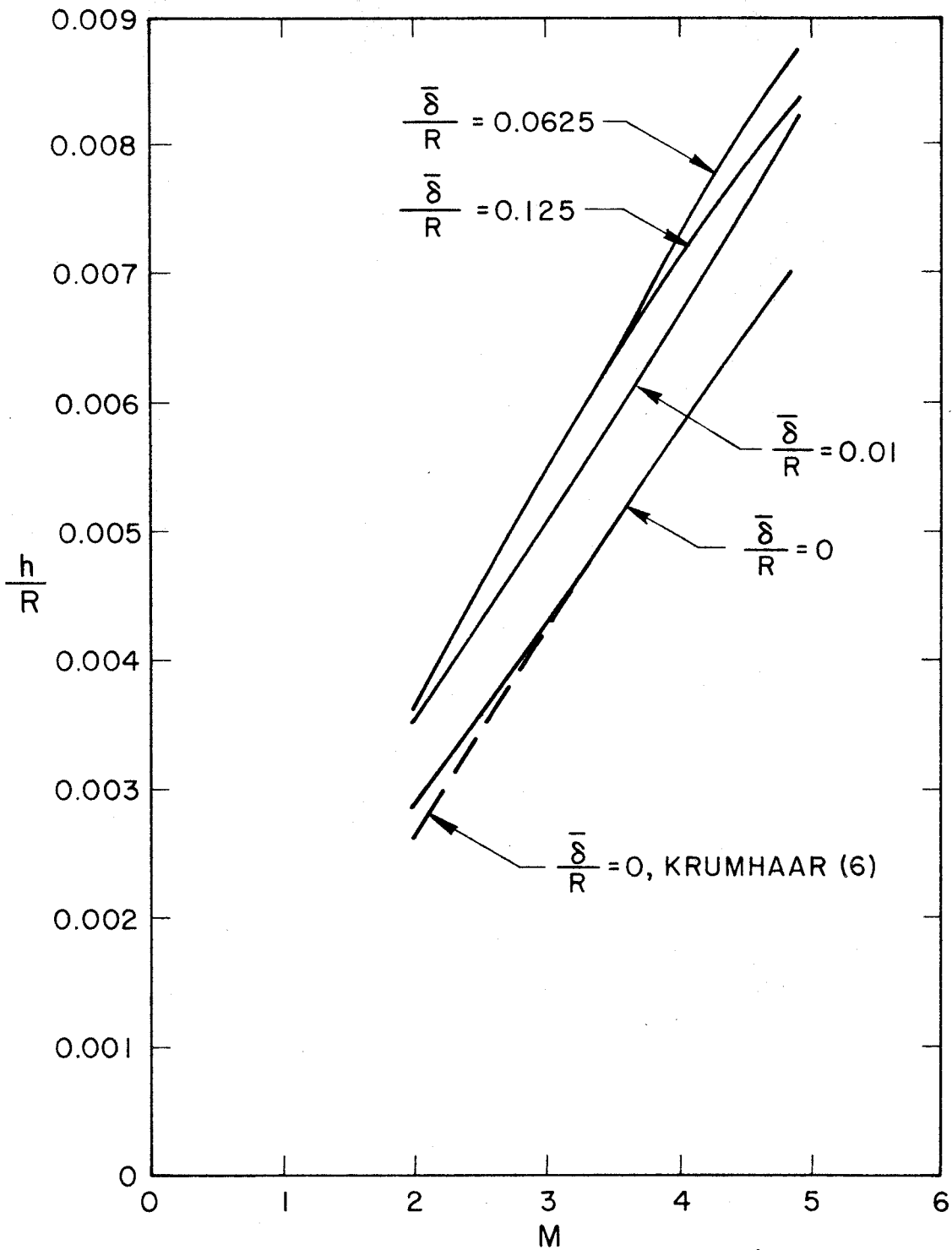


Fig. 13. Thickness Ratio Required to Prevent Flutter for a Copper Cylinder at Sea Level, $R/L = 0.5$, $M_\delta = 0.5$.

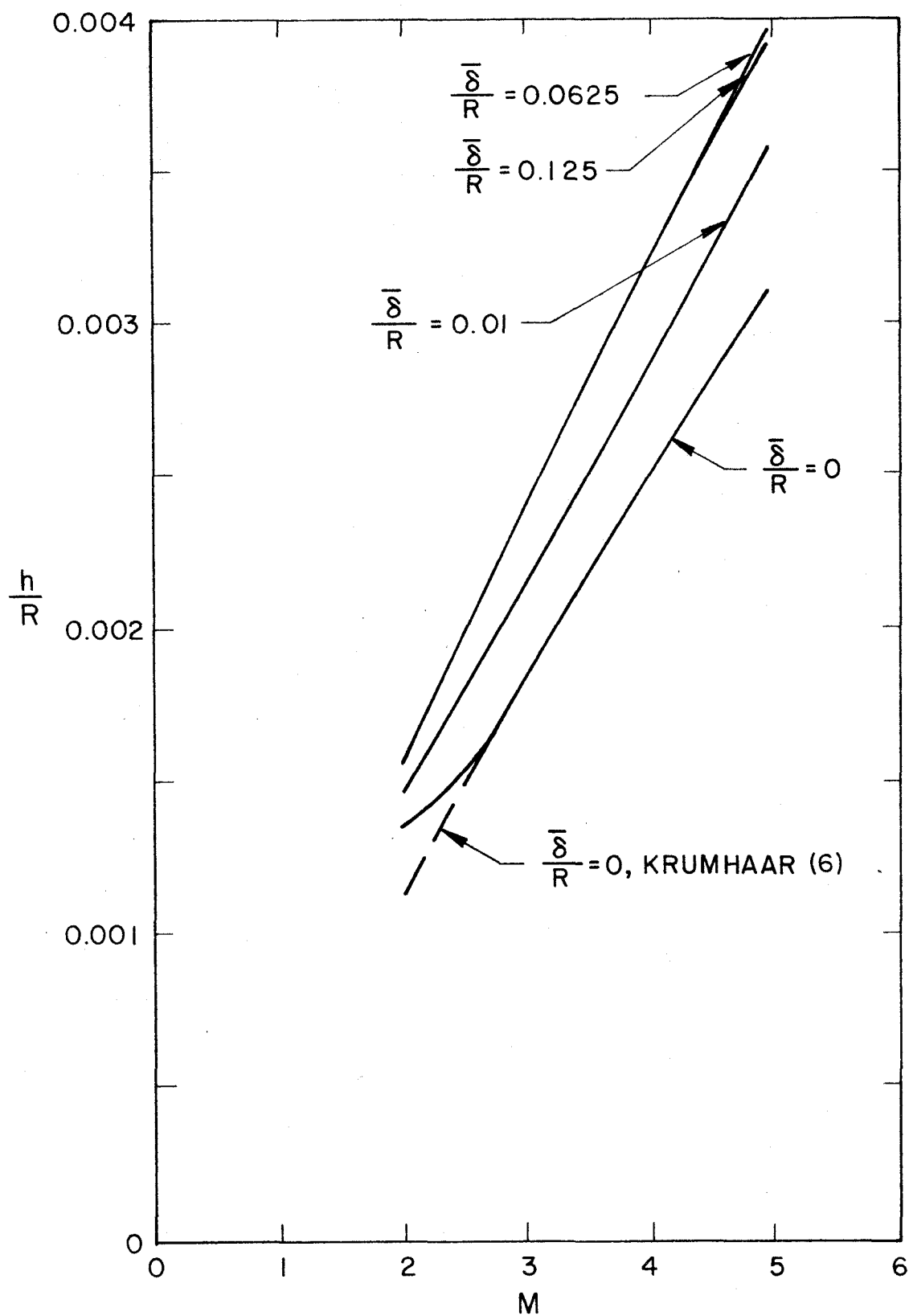


Fig. 14. Thickness Ratio Required to Prevent Flutter for a Copper Cylinder at 50,000 feet. $R/L = 0.5$, $M_0 = 0.5$.

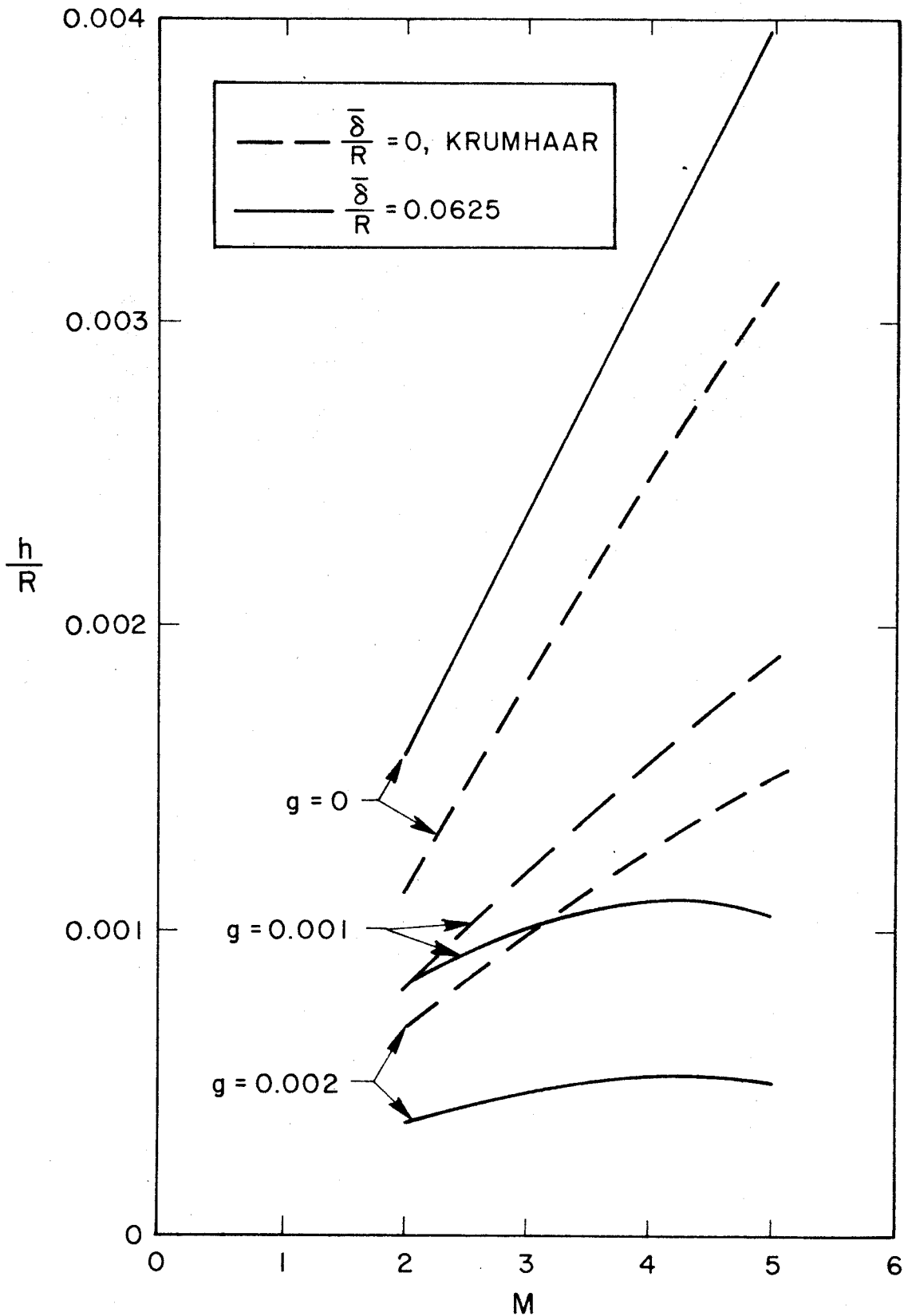


Fig. 15. Effect of Structural Damping in Addition to a Typical Boundary Layer. 50,000 Feet. $M_\delta = 0.5$.

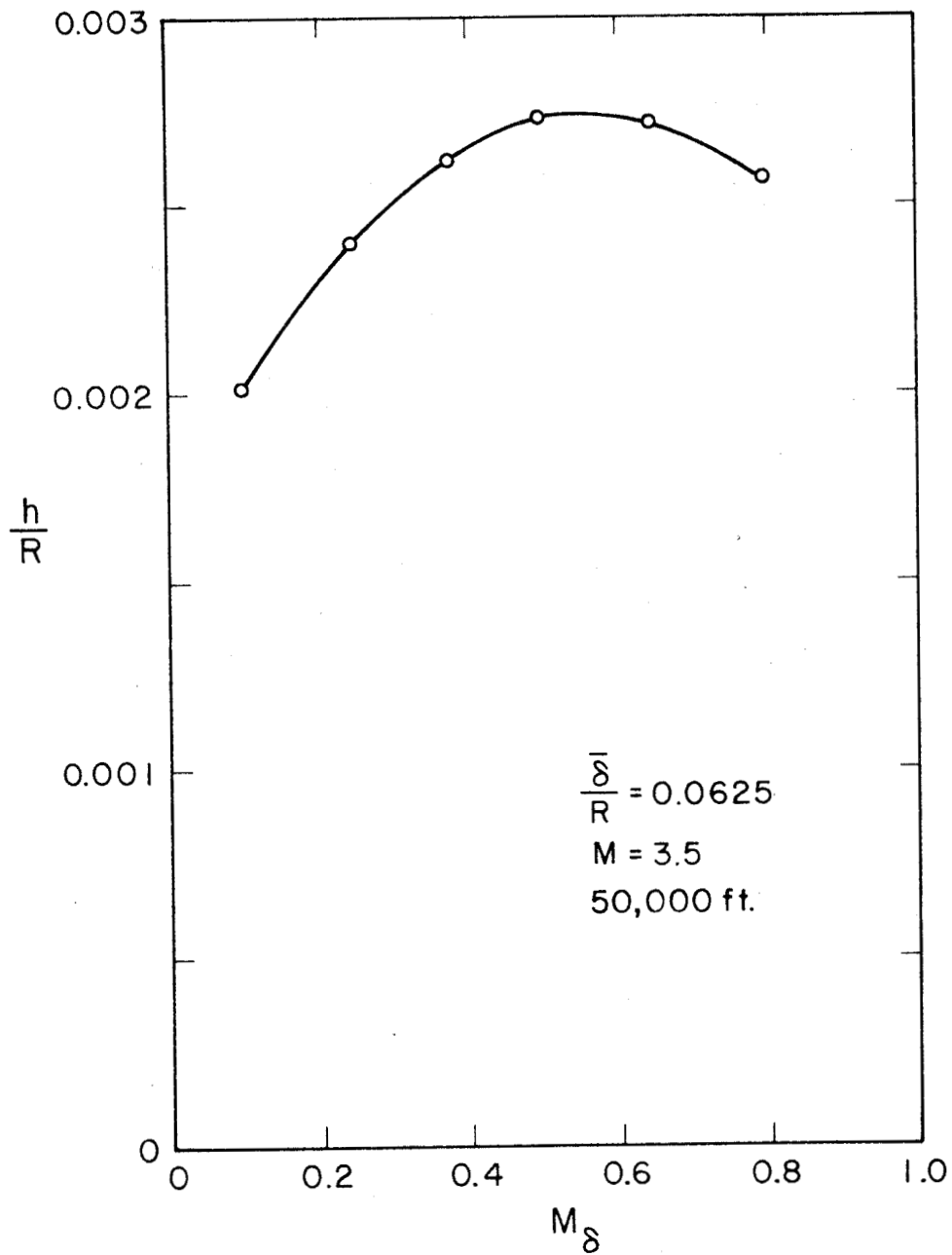


Fig. 16. Effect of the Choice of M_δ on a Typical Flutter Point.